The Hashemite Kingdom of Jordan
Scientific Research Support Fund
The Hashemite University

JJEES

Jordan Journal of Earth and Environmental Sciences

Indexed by Scopus
ELSEVIER

Volume (14) Number (4)

Cover photo © Deema Alawawdeh

JJEES is an International Peer-Reviewed Research Journal

ISSN 1995-6681 jjees.hu.edu.jo December 2023

Jordan Journal of Earth and Environmental Sciences (JJEES)

JJEES is an International Peer-Reviewed Research Journal, Issued by Deanship of Scientific Research, The Hashemite University, in corporation with, the Jordanian Scientific Research Support Fund, the Ministry of Higher Education and Scientific Research.

Editorial Board:

Associate Editorial Board: (Arranged Alphabetically)

International Advisory Board: (Arranged Alphabetically)

Editorial Board Support Team:

Submission address:

Manuscripts should be submitted electronically to the following e-mail:

jjees@hu.edu.jo

For more information and previous issues:

www.jjees.hu.edu.jo

Hashemite Kingdom of Jordan

Scientific Research Support Fund

Hashemite University

Jordan Journal of Earth and Environmental Sciences

JJEES

An International Peer-Reviewed Scientific Journal

Financed by the Scientific Research Support Fund

Volume 14 Number (4)

http:// jjees.hu.edu.jo/

ISSN 1995-6681

King Talal Dam, Jordan.
Photographed by Deema Alawawdeh - Student at the Hashemite University - 2023

JJEES
Jordan Journal of Earth and Environmental Sciences

JJEES

Jordan Journal of Earth and Environmental Sciences

JJEES (2023) 14 (4): 241-253
ISSN 1995-6681

Landfills in the Context of Municipal Solid Waste Management in Lebanon: A review focusing on Greater Beirut Area

Rana Sawaya[1*], Heba Kourani[2], Jalal Halwani[1], Nada Nehme[2]

[1]Lebanese University, Water and Environment Science Lab, Tripoli, Lebanon
[2]Lebanese University, Faculty of Agriculture Engineering and Veterinary Sciences, Dekwaneh, Lebanon

Received August 31, 2022; Accepted May 27, 2023

Abstract

Municipal solid waste management has long been an unresolved problem in Lebanon. Management strategies were crisis-ridden instead of being proactive and sustainable. The history of this sector in Lebanon is highly dictated by the political unrest in the country, weak governance, and late public awareness of the environmental impact of waste generation and disposal. These factors have imposed the only alleged management option adopted by the public sector which is centralized landfilling that covered 50 % of the country and persisted for 30 years. With the chapter on the mega-landfills coming to an end, this report's objective is to describe the landfilling systems as there is a lack of published data on them. Furthermore, the overreliance on landfills through continuous land exploitation is extending their lifespan momentarily especially since unsorted wastes are being disposed of further to the Beirut blast explosion year 2020. The methodology of data compilation was from published articles accompanied by regular visits to the landfills' managing entities. Open dumping and burning of waste have so far prevailed over sanitary landfilling and waste recovery. Thus, there is an urgent call to divert waste from chaotic open disposal and then divert waste from landfills as much as possible. It can be concluded that the application of integrated solid waste management law 80 that encourages waste minimization techniques through sustainable practices related to reusing and recycling waste is of crucial importance. Additionally, and with the scarcity of published data on landfills, this review hopes to lead to communication among Lebanese citizens and stakeholders and with other countries to exchange both scientific and practical experiences.

Keywords: *Lebanon, Environment, Solid waste management, Landfills.*

1. Introduction

The constant accumulation of solid waste in the environment calls for unprecedented measures. Although environmental awareness has encouraged sustainable behavior, the rate of diffusion of municipal solid waste has always exceeded its rate of reuse and recovery (Rezaeisabzevar et al., 2020; Morales, 2020). Globally, most waste (37%) is dumped in landfills and 33% is disposed of in open dumps (Kaza et al., 2018). The Arab countries are considered one of the world's highest per capita waste generators. The United Arab Emirates achieved a municipal solid waste generation per capita of 2.2 kg which is amongst the highest rates worldwide followed closely by Qatar, Kuwait, Saudi Arabia, Oman, and Bahrain. Hence, around 150 million tons of total urban waste are generated in the Gulf Cooperation Council (GCC) annually, with municipal solid waste being the second largest stream after construction and demolition wastes (Mani, 2020). Thus, the sight of wastes dumped in open spaces, deserts, and water bodies is very common due to the deficiency of garbage collection and disposal facilities in addition to a lack of awareness towards waste management and a lack of research on solid waste (Zyoud et al., 2015). Open dumps host potential pathogenic microorganisms which contaminate the soils posing major public health risks (Eghomwanre et al., 2020). Several factors contributed to the ascending waste crisis in the GCC such as rapid urbanization, a construction boom, industrial growth, and improved lifestyle. The organic material constitutes the greatest portion of the wastes in the Gulf states followed by a major part of recyclables. Interestingly, Lebanon shares with the UAE having high waste recovery rates (23 and 27% respectively) (Thabit et al., 2023). Although the countries in the MENA region have similar waste constituents, their methods of landfilling MSW are various (Jaradat and Al-Khashman, 2013). Landfilling of wastes remains the most practiced disposal method.

In Lebanon, solid waste management (SWM) continues to be a complex issue due to deficit implementation of modern SWM practices, non-uniform governmental plans, inadequate environmental awareness, and lack of governmental support (MoE/GFA/EU, 2017; MoE/UNDP/GFA, 2017; MoE/UNDP/ECODIT, 2011). Additional challenges in the SWM sector are the immigration of Syrian refugees year 2011, poor legislative framework, and lack of law enforcement (De Quero-Navarro et al., 2020; MoE/UNDP, 2017; MoE/EU/UNDP, 2015).

Municipal solid waste (MSW) makes up about 90% of

* Corresponding author e-mail: rana.sawaya1313@gmail.com

the total solid waste generated in Lebanon. MSW's average generation per capita is 1.05 kg/d. The high production rate, 1.2 kg/d, mainly corresponds to the region of Beirut and part of Mount Lebanon. Organic wastes are the largest component of the waste stream averaging 53% followed by potentially recyclable material (31%) then other wastes (16%). As for municipal waste collection, the coverage is high, reaching 99% (Sweep-net, 2014). Only 15% of the waste is treated in sorting facilities where material recovery and composting occur. The private sector has failed to shift from a high percentage of disposal to the recovery of both energy and materials (CDR/LACECO, 2011). Around 50 facilities currently exist throughout Lebanon, however, not all of them are operational and/or functioning efficiently (MoE/UNDP/GFA, 2017).

Greater Beirut Area alone generated 51% of the total MSW generated in the country (MoE/GFA/EU, 2017). The Country Report on Solid Waste Management in Lebanon estimated that Lebanon generated 2.04 million tons of Municipal Solid Waste in 2013.

Until the year 2016, only two sanitary landfills for municipal solid waste, Naameh, and Zahle, were under operation and only 23% of national MSW was being recovered by composting and recycling (Sweep-net, 2014). Only a few non-sanitary landfills were constructed yet around 941 open dumpsites are now spread across the country (MoE/UNDP/ELARD, 2017). The latter receives 50% of the total waste while 30% reaches sanitary landfills (MoE/UNDP/GFA, 2017). The climax of ill management of the waste sector was manifested in the waste piling up in the streets in the regions of Beirut and Mount Lebanon after the closure of Naameh Landfill in 2015. The only other sanitary landfill is Zahle Landfill in the Bekaa district which by now has reached 20 years of operation. It is located in a secondary city but favored by the sense of responsibility of the municipal council and the professionalism of the operator (World Bank, 2007).

The current state of the solid waste sector is a consequence of the history of the solid waste crises and three sectors: the formal sector restructuring itself to ensure a basic service, informal actors compensating the gaps left by the central system through resource recovery, and the decentralized sector trying to provide an alternative to the centralized one. However, total efficiency is being held back as these sectors need yet to cooperate (Azzi, 2017). The ratification of the integrated solid waste management law (Law Number 80) in 2018 pushed discussions relating to the decentralization the MSW management services (MoE, 2018). A recent study foresees a strong viability of the success of the decentralization of MSW management services (Abed Al Ahad et al., 2020). The problems facing Lebanon in the solid waste management sector are the exact ones that the GCC and/or Arab countries are facing and similar solutions can be applied to the Middle Eastern Countries. Furthermore, this sector suffers from the scarcity of reliable and accurate background data and information that one can build upon for the creation of sustainable future strategies and solutions.

Studies by Sawaya et al., 2021, Khadra and Stuyfzand 2014, and Fadel et al., 2002 tackled pollution as a result of leachate infiltration into water resources. Other studies about the composition of municipal solid wastes were demonstrated through papers by Mokbel et al., 2022 and Halwani et al., 2020. However, none of the undertaken studies encompassed the prime landfills with all their aspects while shedding light on the basic problems facing this sector with adequate solutions.

Thus, this paper provides a thorough brief on the waste management status in Lebanon with an emphasis on landfills in the context of individual landfill design and characteristics. As the waste crisis is repetitively reoccurring, and as the landfilling solution is the only disposal mode adopted throughout the years, the landfills in Lebanon are being overexploited. This overreliance is being additionally demonstrated after the Beirut blast year 2019 leading to the entry of unsorted wastes into the landfills. Thus, this literature is crucial as it reveals the successful and unsuccessful experiences of the landfills which will allow enhancement of the landfill statuses via possible future upgrading of the technical and environmental features of the landfill sites and/or landfill mining. Furthermore, it will highlight the need to adopt an overall sustainable waste management strategy.

1. History of Solid Waste Management

During the period 1900-1975, the responsibility of waste collection, treatment, and disposal was endorsed to municipalities. However, even then, the practices were described as unsatisfactory and uncoordinated. The period of the civil war (starting the year 1975) is considered the turning point for the waste collection industry.

1. 1975–1990: Civil War era

Circumstances of war split regions from each other. Most of the country's infrastructure was ravaged whereby solid waste facilities including refuse collection trucks, containers as well and other waste-related equipment were destroyed and/or nonfunctional due to the complete absence of maintenance. Jumbled waste disposal actions were taking place with the intermingling of wastes from hospitals to hazardous and others (World Bank, 1995). Two coastal dumpsites were created in the Normandy and Bourj Hammoud areas which received Beirut's municipal and destruction wastes. As for the areas outside the capital, municipal collection, and uncontrolled dumps were the dominant practices.

During 1987 and 1988, around 15800 illegal toxic waste barrels were exported from Italy to Lebanon. (Hägerdal, 2021). Those barrels contain highly toxic substances such as explosive nitrocellulose; outdated adhesives, organophosphate pesticides, solvents, as well as outdated medication; oil residues, and heavy metals (Holder, 1995). In 1989, an agreement referred to as Taef (Saudi Arabia) was signed and was considered the foundation for ending the civil war and restoring political normalcy to the distorted country.

2. 1990–2015: the post-war era or Sukleen's monopoly

The war created vast economic and social wounds. Therefore, the country witnessed the creation of organizations that aimed to manage reconstruction and state

reform. The key ones are the Council for Development and Reconstruction (CDR) and the Office of the Minister of State for Administrative Reform (OMSAR). These institutions today are responsible for the implementation of the Council of Ministers' decisions via conducting public tendering to plan, design, and build the country's main facilities.

The waste collection and dumping sectors did not improve during the first years after the war. Waste was deposited in bags at street corners and was picked up sporadically by trucks. Domestic wastes were mixed with hazardous and hospital ones. Also, the usual dumpsites were utilized and the compiled waste was often put on fire as a consequence of infrequent collection (World Bank, 1995). The resumption of adequate waste collection services was adopted the year 1994 due to private sector contracting. This is the result of the international aid provided through the NERP (National Emergency Recovery Program) coupled with the extensive efforts of the CDR. Sukleen, which is part of the Averda group company, was given the responsibility of managing city cleaning and waste collection. This company ruled the waste management sector for approximately two decades (Nuwayhid et al., 1996).

3. Waste Crises and Emergency Responses

1. Waste Crisis 1997: Emergency Response Plan 1997-2005

The year 1997 witnessed severe protests from civils against the outdated Amrousieh incinerator's harmful emissions as well as the dumping methods practiced at the Bourj Hammoud dump. This led the protestors to burn the incinerator in June of the same year as they accused the government of carelessness regarding health and environmental issues (World Bank, 2011). Based on the above, the Ministry of the Environment has set a 7-year emergency solid waste management plan (1997-2005) to be implemented by the CDR. Solid waste management contracts were issued to the private sector company Averda Group through its sister companies (Sukleen and Sukomi). The responsibilities included sweeping, collection, treatment, and disposal (CDR, 2006). The former services were performed by Sukleen whereas the latter which included sorting, baling, wrapping recycling, composting, and landfilling was attributed to Sukomi. The zone of coverage encompassed most of the Greater Beirut area (34 municipalities). Governorates besides Beirut and Mount Lebanon (800 municipalities) relied on local dumps. Bourj Hammoud dump was closed and a new sanitary landfill referred to as Naameh landfill was established. Supervision of tasks of Sukleen and Sukomi was handed to D.G. Jones and Laceco respectively. The major gap in the system was over-reliance on landfilling as the majority of the waste (80%) was being deposited. Also, alternating composting performance and minor levels of recycling, as well as a high net cost of $130/ton, was the case. As a direct consequence, the Naameh landfill has exceeded its original design capacity due to the incapability of the government to provide an alternative site and increase treatment capacities. Consequently, the contract with the mentioned private companies was being extended repetitively (CDR, 2015).

2. Waste Crisis 2015: Emergency Response Plan 2016–2020

Naameh landfill which was an emergency response against the Bourj Hammoud civil war dumpsite has become a bomb leading to a waste crisis year 2015. A secondary factor that worsened the situation was the mismanagement of private waste management contracts. Overreliance on the Naameh landfill has led to the extension of Averda's contract several times (Boswall, 2019). Initially, the landfill was intended to operate for ten years and receive a maximum amount of two million tons of waste. Yet, it stayed for eighteen years and held within its premises fourteen million tons of waste. The last six months' extension of the landfill's lifetime promised its closure on July 17, 2015. Meanwhile, CDR had to run public tenders to attract bidders for waste treatment in six operating areas. Potential landfill sites were identified in each zone. The tendering process was repeated for three rounds to conform with the validity requirements.

On the above-mentioned closure date, angry protestors blocked the site's entrance marking the beginning of a critical waste crisis. Furthermore, the council of ministers rejected the tenders' results one month later. As a result, all the waste services stopped leading to an eight-month crisis whereby mountains of waste sometimes reaching a height of 7 meters accumulated in proximity to neighborhoods. An estimated 20,000 tons of rotting waste were found in Beirut streets at the peak of the summer season. Three solutions were foreseen by the government for resolving the issue which are incinerating wastes, exporting wastes to Africa and Russia, and initiating two temporary landfills in Srar (North Lebanon) and Bekaa regions.

An emergency response plan was proposed and adopted by the Council of Ministers on March 12, 2016; nearly a year after the crisis. As a primary step, the companies responsible for waste treatment in Beirut and its suburbs were announced. Three short-term solutions were proposed:

- Reopening Naameh landfill for two months to get rid of the piled-up wastes over the last eight months and establishing two temporary landfills (lifetime of 4 years) in the Bourj Hammoud and Costa Brava regions located in Northern and Southern Beirut respectively.
- Reconsidering the energy recovery process as a shift from landfilling to incineration through the construction of waste-to-energy plants with a capacity of 2000 tons per day.
- Restressing the likelihood of municipalities managing their wastes using proper methods.

3. Landfilling aspects

Landfills are inevitable to integrated waste management because they provide the only terrestrial sink for hazardous substances that would otherwise be dispersed into the environment (Touze-Foltz et al., 2020). If operated sustainably, landfills may also represent a way to return materials and substances to the environment by applying material recovery (Powrie et al., 2014).

When designing a landfill, multiple technical factors which have a significant environmental impact should be considered such as location, liner systems, leachate collection, biogas control, and capping (USEPA, 2021; Al

Zaghrini et al., 2019; Katsumi et al, 2001). Dumpsites in Lebanon which include open dumping and open burning are a major threat to water resources and air quality and may pose significant health and carcinogenic risks (Nehme et al., 2021; Mouganie et al., 2020; Borjac et al., 2019; Khalil et al., 2018; Hilal et al., 2015). Moreover, large dumpsites or landfills for municipal solid waste that have been created and/or constructed adjacent to the seashore such as Tripoli, Bourj Hammoud, Costa Brava, and Saida pose a threat to seawater quality (Ecodit, 2015). Coastal landfills pollute water and sediments with microplastics (Kazour et al., 2019) and trace metals (Ghosn et al., 2020; Merhaby et al., 2018) which may reach biota and potentially harm marine organisms. They may be also linked with moderate coastal vulnerability (Ghousseina et al., 2018). Way before the 2015 waste crisis, landfills have already contributed by 5% to the coastal marine pollution of terrestrial origin (Shaban, 2008).

4. Lebanon's primary sanitary landfills

1. Naameh Sanitary Landfill

The CDR in consultation with the MoE and the sector implementation unit (SIU-3) adopted an emergency plan for MSW management in the Greater Beirut Area. The plan consisted of developing an integrated MSW management system that includes the following facilities:

- The Amrousieh and Karantina facilities for sorting and processing raw MSW
- The warehouse storage facility for sorting all bulky and recyclable materials
- The Naameh Landfill site for disposing of sorted MSW
- The Bsalim Landfill for disposing of inert and bulky materials

The emergency plan included collecting MSW from the Greater Beirut Area and transporting them to the Amrousieh and Karantina facilities. At these processing plants, the MSW was sorted into reject, recyclable, and compostable materials. The reject material was then compressed, wrapped, and baled for ultimate disposal at the Naameh Landfill site. Recyclable materials were separated and where possible sold. Compost was supplied to farmers without charge. Inert and bulky materials were transported to and ultimately disposed of at the Bsalim Landfill. The CDR commissioned Sukomi to develop and operate these facilities. To ensure proper development and operations, CDR retained LACECO as the consultant to provide technical assistance to the government through the supervision of the operator's activities at the site (Sweep-net, 2014).

The Naameh landfill site is situated in the Southern coastal zone of Lebanon, some 15 km south of Beirut and 4 km from the coastline at an average altitude of 250 m above sea level (Figure 1).

Figure 1. Map of the controlled landfills in Lebanon by the year 2021.

It started operation in October 1997 whereby it received baled waste rejects, a big fraction of putrescibles not sent to the composting plant due to its limited capacity, and finally the recyclable materials which were not recovered from the raw MSW. The original shelf-life of the landfill was 10 years with an expected capacity not exceeding 3 million tons of solid waste. However, the landfill underwent a series of extensions which lengthened its operation an additional 8 years where it held within its premises around 14 million tons of waste from the Greater Beirut Area. The landfill covers an area of 300,000 m^2. It is worth mentioning that the height of the waste ranged from 10 m at the lowest point to 100 m at some points making it one of the deepest landfills worldwide (El-Fadel et al., 2002).

Naameh landfill is considered one of the prime sanitary engineered landfills in the Middle Eastern area. The Naameh site was designed and managed within the guidelines and principles followed by established control and management of UK and European landfills. Golder Associates (UK)Ltd was appointed by Sukomi Landfill Projects to carry out the project management of the construction Quality Assurance during the construction of the landfill.

The ground profiles at Naameh underwent filling and re-compacting of the valley floor to allow the formation of a stable subgrade followed by a geotextile protection layer (500 g/m2). Above this layer comes the primary component referred to as geomembrane or Flexible Membrane Liner (FML) composed of HDPE (2.0 mm) material that is manufactured to a consistent standard with high manufacturing quality control at plants in either the USA or Germany. Each layout represents a panel, and adjacent panels were welded with purpose-designed machines by experienced installers. All liner construction work was fully supervised and subjected to certified quality auditor inspection, testing, and documentation. Above the FML additional protection layers of geocomposite, sand, and more geotextile (500 g/m2) were placed (Figure 2).

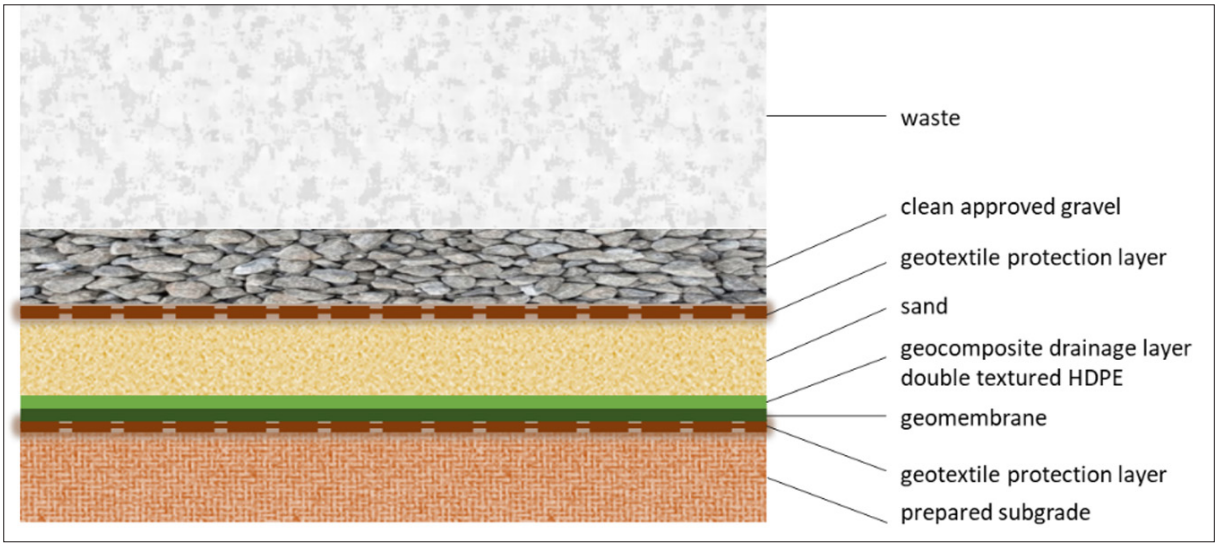

Figure 2. A diagram of the protective liner system in Naameh Landfill (Laceco, 2020).

Once in place, a drainage system was installed for the efficient removal of the leachate from the base of the landfill. It consists of a network of perforated pipes acting as preferential drainage pathways within a coarse aggregate blanket. The drainage system was brought to the lowest part of the relevant cell and connected to tubular leachate towers. Leachate was removed from these towers by periodic pumping to maintain leachate levels at a required minimum. The leachate is then taken to treatment and disposal. Therein, it passes through two stages of treatment: chemical and microbiological (sequential batch reactor).

During bale stacking, a pattern of gas wells was simultaneously constructed. Cells were interconnected by pipework. The collected gas went through the flaring system to prevent the discharge of methane gas into the environment and control odors about the volumes of gas processed (Figure 3).

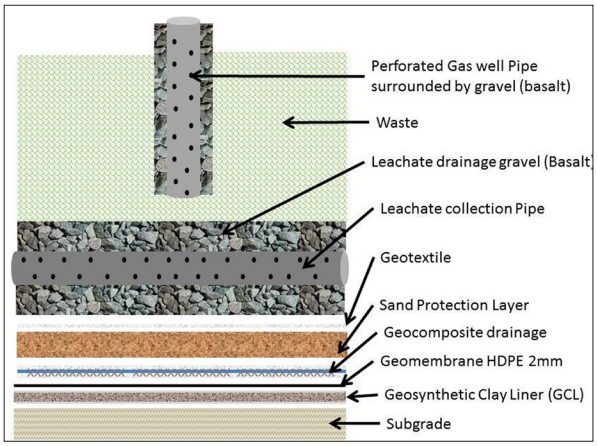

Figure 3. A diagram of the protective liner system with gas wells (Sawaya et. al, 2021).

At last, the landfill was subjected to closure via the construction of a special cap that shall prevent the ingress of rainwater into the wastes (Figure 4). After the closure of the Naameh landfill, two landfills were initiated to receive wastes from the Greater Beirut Area and are referred to as Costa Brava and Bourj Hammoud.

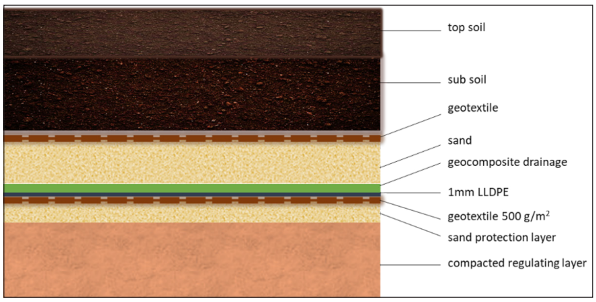

Figure 4. A diagram of the final capping system in Naameh Landfill (Laceco, 2020).

2. Zahle Sanitary Landfill

Zahle Sanitary Landfill is located in the Bekaa Valley in the Caza of Zahle. It receives waste from the City of Zahle and 18 neighboring municipalities. The World Bank funded its construction in 1998 so that it could handle 150 tons per day. This corresponds to eight percent of the waste generated in Lebanon (MoE/UNDP/ECODIT, 2011). In 2001, SERDIM with its partner SCS engineers was selected by the Municipality of Zahle, the CDR, and the World Bank to operate the landfill and to remediate Zahle's old dump site (Serdim Liban). Besides collecting about 180 tons of municipal waste, recyclable materials were being sorted by the private sector contracted at competitive prices. By 2013, 10% of incoming waste was being recycled (Chamieh et al., 2016).

The landfill was comprised of 3 independent disposal cells. The base of the cells was lined with a composite liner containing 60 cm of compacted clay covered by a 1mm HDPE geomembrane Leachate is removed by a series of 4 submersible pumps and relocated to a storage basin which is also equipped with a liner system. The leachate reaches the pumps by pipes fitted inside a sand and gravel layer and placed over the liner system. A modern LFG (landfill gas) extraction and destruction system was installed and operated. The system consists of wells installed in the waste connected to a piping system, a blower, and a flare.

SERDIM-SCS accepted, processed, sorted, and disposed of over 39,000 tons of waste. Each of the three initial cells

was conFigured to be 14 m in height (from the cell bottom) with 4v:1h side slopes. After an assessment of the landfill's design, SERDIM-SCS combined the three cells into one large unit to increase the total capacity. Thus, the height was increased to 24 m and the side slope grades changed to 3v:1h doubling the capacity of the landfill.

Concerning the old dumpsite in the same area in Zahle, it has also been receiving waste from the Municipality of Zahle and other communities for the last 30 years. It occupied 15,000 m^2 and was over 25 m in height that it started to spill over adjacent properties. The waste was frequently burned to decrease its volume and only a small amount of cover soil had been applied over the years. The actual amount of waste disposed of at the old dump was eventually at least 225,000 m3. SERDIM-SCS removed them to one cell of the controlled landfill and returned the old dump site to its original ground elevation which became an open field ready for other uses.

The landfill receives five types of solid waste: household waste, retail waste, organic waste from parks and gardens, market waste, and demolition waste from households. The non-recyclable waste is either landfilled or composted. As the quality of the compost formed has not yet reached the commercial standard, it is currently used as a soil cover for the landfill. Leachate is collected and sent to Al-Ghadir's wastewater treatment station (south of Beirut) because the constructed leachate treatment plant is not yet operational. The treatment and disposal facilities of Zahle include several technical components: (1) a sorting and processing plant with an average capacity of 250 tons/day, (2) a composting plant with an average capacity of 90 tons/day, (3) a sanitary landfill, (4) a leachate treatment plant with a treatment capacity of 35m3/day, (5) a gas flaring unit with a maximum capacity of 300 Nm3 (normal cubic meter) per hour, and (6) a non-operational sorting and processing facility with an average capacity of 60 tons/day (Farah et al., 2019).

With increasing the recycling and composting capacities, the landfill's lifespan was increased from 17 years to 26 years and the costs of both its treatment and disposal operation and maintenance were reduced by two-thirds (World Bank, 2011).

3. Greater Beirut's alternative sanitary landfills

1. Costa Brava Landfill

The Costa Brava Landfill was opened in April 2016. It is one of the two landfills that have been suggested by the Lebanese government as a solution to the eight-month trash crisis that the country went through in 2015. It is located on the southern coast of Beirut, 167 meters away from the national airport (Rafic Hariri Airport). Al-Jihad Group for Commerce and Contracting (JCC) was contracted by CDR to construct and operate the landfill. In the process of landfill construction, JCC reclaimed 500,000 m^2 from the sea. This site receives around 1200 tons of sorted wastes from parts of Beirut and Choueifat areas as well as a small portion from other parts of Mount Lebanon cities. Further to the Beirut explosion on 4th August 2020, all the wastes entering the landfill were unsorted. The total amount of waste received until July 2021 is 2.5 million tons of waste.

Costa Brava landfill consists of 2 cells, 1 and 2 (2A and 2B), separated by 30 m by the Ghadir River. Cell 1 was divided into two phases (I and II). Phase I covered an area of 130,000 m2 and it stopped receiving the waste year 2018 whereby it held within its premises 1,200,000 tons of waste. This area was fully capped and another phase II as an extension to cell 1 is in the initiation and preparation phases for receiving around 780,000 tons of waste in a 78,480 m2 area (FFigure 5).

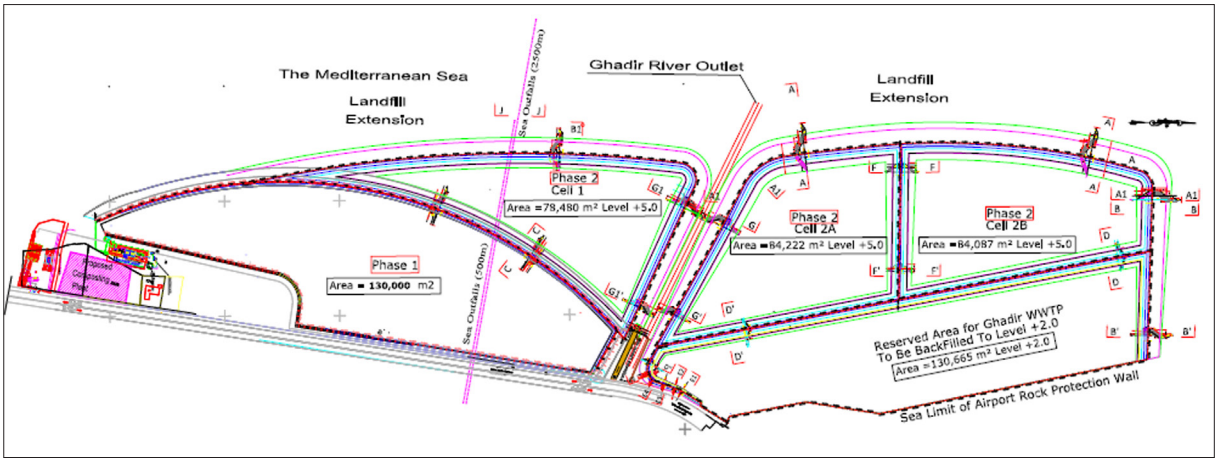

Figure 5. A diagram of the general layout of Costa Brava Landfill according to the phases, cells, and area (CDR, 2020).

The current cells (2A and 2B), which are presently receiving wastes, extend through areas of 84,222 m^2, and 84,087 m2 respectively. They rise 16 m above sea level. The capacity of cell 1 is 1.3 mm3 and the capacity of cell 2 is 2.5 mm3 of which 1.75 mm3 tons are already occupied. In addition to the cells, there is a reserved area for a new Ghadir WWTP to be backfilled to level +2.0 spaced 130,665 m2.

The floor base of the landfill was initiated via compaction of the floor followed by a grading layer (15 cm), clay (60 cm), HDPE geomembrane layer (2.5 mm), geotextile (500 g/m2), sand (30 cm), and another geotextile layer then the wastes with a daily sand cover added above them (Figure 6). Only part of cell 1 was capped. The capping system consists of protective soil (25 cm), grading layer (15 cm), clay (50 cm), HDPE geomembrane (2.5 mm), sand (30 cm), agricultural soil (60 cm), and the final vegetative cover (FigureFigure 7).

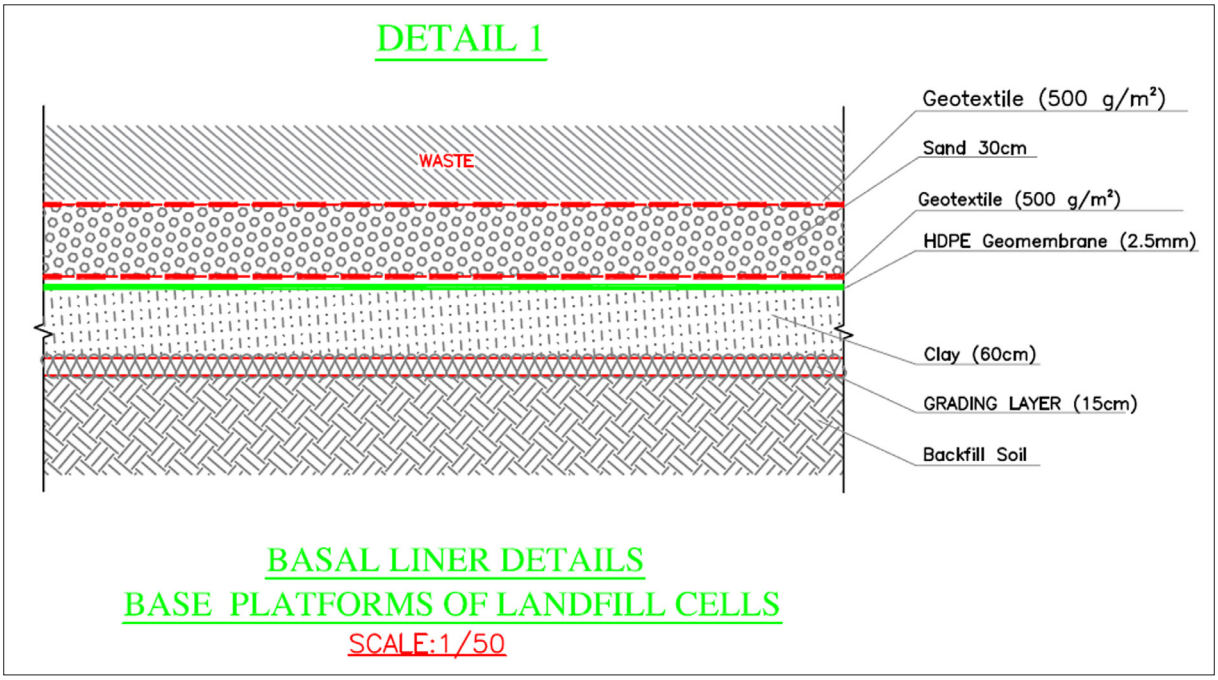

Figure 6. A diagram of the protective liner system in Costa Brava Landfill (CDR, 2020).

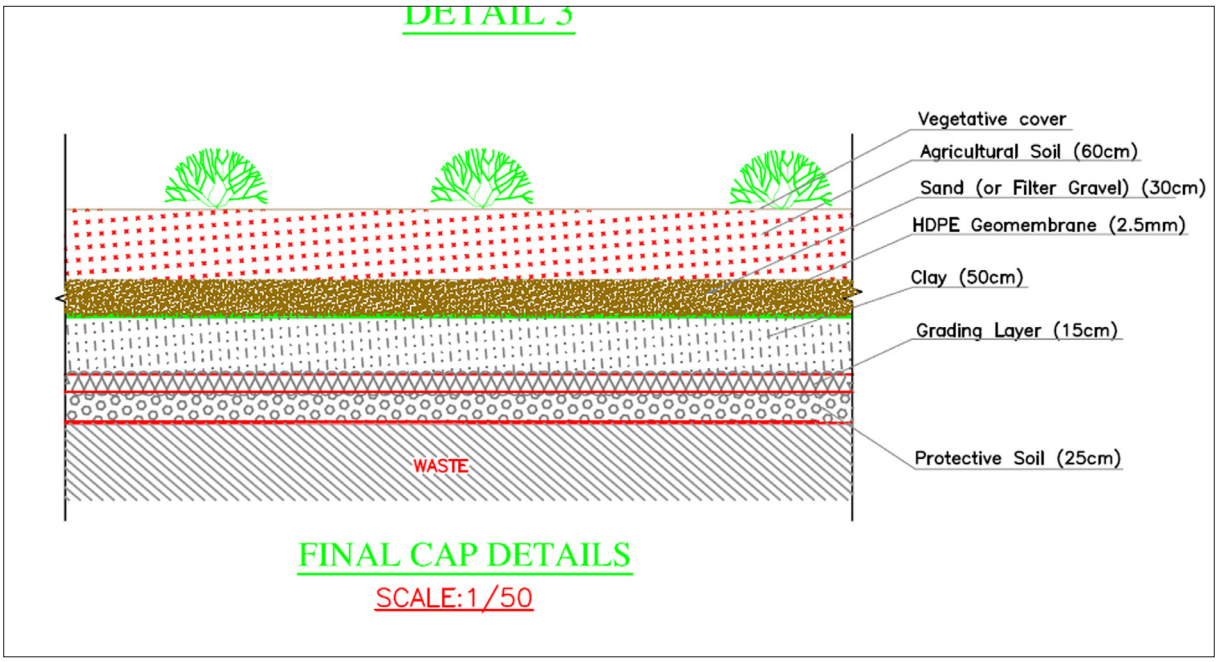

Figure 7. A diagram of the final capping system in Costa Brava Landfill (CDR, 2020).

Leachate resulting from the waste degradation process is gathered via a leachate collection system (200 Ø HDPE pipes, sump pits, leachate wells and submersible pumps) and further treated via two leachate treatment systems each about a phase. The leachate plant responsible for phase I was initiated by EMIT (an Italian company) in 2017 and offered three stages of treatment: physical/chemical, biological, and reverse osmosis (RO) system. The flow rate is 120 $m^{3/day.}$ Another treatment system initiated by Hofsteler (a Swiss company) encompassed leachate from phase II and consisted of physical/chemical, MBR, and RO systems for both the leachate and permeate. This system is currently nonfunctional due to the unavailability of sulfuric acid and its flow rate is around 120 m3/day. The water resulting from both treatments is being reused in dust control.

The biogas resulting from the waste degradation process is collected through a gas network and undergoes flaring at a combustion temperature of greater than 1000 degrees Celsius and a flow rate of 320-1600 m3/h. There are 63 gas wells in the landfill present (CDR, 2020).

Amidst the continual waste management crisis and absence of sustainable solutions, the landfill's life span was extended for an additional 4 years.

2. Bourj Hammoud–Jdeideh Landfill

Bourj Hammoud landfill is located on the northern coast of Beirut. It was fated to receive waste from the 1950s till 1990. Informal practices of open dumping especially on the coast prevailed during the years of civil and regional war (1975-1990). By the end of the war, tons of waste had accumulated by the Bourj Hammoud seashore. Nevertheless, the majority of the waste was dumped after the war, as the uncontrolled dump was declared an official landfill by a governmental decision. After the Civil War, the landfill received around 3,000 tons of waste daily. By 1997, the dump had far exceeded its capacity inevitably becoming an environmental and public health hazard. The situation led to a major protest by the inhabitants of Bourj Hammoud as the landfill was not only a dump site for the region, but also all the suburbs of Beirut and Mount Lebanon. Meanwhile, an incinerator in Amrousieh was supposed to back up the waste disposal process to Bourj Hammoud. However, this plan which was also government-based, failed as community protestors set the incinerator on fire. Eventually, the government closed the landfill on July 20, 1997, but without rehabilitation.

For years, Bourj Hammoud dumpsite released an estimated 120,000 tons of leachate annually equivalent to at least half the leachate produced by three main coastal dumpsites in Lebanon (Tripoli, Bourj Hammoud, and Normandy) (EU, 2006). However, LFG generation dropped rapidly to half its peak level only 4 years after landfill closure (El-Fadel et al., 2012).

As history repeats itself, after the solid waste crisis in 2015 and waste piling up on the streets, the government decided to rehabilitate the old Bourj Hammoud Landfill and open one next to it: the Jdeideh Landfill.

The Bourj Hammoud solid waste dump occupied a surface area of 163000 m^2 and rose to about 55 m above sea level with extremely steep side slopes. The waste, estimated at 6 million cubic meters, consists of demolition debris, excavation material, municipal solid waste, industrial waste, and hospital waste. Slope failure could occur at any time because the slopes are highly unstable and the underlying subsoil is a thick layer of soft clay which intensifies the stability problems. A consulting firm, Associated Consulting Engineers (ACE), was assigned to rehabilitate the old landfill (LINORD development project). The project had to solve the problems of soil instability, as well as leachate and gas generation, and aim at transforming the dump into a district park.

Bourj Hammoud garbage mountain was used as a backfill for the construction of these two new landfills. Hence, around 3.5 million cubic meters of waste, of which more than 50% were construction and demolition waste, while the rest were municipal waste, were excavated from the old dump and moved to the new nearby landfill, next to the fishing port. They were also used to reclaim land on the sea for building these new landfills and creating land for the municipalities.

The reason behind building two landfills instead of one is the area restrictions. The area between Bourj Hammoud Landfill and Jdeideh Landfill is 250 meters of seawater (Figure 8) which is the only passage of oil and gas pipes for the country. This zone is reserved for petroleum companies.

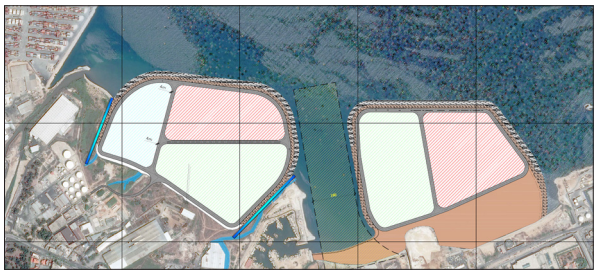

Figure 8. A map of Bourj Hammoud (left)-Jdeideh (right) Landfills general layout concerning the location and cells (CDR, 2020).

Bourj Hammoud landfill consists of 8 cells occupying 126,400 m^2 while the 11 cells of Jdeideh's landfill occupy 122,700 m2. It is noted that the Bourj Hammoud landfill reached full capacity, while 10 cells of the Jdeideh landfill are fully occupied and the 11th is now receiving waste. From the Bourj Hammoud landfill area, 97,400 m2 were reclaimed and given to the municipality while 119,500 m2 were reclaimed from Jdeideh as a public domain. Furthermore, around 65,000 m2 of the Bourj Hammoud landfill was kept to construct a wastewater treatment plant for Beirut.

Bourj Hammoud landfill closed in February 2019 and it has reached 20 m in height. It is noted that minimal leachate is being produced while biogas is still being emitted. Jdeideh landfill reached 15.5 m in height now.

The landfill land lies 0.5 m above sea level. First, 40-50 cm stabilized soil and then a protection and leveling layer (10 cm) were added. The landfill liner system consists of 3 layers: GCL (geosynthetic clay liner), which is composed of 2 layers of geotextile impregnated with bentonite, then 2 mm HDPE, and lastly geotextile 800 g/cm2. Finally, a drainage layer of 10-30 mm was added (Figure 9).

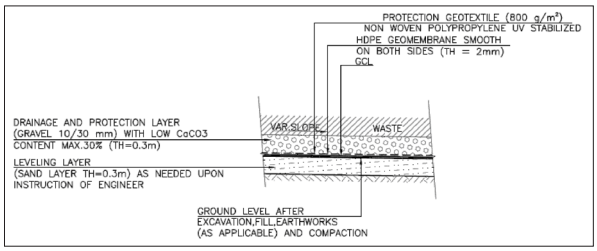

Figure 9. A diagram of the protective liner system in Bourj Hammoud-Jdeideh (CDR, 2020).

Capping consists of 5 layers (Figure 10). It starts with a leveling layer of sand around 0.3 m. Next, there are GCL, HDPE geomembrane textured at both sides (TH= 2 mm), protection geotextile (800 g/m^2) of non-woven polypropylene UV stabilized. Capping ends with a drainage and protection layer (gravel 10/30 mm) with low CaCO3 with a content maximum of 30% (TH= 0.3 m).

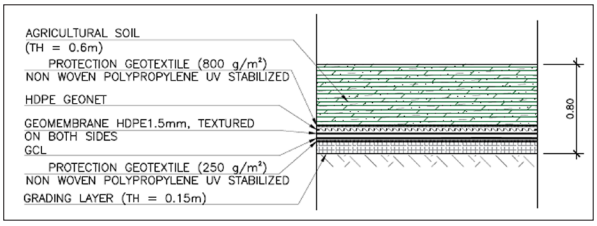

Figure 10. A diagram of the final capping system in Bourj Hammoud Landfill (CDR, 2020).

There are two leachate treatment plants, one for each landfill. Leachate circulates through corrugated 400mm diameter pipes (to allow aeration) and then reaches a leachate pond covered with grids to reduce evaporation and smell, after which they are pumped to a tank with blowers for aeration. Two leachate treatment plants include only reverse osmosis (RO) aided by a pH dosing pump (injection of sulfuric acid or caustic soda). The RO container plant for leachate treatment allows 120 m^3/d, has 3 stages, and a 69 bar max operating pressure of the leachate stage, with 85% yield and 5 m^3/hour recovery. It is worth mentioning that a gas flaring system was installed by an Italian company. However, the system did not operate due to the COVID-19 outbreak and the Beirut blast which prevented the operators from performing the necessary commissioning and training. Thus, the gas resulting from the landfilled wastes is being emitted into the atmosphere. Further to the Beirut explosion on 4th August 2020, all the wastes entering the landfill were unsorted. The total amount of waste received until July 2021 is 2 million tons of waste.

6. Other controlled landfills in Lebanon

1. Tripoli Landfill

Tripoli landfill is located alongside the coastline, adjacent to the Abou Ali River estuary, and north of the port of Tripoli. Its estimated area is 60,000 m^2. Tripoli Landfill receives around 450 tons of waste daily from the following cities: Tripoli, El-Bedawi, El-Mina, and El-Qalamon as well as from the north Palestinian refugee camps. Its operation was initiated year 1980 and it was converted to a semi-controlled dump year 2000 (Halwani et al., 2020). The dump's operation was supposed to end the year 2012, however, it is still receiving waste until present without any regard for the associated ecological risks (Halwani et al., 2014).

To contain the open dump and prevent its expansion into the Mediterranean Sea, a peripheral seaside wall was constructed the year 1997. Furthermore, the Union of Al-Fayhaa Municipalities (UFA) initiated a project year 1999 which consisted of shifting the site's operation to that of a controlled landfill through its rehabilitation. Thus, the contractor (BATCO) was assigned by CDR to manage the controlled dump. It enhanced the waste disposal modes via the incorporation of gas extraction wells and flaring units (CDR, 2002).

Tripoli landfill's operation ranged from waste placement, application of daily cover, compaction, and biogas flaring to leachate control (both stopped in 2013) (Halwani et al., 2020).

The landfill holds 1.1 million m3 of waste. with a height of 45 meters (UFA, 2018). The landfilling operation is a simple one consisting of spreading and compacting the waste in layers of approximately 50 cm and then covering it with 15 cm of inert soil material.

The landfill's leachate was drained into pits and it underwent a partial treatment process from years 2009 until 2013. The leachate was subjected to a recirculation procedure whereby it was sprayed and evaporated on the compacted solid waste and then recollected via a peripheral network underneath the waste. However, the continuous increase in the height of the solid waste as well as the construction of the peripheral trenches exposed the system to a great risk as the associated equipment (pumps, etc.) couldn't sustain the variations. The leachate treatment process consisted of an aerobic digester with nitrification and anoxic denitrification; clarification; chlorination; and filtration (sand and carbon filter). However, the efficiency of the treatment was altered due to the increase in the volume and height of solid waste as well as the rainwater ingress which overwhelmed the design capacity of the plant (36 m3/day). Therefore, a fraction of the leachate was recirculated in the landfill and another one was released into the river discharging into the sea (Halwani et al., 2020).

As a replacement for the old flare (500 m3/h), a new one with a higher capacity (1100 m3/h) was installed year 2009. However, the system stopped in 2013 as the height of waste exceeded 32 m and thus the need to elevate the gas wells vertically. Therefore, the biogas released is not being treated and might cause an accidental huge fire which in turn will lead to serious health and environmental impacts (Halwani et al., 2020; Halwani et al., 2017).

OMSAR, with financial support from the European Union, has constructed a sorting and composting plant near the dumpsite area with a capacity of 420 tons/day. However, the plants were stopped just a few weeks later due to complaints from residents about the awful odors detected in the city, low recycling efficiency (less than 5%), and poor compost quality. Those shortfalls resulted from troubleshooting the biofilter and maturation phase of the compost. To solve this issue, technical modifications for the facilities are being looked upon by OMSAR and UFA. The waste entering the landfill is not being sorted except by scavengers who were allowed by UFA to collect recyclables before spreading the waste in the dump.

As the landfill succeeded in reducing the amount of waste disposed from 420 tons/year to 350 tons/year, an extension into a new temporary landfill was performed by reclaiming 60,000 m2. The new landfill started its operation in February 2019. It consists of three cells and the design capacity is for three years. Further to its closure, the rehabilitation process will be initiated (Halwani et al., 2020).

2. Saida Dump

Saida dump was established year 2004. It is located on the seafront, at a distance of 200 meters from commercial units and nearby houses (Farah et al., 2019). The dumpsite is being managed by the municipality of Saida. It receives around 300 tons of waste daily from 15 municipalities. Since its establishment year 1982, it received all kinds of waste

(60% rubble and 40% municipal waste) which piled up to form a waste mountain reaching a height of 55 meters (MoE/UNDP/ECODIT, 2011). It covered an area of 60,000 m^2 and held waste at an estimated volume of 1.2 million m3 which rendered it an enduring eyesore to tourists and residents (Farah et al., 2019; ILO/UNDP, 2011). Thus, countless complaints from residents and fishermen were raised as a result of the severe environmental repercussions with the accompanying adverse impacts on health (UNDP, 2013).

With support from the UNDP as well as the Prince Walid Bin Talal Humanitarian Foundation, the dumpsite was transformed into an enclosed landfill via a mining procedure that allowed for the treatment of waste at the dumpsite (UNDP, 2017). Part of the land was reclaimed for wastewater treatment and gas emanations and another part (33,000 m2) was transformed into a park year 2016. IBC (a private waste contractor) constructed a mechanical and biological treatment plant at a distance of 200 m. An anaerobic digester started its operation in 2013 south of the dumpsite (MoE/UNDP/ECODIT, 2011).

The treatment plant received 500–600 tons of waste daily from areas within and outside the district. Further to sorting, the waste is treated via anaerobic digestion and then processed to generate electricity. Putrescibles are packaged as organic fertilizers, plastics are recycled, and refuse-derived fuel is sent to cement plants (Farah et al., 2019).

The closure of the Naameh landfill year 2015 and the temporary closure of a waste-to-energy facility in Bekaa which received IBC's residual waste after treatment has led to the accumulation of waste at the Saida site. Thus, the quantities of waste received since 2015 have by far surpassed the treatment plant's capacity. Subsequently, IBC got rid of the residuals via shredding with gravel followed by dumping in a nearby sea site enclosed by a breakwater. As a result of the rising local pressure, IBC was obliged to restrict the waste received to Saida and Zahrani districts solely as of the year 2018.

7. Discussion

On an annual and seasonal scale, statistically insignificant increasing and decreasing trends in rainfall are found in the three rain gauging stations that were studied. The rainfall patterns in the three AERs WL3, IL1a, and DL1f have changed differently in each season and annually. These changes show that climate change has influenced the rainfall trends and hence some impacts are faced by the agriculture and aquaculture sector in the country due to these trend changes, even though those are statistically insignificant. In the examined rain gauges, no significant increase or decrease in rainfall was found.

Except for the landfills in Zahle and Naameh, which are located in the interior, all of Lebanon's major landfills are located on the coast: the Costa Brava dump, the Saida sanitary landfill, the Bourj Hammoud landfill, and the Tripoli landfill. The city's landfill is a significant and dangerous part at the same time. If a landfill does not adhere to sanitary landfill regulations, the pollution it causes harms the surrounding areas, particularly the residential areas, when designing an urban metropolis. When choosing a landfill site, it is crucial to maintain a safe and healthy environment because waste pollution threatens the ecosystem and consequently human health and well-being (Halwani et al., 2020).

According to a study done by Amkieh in the year 2021, the residential area of Bourj Hammoud is mostly affected by the landfill because of its proximity to the area and the high-risk weather during the summer. This area is also the most polluted, along with the landfill site in Tripoli City, as the results show that it has the same level of pollution. The climatic circumstances (such as warmth and humidity) are worse in the coastal zone in the summer than in the inward area, which increases the pollution by landfills that influence the nearby zones, and as a result, the pollution degree is higher in the coastal region than the inward area.

The landfilling disposal approach may have several negative effects due to unplanned landfill area development that may lack proper engineering controls or even result in insufficient oversaturation. This could cause leachate to form, which could then escape containment and seep into the groundwater. Therefore, for both engineered and uncontrolled landfill sites, the migration of landfill leachate into groundwater poses a major environmental danger (Baghanam et al., 2020). Even in hygienic engineered landfills with related geomembrane layers, the environmental impact of landfill leakage was repeatedly found. Therefore, it is crucial to evaluate any risk of groundwater pollution brought on by landfill operations (Sawaya et al., 2021; Kanj et al., 2022; Nehme et al., 2020; Nehme et al., 2019; Haydar et al., 2022).

Plans for managing solid waste are typically successfully implemented in industrialized nations, where each has a special strategy that works with its metropolitan infrastructure. Solid waste has long been a problem in Lebanon, but it has become much worse recently in various parts of the country, with differing effects on the environment and the health of the population. There are several factors contributing to this increase, one of which is the populace's consumption-based way of life and lack of awareness of personal responsibility.

The future of MSW management in Lebanon will not be brighter unless the implementation of an effective solid waste management framework is adopted. This will aid in preventing the oversaturation of landfills and the emergence of uncontrolled dumpsites.

The drafted law on integrated solid waste management (law 80) is the solution for the improvement of the system. This law was approved year 2018 and is still awaiting implementation The law is characterized by three basic principles which are: the establishment of the legal framework for solid waste management, sound management of solid wastes through waste minimization practices (sorting at source, recycling, energy recovery), and applying the polluter pays principle and prevention of open dumping. Thus, for the implementation of this law, it is of crucial importance to set and issue application decrees as well as strategies and plans that are missing to obtain an integrated

SWM system in Lebanon. Additionally, the rising economic crisis further aggravated the situation as it hindered the operations of ministries due to the scarce resources and lack of personnel to follow up on the law implementation.

8. Conclusions and Recommendations

Throughout the years there was no adoption of any comprehensive and sustainable solid waste management strategy by the government which aims at solving the continuously occurring waste management crisis. Thus, overreliance on landfills through their expansion is considered a temporary solution that will reach an end sooner or later given the restricted spaces in Lebanon. The Naameh landfill was expected to operate for ten years, but its lifetime was extended to an additional 8 years. History is repeating itself with both Costa Brava and Bourj Hammoud landfills which are being expanded to receive additional waste in the absence of alternative solutions. It can be said that the lack of human resources as well as suitable facilities, corruption, and inefficient technical skills have led to this extensive failure in municipal solid waste management. Hence, the lack of environmental legislation in itself is not the center of the problem but rather the absence of law enforcement and/or the availability of other alternatives. With the absence of sustainable waste management solutions, unsorted wastes will continue entering landfills leading to shortening their lifespan and their overexploitation. This will in turn lead to other waste crises whereby wastes will accumulate on the streets causing adverse environmental effects with associated pollution problems.

Thus, the country requires for the upcoming future, a sustainable development strategy with waste management (minimization, reuse, and recycling) among its main priorities. The key to a sustainable solid waste management system requires an elevated degree of public participation, effective legislation, ample funds, and modern waste management technologies. Improvement of the waste management scenario can be achieved by the implementation of source segregation, encouraging private sector participation via awareness campaigns, availing recycling and waste-to-energy systems, and developing a strong legislative and institutional framework.

References

Abed Al Ahad, M., Chalak, M., Fares, S., Mardigian, P., and Habib, R. R. (2020). Decentralization of solid waste management services in rural Lebanon: Barriers and opportunities. Waste Management and Research. 38(6): 639-648. https://doi.org/10.1177/0734242X20905115

Al Zaghrini, N., Srour, F. J., and Srour, I. (2019). Using GIS and optimization to manage construction and demolition waste: The case of abandoned quarries in Lebanon. Waste Management. 95: 139-149. https://doi.org/10.1016/j.wasman.2019.06.011

Amkieh, Yasmine. (2021). Landfill pollution assessment in residential urban spaces in Lebanon. Architecture and Planning Journal. 27(1): Article 2. https://digitalcommons.bau.edu.lb/apj/vol27/iss1/2

Azzi, E. (2017). Waste Management Systems in Lebanon - The benefits of a waste crisis for improvement of practices. (Degree project in the field of Technology - Civil Engineering and Urban Management and The Main Field of Study the Built Environment, Second Cycle, 30 Credits). KTH Royal Institute of Technology, Stockholm, Sweden. https://kth.diva-portal.org/smash/get/diva2:1139992/FULLTEXT01.pdf

Baghanam, A. H., Nourani, V., Aslani, H., and Taghipur, H. (2020). Spatiotemporal variation of water pollution near landfill site: Application of clustering methods to assess the admissibility of LWPI. Journal of Hydrology. 591: 125581. https://doi.org/10.1016/j.jhydrol.2020.125581

Borjac, J., El Joumaa, M., Kawach, R., Youssef, L., and Blake, D. A. (2019). Heavy metals and organic compounds contamination in leachates collected from Deir Kanoun Ras El Ain dump and its adjacent canal in South Lebanon. Heliyon. 5(8): e02212. https://doi.org/10.1016/j.heliyon.2019.e02212

Boswell, J. (2019). Lebanon: the state of waste. Heinrich Boel Stiftung, Beirut, Middle East. https://lb.boell.org/sites/default/files/2019-12/lebanon_the_state_of_waste_1.pdf

CDR/LACECO. (2011). Supervision of Greater Beirut Sanitary Landfills – LACECO, Annual Report.

CDR. (2002). Annual solid waste report. Council for Development and Reconstruction, Beirut.

CDR. (2006). Basic Services, Solid Waste. Annual report, pp. 111-116; Council for Development and Reconstruction, Beirut.

CDR. (2015). Collection and Disposal of Municipal Solid Waste in Lebanon, Lot 1. Beirut City and Northern and Southern Suburbs. Request for proposals. Part I, Instructions to bidders.

CDR. (2020). Unpublished report.

Chamieh, N., Abiad, M., Doumani, F., Abdelnour-Tohme, K. (2016). Economic Instruments to Create Incentives or Recycling in Lebanon. EU, GFA. Support to Reforms – Environmental Governance, Beirut, Lebanon EuropeAid/134306/D/SER/LB/3

Clemente Holder, R. (1995). In Washington Report on Middle East Affairs, June 1995, Page 89. Available at: http://www.wrmea.org/1995-june/waste-dumping-during-civil-war-ignites-debate-in-lebanon.html

DeQuero-Navarro, B., Barakat, K. A., Shultz, C. J., Araque-Padilla, R. A., and Montero-Simo, M. J. (2020). From Conflict to Cooperation: A Macromarketing View of Sustainable and Inclusive Development in Lebanon and the Middle East. https://doi.org/10.1007/s00267-020-01300-w

Ecodit. (2015). Strategic environmental assessment for the New Water Sector Strategy for Lebanon.

Eghomwanre, A., Obayagbona, N., and Ilontumhan, C. (2020). A Microbiological and Physicochemical Assessment of Top Soils from Makeshift Open Waste Dumpsites in the Premises of Some Schools in Benin City. Jordan Journal of Earth and Environmental Sciences.11(1): 71-76.

El-Fadel, M., Abi-Esber, L., and Salhab, S. (2012). Emission assessment at the Burj Hammoud inactive municipal landfill: Viability of landfill gas recovery under the clean development mechanism. Waste management. 32: 2106-2114. https://doi.org/10.1016/j.wasman.2011.12.027

El-Fadel, M., Bou-Zeid, E., Chahine, W., and Alayli, B. (2002). Temporal variation of leachate quality from pre-sorted and baled municipal solid waste with high organic and moisture content. Waste Management. 22: 269-282. https://doi.org/10.1016/S0956-053X(01)00040-X.

EU: Support to DG Environment for the development of the Mediterranean De-pollution Initiative "Horizon 2020": Review of Ongoing and Completed Activities. European Commission (2006).

Farah, J., Ghaddar, R., Nasr, E., Nasr, R., Wehbe, H., and Verdeil, E. (2019). Solid Waste Management in Lebanon: Lessons for Decentralisation. pp.40. https://halshs.archives-ouvertes.fr/halshs-02407660v2

Ghosn, M., Mahfouz, C., Chekri, R., Ouddane, B., Khalaf, G., Guérin, T., Amara, R., and Jitaru, P. (2020). Assessment of trace element contamination and bioaccumulation in algae (Ulva lactuca), bivalves (Spondylus spinosus), and shrimps (Marsupenaeus japonicus) from the Lebanese coast. Regional Studies in Marine Science; 39: 101478. https://doi.org/10.1016/j.

rsma.2020.101478

Ghousseina, Y., Mhaweja, M., Jaffal, A., Fadel, A., El Hourany, R., and Faour, G. (2018). Vulnerability assessment of the South-Lebanese coast: A GIS-based approach. Ocean and Coastal Management. 158: 56–63. https://doi.org/10.1016/j.ocecoaman.2018.03.028

Hägerdal N. (2019). Toxic waste dumping in conflict zones: Evidence from 1980s Lebanon, Mediterranean Politics. 26(2): 198-218. https://doi.org/10.1080/13629395.2019.1693124

Halwani, J., Merhaby, D., Fawal, N., Ouddane, B. (2014). Land-based sources of pollution to the Coastal (Lebanon). In: International symposium on water pollution and environmental impacts in Mediterranean Basin, Nov 24–27. Sousse, Tunisia.

Halwani, J., Amine, H., Hamze, M., and Baroudi, M. (2017). Les Risques environnementaux de la décharge sauvage de déchets de Tripoli (Liban) et son impact sur la santé humaine. 3ème colloque international francophone en environnement et santé, ULCO, 23–25 Octobre 2017. Dunkerque-France.

Halwani, J., Halwani, B., Amine, H., and Kabbara, M. B. (2020). Waste Management in Lebanon—Tripoli Case Study. In: Negm A., Shareef N. (Eds) Waste Management in MENA Regions. Springer Water. Springer, Cham. https://doi.org/10.1007/978-3-030-18350-9_11

Haydar, C. M., Tarawneh, K., Nehme, N., Amaireh, M., Yaacoub, A., and Diab, W. (2022). Heavy metals content in water and sediments in the Upper Litani River Basin, Lebanon. Journal of Geoscience and Environment Protection. 10: 139-158. https://doi.org/10.4236/gep.2022.107010

Hilal, N., Fadlallah, R., Jamal, D., and El-Jardali, F. (2015). K2P Evidence Summary: Approaching the Waste Crisis in Lebanon: Consequences and Insights into Solutions. Knowledge to Policy (K2P) Center. Beirut, Lebanon. AUB, Faculty of Health Sciences. https://www.aub.edu.lb/k2p/Documents/K2P%20Evidence%20Summary%20Waste%20Management_Final_%20Dec%2014%202015.pdf

Huerta Morales, A. (2020). Exploring Paradoxical Tensions in Circular Business Models—Cases from North Europe. Sustainability 12(18): 7577. https://doi.org/10.3390/su12187577

ILO and UND. (2011). Green Jobs Assessment in Lebanon. Synthesis Report, 13 pages, International Labour Organization (ILO) Geneva. https://www.ilo.org/global/topics/green-jobs/publications/WCMS_168091/lang--en/index.htm

Jaradat, A., and Al-Khashman, O. (2013). Evaluation of the Potential Use of Municipal Solid Waste for Recovery Options: A Case of Ma'an City, Jordan. Jordan Journal of Earth and Environmental Sciences. 5(1): 9-15.

Kanj, F., Sawaya, R., Halwani, J. and Nehme, N. (2022). Mercury prediction in groundwater of Naameh Landfill using an Artificial Neural Network (ANN) model. Green Technology, Resilience, and Sustainability. 2, 3. https://doi.org/10.1007/s44173-022-00003-1

Katsumi, T., Benson, C. H., Foose, G. J., and Kamon M. (2001). Performance-based design of landfill liners. Engineering geology. 60 (1-4): 139-148. https://doi.org/10.1016/S0013-7952(00)00096-X

Kaza, S., Yao, L., Bhada-Tata, P., and Van Woerden, F. (2018). What a Waste 2.0: A Global Snapshot of Solid Waste Management to 2050. World Bank.

Kazour, M., Jemaa, S., Issa, C., Khalaf, G., Amara, R. (2019). Microplastics pollution along the Lebanese coast (Eastern Mediterranean Basin): Occurrence in surface water, sediments, and biota samples. Science of the Total Environment 696: 133933 https://doi.org/10.1016/j.scitotenv.2019.133933

Khadra, W. M., and Stuyfzand, P. J. (2014). Separating baseline conditions from anthropogenic impacts: Example of the Damour coastal aquifer (Lebanon). Hydrological Sciences Journal. 59: 1872–1893. https://doi.org/10.1080/02626667.2013.841912

Khalil, C., Al Hageh, C., Korfali, S., Khnayzer R. S. (2018). Municipal leachates health risks: Chemical and cytotoxicity assessment from regulated and unregulated municipal dumpsites in Lebanon. Chemosphere. 208: 1-13. https://doi.org/10.1016/j.chemosphere.2018.05.151

Laceco. (2020). Private company and consultatnt, unpublished local report.

Mani, I. Solid Waste Management Challenges in GCC. (2020). Middle East, Recycling, Waste Management. Echoing Sustainability in MENA. Solid Waste Management Challenges in GCC | EcoMENA

Massoud, M.A., and Mokbel, M. (2022). Determinants of waste characterization in Lebanon and material recovery potential Journal of Material Cycles and Waste Management. 24: 1913-1922. https://doi.org/10.1007/s10163-022-01445-2

Merhaby, D., Ouddane, B., Net, S., and Halwani, J. (2018). Assessment of trace metals contamination in surficial sediments along Lebanese Coastal Zone. Marine Pollution Bulletin 133: 881–890. https://doi.org/10.1016/j.marpolbul.2018.06.031

MoE/EU/UNDP. (2015). Lebanon Environmental Assessment of the Syrian Conflict and Priority Interventions. Updated Fact Sheet-December 2015. EASC Report, Beirut, Lebanon https://www.undp.org/content/dam/lebanon/docs/Energy%20and%20Environment/Publications/FINAL-EASC-FactSheet2015-EN.pdf

MoE/GFA/EU. (2017). Support to Reforms-Environmental Governance (StREG) Programme. Layman Report, Beirut, Lebanon. http://www.databank.com.lb/docs/20171227-StREG_layman-Final.pdf

MoE/UNDP/ECODIT. (2011). State and trends of the Lebanese environment. Available at: https://www.lb.undp.org/content/lebanon/en/home/library/environment_energy/state--trends-of-the-lebanese-environment. html

MoE/UNDP/ELARD. (2017). Updated Master Plan for The Closure and Rehabilitation of Uncontrolled Dumpsites Throughout the Country of Lebanon. Volume A.

MoE/UNDP/GFA. (2017). Assessment of Solid Waste Management Practices in Lebanon in 2015. The report, Support to Reforms – Environmental Governance. Beirut, Lebanon. Project Identification No. EuropeAid/134306/D/SER/LB/3 Service Contract No: ENPI/2014/337-755. http://www.moe.gov.lb/getattachment/ddd7eb2d-ccc2-4e7d-af0a-ea39562544c2/Assessment-of-Solid-Waste-Management-Practices-in-Lebanon-2015-Final-Report.September-2017.aspx

MoE/UNDP. (2017). Nationally Appropriate Mitigation Action NAMA in Lebanon's Municipal Solid Waste Sector NAMA Proposal and Design Document.

MoE. (2018). Policy Summary on Integrated Solid Waste Management in Lebanon Report. http://www.moe.gov.lb/getattachment/cca17155-ac13-4cf3-83c1-6c5baee40df4/Policy-Summary-for-Jan-2018.aspx

Mouganie, P.; Ajeeb, R., and Hoekstra, M. (2020). The Effect of Open-Air Waste Burning on Infant Health: Evidence from Government Failure in Lebanon, IZA Discussion Papers, No. 13036, Institute of Labor Economics (IZA), Bonn.

Nehme, N., Moussa Haydar, C., Al-Jarf, Z., Abou Abbass, F., Moussa, N., Youness, G., and Tarawneh, K. (2021). Assessment of the physicochemical and microbiological water quality of Al-Zahrani River Basin, Lebanon. Jordan Journal of Earth and Environmental Sciences. 12 (3): 206-213.

Nehme, N., Haydar, C. M., Diab, W., and Tarawneh, K. (2019). Assessment of heavy metal pollution in the sediments of the Lower Litani River Basin, Lebanon. Jordan Journal of Earth and Environmental Sciences. 10(2): 104-112. https://doi.org/10.4236/gep.2022.107010

Nehme, N., Haydar, C.M., Dib, A., Ajouz, N. and Tarawneh, K. (2020). Quality assessment of groundwater in the Lower Litani Basin (LLRB), Lebanon. Geosciences Research. 5. https://dx.doi.org/10.22606/gr.2020.51001

Nuwayhid, R. Y., Ayoub, G. M., Saba, E. F., and Abi-Said, S.

(1996). The solid waste management scene in greater Beirut. Waste Management and Research. 14(2): 171–187. https://doi.org/10.1177%2F0734242X9601400207

Powrie, W., Beaven, R. P., and Richards, D. J. (2014). Landfill Aftercare: Meeting the Challenge. Engineers Australia. pp. 219–226.

Rezaeisabzevar, Y., Bazargan, A., and Zohourian, B. (2020). Landfill site selection using multi-criteria decision making: Influential factors for comparing locations. Journal of Environmental Sciences 93, 170–184. https://doi.org/10.1016/j.jes.2020.02.030

Sawaya, R., Halwani, J., Bashour, I., and Nehme, N. (2021). Assessment of the leachate quality from municipal solid waste landfill in Lebanon. Arabian Journal of Geosciences. 14: 2160. https://doi.org/10.1007/s12517-021-08502-4

Serdim Liban. (2021). Zahle Project. http://www.serdimliban.com/zahle.htm Accessed 4 March 2021

Shaban, A. (2008). Use of Satellite Images to Identify Marine Pollution along the Lebanese Coast. Environmental Forensics. 9(2): 205-214. http://dx.doi.org/10.1080/15275920802122296

Sweep-net. (2014). Country Report on the Solid Waste Management in Lebanon. Deutsche Gesellschaft für Internationale Zusammenarbeit (GIZ), Germany. https://www.retech-germany.net/fileadmin/retech/05_mediathek/laenderinformationen/Libanon_RA_ANG_WEB_Laenderprofile_sweep_net.pdf

Thabit, Q., Nassour, A., and Nelles, M. (2023). Facts and Figures on Aspects of Waste Management in the Middle East and North Africa Region. Waste. 1(1): 52-80. https://doi.org/10.3390/waste1010005

Touze-Foltz, N., Xie, H., and Stoltz, G. (2020). Performance issues of barrier systems for landfills: A review. Geotextiles and Geomembranes. https://doi.org/10.1016/j.geotexmem.2020.10.016

UFA. (2018). Tripoli Environment and Development Observatory. Union of Al-Fayhaa Municipalities, Annual report.

UNDP. (2013). The Rehabilitation of Saida Dumpsite. Project Document. MoE/CDR/UNDP, Lebanon. https://info.undp.org/docs/pdc/Documents/LBN/Prodoc%20Saida%20Rehab%20signed%20by%20All%2014%2005%2013.pdf

UNDP. (2017). Updated master plan for the closure and rehabilitation of uncontrolled dumpsites, Prepared by ELARD, MoE-UNDP. https://www.lb.undp.org/content/lebanon/en/home/library/environment_energy/MASTER-PLAN-FOR-THE-CLOSURE-AND-REHABILITATION.html

USEPA. (2021). Landfills. U.S. Environmental Protection Agency https://www.epa.gov/landfills. Accessed 24 June 2021

World Bank. (1995). Staff Appraisal Report – Lebanese Republic, Solid Waste / Environmental Management Project. Report No. 13860-LE. https://documents1.worldbank.org/curated/en/484871468772183406/pdf/multi0page.pdf

World Bank. (2007). Project Performance Assessment Report (PPAR) on the Emergency Reconstruction and Rehabilitation Project and the Solid Waste and Environmental Management Project in Lebanon. Report No.: 38473. https://ieg.worldbankgroup.org/sites/default/files/Data/reports/ppar_38473.pdf

World Bank. (2011). Republic of Lebanon, Country Environmental Analysis, Report No. 62266-LB, Sustainable Development Department (MNSSD), Middle East and North Africa Region.

Zyoud, S.H., Al-Jabi, S.W., Sweileh, W.M. et al. (2015). The Arab world's contribution to solid waste literature: a bibliometric analysis. Journal of Occupational Medicine and Toxicology. 10: 35 https://doi.org/10.1186/s12995-015-0078-1

JJEES

JJEES (2023) 14 (4): 254-257
ISSN 1995-6681

Jordan Journal of Earth and Environmental Sciences

Estimating National Emissions of Greenhouse Gases from Food Systems in Jordan

Rama Mazahreh* and Mahmoud Abu-Allaban

Department of Water Management and Environment, Faculty of Natural Resources and Environment, The Hashemite University, Al-Zarqa, Jordan

Received January 19, 2023; Accepted May 27, 2023

Abstract

Global warming has become a main challenge that threatens life on Earth. It is mainly blamed on the unprecedented levels of atmospheric greenhouse gases emanating from natural and anthropogenic sources including food systems that encompass different processes including agricultural practices, food packaging, refrigeration, transportation, and disposal of food waste. Therefore, signatory nations to the Paris Agreement are called upon to assess the contributions of their food systems to national budgets of greenhouse gases and to take necessary actions to reduce these emissions.

In this paper, we present the findings of an attempt to quantify the national emissions of greenhouse gases emanating from food systems in Jordan based on validly published emission rates and locally relevant agricultural data reported by the Jordanian Department of Statistics including cultivated areas, harvested goods, and imported food items. Our calculations revealed that more than 12.5 million tons of carbon dioxide equivalent in 2019 were generated by food systems in Jordan constituting about 47% of the total national emissions in that year. The transportation sector is found to be a main emitter of carbon dioxide???, making imported meat and rice the main generators of carbon dioxide in the food systems in Jordan. Landfilling of food remains or losses generate massive quantities of greenhouse gases with no social gain.

Keywords: *Food systems, Carbon footprint, Global warming, Pollution, Climate change*

1. Introduction

Global warming has become a catalyst that affects all aspects of life on Earth, whether they are political, social, economic, or environmental. In response to growing concerns over the increasing abundances of atmospheric greenhouse gases, tremendous efforts have been spent worldwide to come up with initiatives and regulations that call upon cutting emissions of greenhouse gases (GHGs) including carbon dioxide, methane, nitrous oxide, ozone, chlorofluorocarbons, and sulfur hexafluoride to combat global warming.

As a phenomenon, global warming has elicited heated debate among the scientific community, but there is a consensus maintains that the greenhouse effect and its influence over climate change is a real and tangible occurrence (Abu Sada et al., 2015; Salahat and Al-Qinna, 2015; Al-Qinna, 2018), and that humans are contributing to the rise of global temperature by adding greenhouse gases to air. Potential implications of global warming particularly include sea level rise because of thermal expansion of water and melting of the ice cap, storm surges, windstorms, flooding, heat waves, drought, food insecurity, food, and water-borne diseases, vector-borne diseases, intensive power consumption for heating, cooling, water energy, and water stress (Pender, 2008; Hunt, 2010).

Curbing global warming isn't an easy task or a simply achieved goal, but it starts by taking steadfast commitments to reduce emissions of GHGs by creating alternative sources of energy to replace these fossil fuels, removing carbon dioxide from emissions at the source, eliminating the use of chlorofluorocarbons, afforestation, developing agricultural techniques that release less carbon dioxide to the atmosphere, setting rigorous emissions regulations, and changing our dietary regimes as food systems are major sources of certain emissions, particularly methane from livestock and carbon dioxide from machinery and refrigeration.

Food systems include the full spectrum of actors and their interconnected value-adding activities that are involved in the production, aggregation, processing, distribution, consumption, and disposal of food products that come from the agricultural, livestock, forestry, fisheries, and food industries, as well as the larger economic, societal, and natural environments in which they are embedded (Westhoek et al., 2016). Emissions generated by the food systems make up a sizable fraction of all greenhouse gas emissions made by humans and as a result, they play a role in global warming (Vermeulen et al., 2012). Finding ways to lessen the food system's contribution to GHG emissions is consequently a major challenge for its sustainability. Understanding the sources and processes of greenhouse gas emissions across the entire food system is crucial to address and reduce the contributions of the food system to global warming. It's also crucial to comprehend how different approaches to structuring various aspects of the food system can lead to varying amounts of emanated GHGs.

Fertilizers, pesticides, manure, agriculture, and changes in land use combined account for around 24% of global GHG emissions. Other contributions come from later stages

* Corresponding author e-mail: ramabmazahreh@gmail.com

in the food system including packaging, retail, transport, processing, food preparation, open burning, refrigeration, storage, catering consumption, and waste disposal (Garnett et al., 2016, Li et al., 2022).

Due to its enormous greenhouse gas (GHG) footprint, food loss and waste worsen the climate change challenge. Food waste produces methane, a strong greenhouse gas when dumped in domestic landfills. The relationship between food loss and waste and climate change reveals a crucial connection between agriculture, supply chain resilience, and climate change. In contrast, supply chain resilience and agriculture are both negatively impacted by extreme weather events.

2. Study Aim

The previous introductory section has demonstrated that food systems are potent sources of greenhouse gases; therefore, it is vital to assess national emissions of GHGs to come up with practical initiatives to cut them. Therefore, the main objective of this paper is to quantify the contribution of food systems to the national emission inventory of GHGs in Jordan based on the 2019 agricultural statistics and published carbon footprints.

3. Methodology

The mass of Greenhouse gases (MGHGE) emanating from producing vegetables and fruit is estimated by multiplying the annual produced mass (APM) of an item by its carbon footprint (CFP). i.e.:

$$\mathbf{MGHGE = APM \times CFP} \quad \text{.....(1)}$$

Statistics of cultivated land and main crops are procured from the Department of Statistics (Department of Statistics, 2019). The main crops cultivated in Jordan in 2019 were mainly Fruit Trees, Vegetables, and Field Crops. A large portion of the cultivated areas depend on irrigation, which relies intensively on groundwater resources. Areas planted by field crops formed about 49% of the total cultivated area in 2019 followed by fruit trees and vegetables which make up about 36% and 15% of the total cultivated areas in Jordan, respectively.

4. Results and Discussion

4.1 National GHGs Associated with Vegetables and Fruits

Agriculture is an important contributor of carbon dioxide, methane, and nitrous oxide with meat and fisheries being the top producer of greenhouse gases. The total greenhouse gas (GHG) emissions caused directly and indirectly by a kilogram of a food item is termed the "carbon footprint" of that food (Werner et al., 2014). The highest carbon footprints are produced by meat, cheese, and eggs. Fruits, vegetables, beans, and nuts have significantly smaller carbon footprints (Clune et al., 2017). To calculate the national emissions of GHGs associated with the production of vegetables and fruit in Jordan in 2019 due to cultivation, transportation, and food loss we have employed formula (1). The attained quantities are summarized in Table 1.

Jordanians consume various types of vegetables and fruits, but they rely mainly on citrus fruit, dates, olives, wheat (bread), lentils, chick-peas, potatoes, tomatoes, squash, eggplants, cucumbers, cabbages, cauliflower, sweet (bell) peppers, and onion. Other items such as parsley, lettuce, and strawberry, are less common in Jordanians' diet, therefore they don't contribute significantly to the national inventory of greenhouse gases.

Table 1. Greenhouse gas associated with vegetables and fruit production in Jordan in 2019 due to cultivation, transportation, and food loss and waste.

Crop	Annual Production (Ton)	CO2 Footprint (kg/kg) (Werner et al., 2014)			GHG Generated/ CO2 Equivalent (Kiloton)		
		Cultivation	Transportation	Waste	Cultivation	Transportation	Waste
Citrus Fruit	123942	0.70	1.05	0.18	86.8	130.1	21.7
Dates	23375	0.44	0.66	0.11	10.3	15.4	2.6
Olives	214994	0.28	0.42	0.07	60.2	90.3	15.0
Wheat	26361	0.25	0.38	0.06	6.6	9.9	1.6
Maize (Green)	20936	0.28	0.42	0.07	5.9	8.8	1.5
Sorghum	279	0.28	0.42	0.07	0.1	0.1	0.0
Barley	66618	0.30	0.45	0.08	20.0	30.0	5.0
Lentils	153	0.90	1.35	0.23	0.1	0.2	0.0
Chick-peas	4232	0.64	0.96	0.16	2.7	4.1	0.7
Clover trefoil	111610	0.15	0.23	0.04	16.7	25.1	4.2
Potatoes	173653	0.34	0.51	0.09	59.0	88.6	14.8
Tomatoes	601370	0.33	0.50	0.08	198.5	297.7	49.6
Squash	53043	0.36	0.54	0.09	19.1	28.6	4.8
Eggplants	55630	0.51	0.77	0.13	28.4	42.6	7.1
Cucumbers	186317	0.51	0.77	0.13	95.0	142.5	23.8
Cabbages	35074	0.29	0.44	0.07	10.2	15.3	2.5
Cauliflower	46799	0.31	0.47	0.08	14.5	21.8	3.6
Sweet peppers	55771	0.29	0.44	0.07	16.2	24.3	4.0
Onion, dry	54500	0.60	0.90	0.15	32.7	49.1	8.2
Total					683	1024	171

4.2 Emissions of GHGs Associated with Rice Import and Consumption

Rice is not cultivated locally, it is rather imported from remote sources including Egypt, the USA, Pakistan, India, and other South Asian states, which implies that a large portion of its carbon footprint is attributed to transportation. Rice has gradually become a main constituent of Jordanians' daily meals and it's an important ingredient of the national dish (Mansaf) that is cooked and served in social gatherings and celebrations including wedding and funeral banquets. The carbon footprint of rice is reported by Werner et al. (2014) to be 3.74 kg per kilogram of rice. When multiplying this value by the Jordanians' rice consumption in 2017 (194 kt), the answer is 726 kilotons of CO2 equivalent, which is about 39% of the total emissions from vegetables and fruits that appear in Table 1. This finding places an important and ethical responsibility on governmental authorities, community leaders, religious preachers, and social activists to work toward changing the habits of offering vast rice quantities in wedding and funeral banquets that end up being dumped in domestic landfills for more production of methane and other greenhouse gases.

4.3 Emissions of GHGs Associated with Animal-Derived Food

Jordan enjoys mild weather throughout the year with a small annual and diurnal temperature means, which offers excellent conditions for growing chicken and other poultry species. This encouraged the investment in growing chicken for their meat and eggs, which then became the main source of protein for most Jordanians. however, beef and lamb meat markets depend mainly on imported rather than growing local livestock because of the low precipitation that is required to support and maintain natural grazing thereby forcing livestock owners to rely on expensive fodder to feed their animals, which puts extra cost on local meat production. Seafood is relatively new to Jordanians' diet due to a lack of local sources. Historically, total fish consumption in Jordan reached an all-time high of 47.8 kt in 2013 and an all-time low of 1.07 kt in 1961 (FAOSTAT, 2022).

Jordanians' consumption of meat, milk, eggs, and vegetable oil reported by FAOSTAT are available up to the year 2013. Therefore, we assumed that the 2013 per capita of these products remained the same until the year 2019 (the same year for vegetables and fruits reported by the Department of Statistics). This assumption is 90% valid as can be seen from the time series plots for these food items illustrated on the FAOSTAT webpage. This implies that the calculated carbon dioxide equivalent of GHGs generated from animal products and vegetable oil presented in this paper (Table 2) is about 80%-90% accurate.

Table 2. Carbon Dioxide Equivalent of Greenhouse Gases Emanated from Meat products and vegetable oil.

Meat	2013 Total Meat Consumption (kt) (FAOSTAT, 2022)	2013 Per Capita Meat Consumption (kg)	Estimated 2019 Total Meat Consumption (kt)	CO2 Footprint (kg) (Werner et al., 2014)	2019 CO2 Equivalent (kt)
Poultry	239	28.1	284.0	6.9	1959.5
Beef	52.9	6.2	62.9	68.8	4324.6
Lamb And Goat	39.1	4.6	46.5	39.2	1821.2
Fish	47.8	5.6	56.8	5.4	306.7
Eggs	49.1	5.8	58.3	4.9	285.9
Milk	280.4	33.0	333.2	1.9	633.0
Veg. Oil	151	17.8	179.4	3.2	574.2
Total					9905.1

4.4 Reducing Greenhouse Gases Emanated from Food Systems

Table 3 summarizes the findings of the previous sections. As can be readily learned from the table, it is evident that the food systems in Jordan generated more than more than 12.5 million tons. The 12.5 million ton makes up about 47% of the total Jordanian greenhouse gases emanated nationwide which is 26.5 million kt of carbon dioxide equivalent (World Data Atlas, 2022). There was a lot of carbon dioxide equivalent released by the food systems, but it's important to remember that people need food to survive.

Table 3. Summary of CO2 equivalent associated with producing, importing, consuming, and wasting food in Jordan in 2019.

Food	2019 CO2 Equivalent (kt)
Meat	8105
Fish	307
Eggs	286
Milk	633
Veg. Oil	574
Vegetables and Fruits	1878
Rice	726
Total	12509

The quantity of greenhouse gas emissions brought on by the production of food that is never consumed is harder to comprehend. Some food that Jordanians produce, or import is wasted by shops, eateries, and customers, or it spoils or spills throughout the supply chain. Therefore, local authorities and stockholders are invited to work toward minimizing food losses and waste to prevent producing unnecessary greenhouse gases. The Paris Agreement mandates signatory nations to update or resubmit their Nationally Determined Contributions plans (NDCs) every five years. Therefore, Jordanian authorities and legislators should seize this opportunity to adopt more ambitious initiatives and measures to reduce greenhouse gas emissions from food systems by reducing food losses and waste, improving food transport and distribution methods, and controlling methane emissions from livestock whether imported or raised locally.

Fruit and vegetable waste (FVW) are produced in enormous amounts in markets and are an annoyance in municipal landfills. When dumped in domestic landfills, anaerobic microbes decompose food and other organic waste into biogas, composed mainly of methane and carbon dioxide. A field survey on Ma'an found that a large constituent of

domestic solid waste in this southern Jordanian governorate is food remains and organics (Jaradant and Al-Khashman, 2013), making it a major source of methane, the potent greenhouse gas (Tavakoli, 2017). The municipality of Irbid thought of turning the FVW into compost to prevent methane production and provide local farmers with chemical-free fertilizers and soil conditioners. Adopting similar initiatives and practices by other municipalities throughout Jordan is vital to reducing national emissions of greenhouse gases from wasted fruit and vegetables.

5. Summary and Conclusions

Food systems involve major sources of carbon dioxide, nitrous oxide, and methane including agricultural practices, food packaging, and refrigeration, hauling of food products from sources to end users, and disposing of food losses and waste. This implies that any plan that aims to cut emissions of greenhouse gases shall control emissions from food systems locally, regionally, and globally. This necessitates national quantification of greenhouse gasses emanating from food systems to plan carbon cuts accordingly.

This paper presents the main estimates of the food system's contribution to the national budget of greenhouse gases. Main vegetables and fruit produced in Jordan include Citrus Fruit, Dates, Olives, Wheat (Bread), Lentils, Chick-Peas, Potatoes, Tomatoes, Squash, Eggplants, Cucumbers, Cabbages, Cauliflower, Sweet (Bell) Peppers, and Onion. Transportation and distribution of food products, including air and sea shipping of meat products are the main emitters of greenhouse gases, therefore national initiatives to reduce the contribution of food systems to national emission inventory of greenhouse gases have to adopt restrictive regulations and innovative practices to reduce food imports. Reducing the total distances traveled by trucks that transport vegetables and fruit from producers to consumers could significantly cut GHGs emissions from food transport. Food losses and waste are among the unnecessary components that contribute a large portion of the national greenhouse gases. Rice is particularly important in this aspect because rice paddies are the main sources of methane production. In addition, all rice consumed or wasted in Jordan is imported from remote sources, thus generating tons of transport-emitted carbon dioxide. Therefore, Jordanian authorities and community activists are invited to advocate food conservation and minimize food waste in large gatherings such as wedding feasts and other celebrations. Healthier vegetarian diets are among the good food habits that would help Jordanians reduce the food system's contribution to the national emission inventory of greenhouse gases.

The paper offers several actions that can be nationally adopted to cut off greenhouse gases emanating from food systems. The actions include reducing land-use change and conversion of natural habitats, reducing food loss and waste, improving food transport and distribution means, reducing methane emissions from livestock, and shifting to healthier and more sustainable diets with a higher proportion of plant-based than animal-based foods.

Acknowledgment

This paper is part of a thesis prepared by the first author and submitted to the graduate school at Hashemite University as a partial fulfillment of a master's degree in environmental sciences and management.

References

Abu Sada, A.; Abu-Allaban, M.; Al-Malabeh, A., 2015. Temporal and Spatial Analysis of Climate Change at Northern Jordanian Badia. Jordan Journal of Earth and Environmental Sciences, 7(2): 87-93.

Al-Qinna, M. I., 2018. Analyses of Climate Variability in Jordan using Topographic Auxiliary Variables by the Cokriging Technique. Jordan Journal of Earth and Environmental Sciences, 9(1): 67-74.

Clune, S., E. Crossin, and K. Verghese., 2017. A systematic review of greenhouse gas emissions for different fresh food categories. Journal of Cleaner Production, 140:766-783.

Department of Statistics, 2019. Agricultural Statistics Bulletin. Amman, Jordan. http://dosweb.dos.gov.jo/DataBank/Agri/Agr_2019.pdf

FAOSTAT. Webpage of Food and Agriculture Organization of the United Nations Statistics Division.Viale delle Terme di Caracalla. Accessed on (10/8/2022). https://www.fao.org/statistics/en/

Garnett, T., Smith, P., Nicholson, W., and Finch, J., 2016. Food systems and greenhouse gas emissions (Foodsource: chapters). Food Climate Research Network, University of Oxford.

Hunt, A., Watkiss, P., 2010. Climate change impacts and adaptation in cities: a review of the literature. Climatic Change, 104(1), 13–49.

Jaradat, A. and Al-khashman, O., 2013. Evaluation of the Potential Use of Municipal Solid Waste for Recovery Options: A Case of Ma'an City, Jordan. Jordan Journal of Earth and Environmental Sciences, 5(1): 9-15.

Li, M., Jia, N., Lenzen, M., et al., 2022. Global food miles account for nearly 20% of total food-systems emissions. Nat Food 3: 445–453.

Salahat, M., and Al-Qinna, M., 2015. Rainfall Fluctuation for Exploring Desertification and Climate Change: New Aridity Classification. Jordan Journal of Earth and Environmental Sciences, 7(1): 27-35.

Tavakoli, A., 2017. How Precisely «Kaya Identity» Can Estimate GHG Emissions: A Global Review, 8(2): 91 – 96.

Pender, J. S., 2008. What Is Climate Change? And How It Will Affect Bangladesh. Briefing Paper. (Final Draft). Dhaka, Bangladesh: Church of Bangladesh Social Development Programme. ACADEMIA.

Vermeulen, S. J., Campbell, B. M., Ingram, J. S. I., 2012. Climate Change and Food Systems. Annual Review of Environment and Resources, 37(1), 195–222.

Werner, L., F., Flysjö, A., Tholstrup, T., 2014. Greenhouse gas emissions of realistic dietary choices in Denmark: The carbon footprint and nutritional value of dairy products. Food and nutrition research, 58: 20687.

Westhoek, H., Ingram J., Van Berkum, S., Özay, L., and Hajer M., 2016. Food Systems and Natural Resources. A Report of the Working Group on Food Systems of the International Resource Panel, UNEP.

World Data Atlas webpage. Accessed on (9/8/2022). https://knoema.com/atlas/Jordan .

JJEES

JJEES (2023) 14 (4): 258-267
ISSN 1995-6681

Jordan Journal of Earth and Environmental Sciences

Geochemical Discriminant for Provenance, Source Area Weathering and Paleoredox of Some Shale Deposits in Edo State, Nigeria

Martins Ilevbare* and Adeleye Rita A.

Geology Department, Afe Babalola University, Ado-Ekiti, Edo State, Nigeria

Received February 19, 2023; Accepted June 13, 2023

Abstract

The shale samples from Uzebba, Ayoguiri, and Ugbenor within Edo State, Anambra basin, southern Nigeria, were geochemically analyzed for major oxides, trace elements, and mineral content. The trace element ratios from the paleoredox inferences revealed that the shale samples were deposited in an oxic environment (Ni/Co, V/Cr, and V/V+Ni) except for V/Ni which was deposited in a dysoxic - oxic environment. The ancient climate condition of the shale was a semi-arid climate with increasing chemical maturity and the bivariate relations (SiO_2 vs. Al_2O_3) authenticating that the shale was terrestrially sourced. The Al_2O_3/TiO_2 (13.48) indicates that the provenance of the shale is from a felsic source. The bivariate relationship of (SiO_2 vs. Al_2O_3+Na_2O+K_2O) suggests a semi-arid paleoclimate with increasing chemical maturity in a phanerozoic shale environment. The data obtained from the study, showed that the average values of the following weathering indices: the Plagioclase Index of Alteration (PIA) with a value of 91.00% (73.58-98.43), the Chemical Index of Alteration (CIA) of value 74.33% (65.18-78.25), the Chemical Index of Weathering (CIW) with a value of 93.12% (73.58-98.43) and the Mineralogical Index of Alteration (MIA) valued at 48.67% (30.36-56.50) which indicates a substantial, moderate to intense chemical weathering with a PIA average indicating a phenerozoic ancient environment. The mineralogy of the shale from the diffractogram profiles were quartz, fluorapatite, calcite and montmorillonite. The predominance of quartz again confirms the resistance of quartz to weathering conditions while the other minerals that are in trace amounts are only indications that they are less resistant to weathering and have dissolved in the solution.

Keywords: *Provenance, Paleoredox, Phenerozoic, Felsic source, Mamu shale*

1. Introduction

Insight into the provenance and paleo-conditions of a sedimentary basin fill is crucial for hydrocarbon exploration/exploitation as well as other paleo conditions. Although the usefulness of the geochemistry of sedimentary rocks in the determination of provenance, maturity, and paleo-conditions has been a global subject, its application is grossly a complex function of the nature of source rock(s), weathering intensity/duration, sedimentary recycling. The geochemical attributes of elements (major and trace elements) in clastic sedimentary rocks are invaluable for construing provenance (Peters and Moldowan, 1993??). Also, the geochemical composition of elements furnishes invaluable information that is germane for paleo-climate (Ilevbare and Omodor, 2020, Cao *et al.,* 2012; Tao *et al.,* 2017) and paleo-redox (Matthew *et al.,* 2019; Mengjiao *et al.,* 2020; El-Hasan and Al-Malabeh, 2008) reconstructions.

Over the last two decades, several studies focusing on sedimentology (Tijani *et al.,* 2010; Onyekuru and Iwuagwu, 2010; Dim *et al.,* 2019) and stratigraphy (Uzoegbu *et al.,* 2013), mineralogy (Akinyemi *et al.,* 2013), palynology (Egboka and Emejulu, 2015), reservoir characterization (Anakwuba and Onyekwelu, 2010; Okwara *et al.,* 2020), petroleum potential (Adebayo *et al.,* 2018; Ogungbesan and Adedosu, 2020), aeromagnetics, (Bello *et al.,* 2017), and gravity modeling (Obasi *et al.,* 2018; Omietimi *et al.,* 2021) have been carried out on the basin.

As a result, this study presents the inorganic geochemistry investigation for Maastrichtian shale sourced from the southern Anambra Basin, Nigeria. To decipher the provenance, maturity, source area weathering, mineral composition, and paleo-redox conditions, which will help provide more information for further exploitation of the basin.

2. Study Area

Fifteen outcrop shale samples were collected from three different communities; Uzebba, Ayoguiri, and Ugbenor, and the field photographs of the outcrop are presented in Figure 1 below. In Uzebba, samples were collected from eleven (11) locations (Figure 2b) and at Ayoguiri and Ugbenor Fugar (Figure 2a), all from Edo-North, Nigeria.

* Corresponding author e-mail: martins.ilevbare@abuad.edu.ng

Figure 1. Exposed Outcrops of Shale in the study area, Edo State, Nigeria.

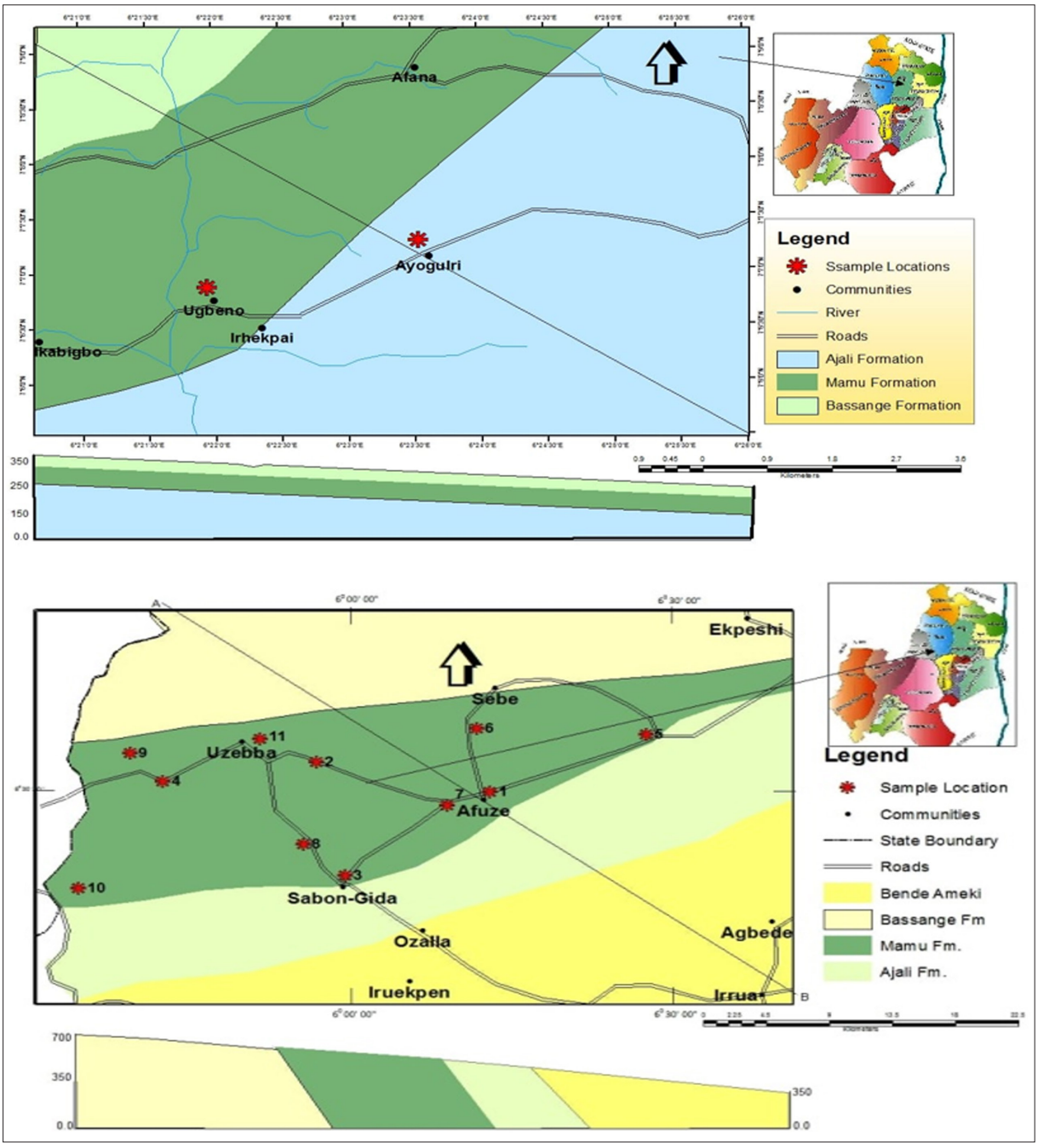

Figure 2. Location map of (a) Ugbenor and Ayoguiri shale (Upper) and (b) Geologic section of Uzebba shale (down).

2. Geologic Settings of the Basin

The Anambra Basin (Figure 3and4) is tiered up with the southern ensemble of the Benue Trough and its genesis is closely related to the evolution of the Benue Trough, which is connected with the separation of Africa from the South American plate in the Mesozoic, which is the opening of the Atlantic Ocean (Burke *et al.,* 1971). There have been several investigations by researchers on the geochemistry of the sedimentary successions of the Anambra Basin (Ilevbare and Imasuen 2020; Ilevbare and Omodolor, 2020; Overare *et al*., 2020; Ilevbare and Omorogieva, 2020).

Although the Formation mechanism is debatable, the majority of studies favor tensional movements that result in rifts, graben-like structures, or a dominant tectonic process of wrenching (Cratchley and Jones, 1965; Stoneley, 1966). (Benkhelil, 1989; Maurin *et al.,* 1986). Evidence supporting the rift model has been gathered through structural, geomorphic, stratigraphic, and paleontological results (Burke *et al.,* 1972; Benkhelil, 1989; Guiraud and Bellion, 1995). Following the emergence of a hotspot, it is now understood to be a folded aulacogen or a failed arm of a triple rift system (Burke and Dewey, 1974; Olade, 1975).

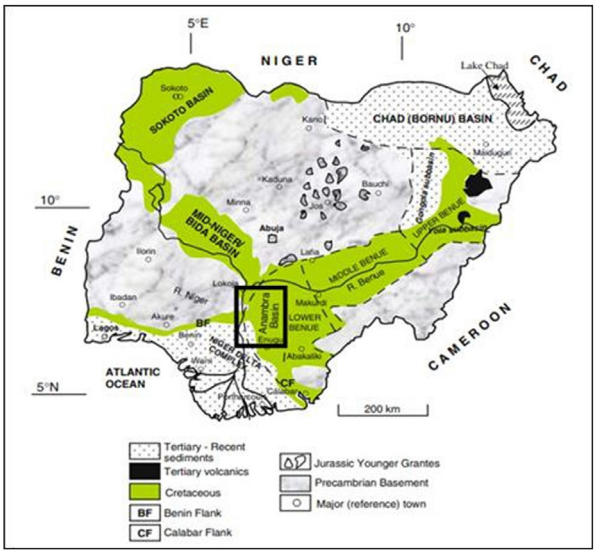

Figure 3. Generalized geological map of Nigeria showing the Anambra Basin in the thick rectangular box (modified after Obaje et. al., 2004).

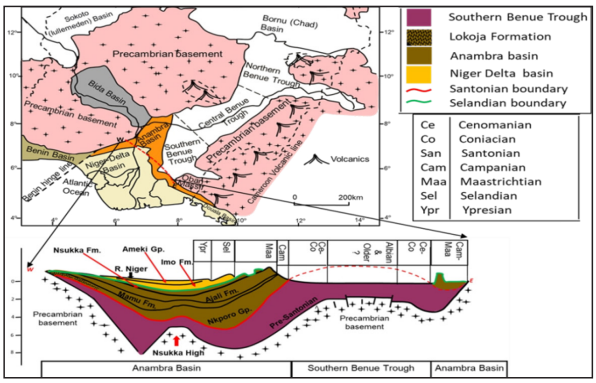

Figure 4. Map of Nigeria showing areas underlain by basement and sedimentary rocks. Below is a W-E cross-section of the Anambra Basin and Southern Benue Trough (after Edegbai et al., 2019a and b).

3. Materials and Methodology

The methods of investigation involved both field study and laboratory analyses. Laboratory investigations of samples for geochemical characteristics were the 15 shale samples were immediately stored in a Ziploc polyethylene bag and preserved at room temperature. Samples were oven-dried and later disaggregated using Porcelain mortar and pestle.

3.1 XRF and LA-ICPMS Analyses

The pulverized shale samples were analyzed with the XRF technique. X-ray fluorescence spectrometry and instrumental neutron activation analysis would be used for sample preparation, as well as major and trace element analysis.

The analytical procedures for XRF are as follows:

Pulverized shale samples were analyzed for the major element using an Axios instrument with a 2.4 kWatt Rh X-ray Tube. Further, the same set of samples was also analyzed for trace elements using LA-ICPMS instrumental analysis; LA-ICP-MS is a powerful and sensitive analytical technique for multi-elemental analysis. The laser was used to vaporize the surface of the solid sample, while the vapor and any particles, were transported by the carrier gas flow to the ICP-MS (Okiotor and Ighodaro, 2020). The detailed procedures for sample preparation for both analytical techniques are reported below.

- Add 10.0000 g ± 0.0009g Claisse flux and fuse in M4 Claissefluxer for 23 minutes.
- 0.2 g of $NaCO_3$ was added to the mix and the sample+flux+$NaCO_3$ was pre-oxidized at 700°C before fusion.
- Flux type: Ultrapure Fused Anhydrous Li-Tetraborate-Li- Metaborate flux (66.67 % $Li_2B_4O_7$ + 32.83 % $LiBO_2$) and a releasing agent Li-Iodide (0.5 % LiI).

3.2 Pressed Pellet Method for Trace Element Analysis

- Weigh 8g ± 0.05 g of milled powder
- Mix thoroughly with 3 drops of wax binder
- Press the pellet with a pill press to 15-tonne pressure in the oven at 100°C for half an hour before analyzing.

Eleven (11) major oxides were analyzed (SiO_2, TiO_2, Al_2O_3, Fe_2O_3, MgO, MnO, CaO, Na_2O, K_2O, $Cr_2O_3$and P_2O_5) as well as seven (7) trace elements ((Ba, Cu, Zn, Cr, Ni, Co, and V) using Phillips PW-1800 X-ray fluorescence (XRF) analyzer

3.3 X-ray diffraction analysis and procedures

The X-ray diffraction studies for mineral identification were conducted as described by Bundy (1993) and Murray and Keller (1993). X-ray diffraction analysis (XRD) was used to determine the mineralogical composition of these samples. Representative samples from shale outcrops were analyzed to assess their whole-rock geochemical compositions.

The analytical procedures for XRD are as follows:

Powdered samples were pelletized and sieved to 0.074mm and later taken to an aluminum alloy grid (35mm x 50mm) on a flat glass plate and covered with paper. Wearing hand gloves, the samples were compacted by gently pressing them with the hand.

Each sample was run through the Rigaku D/Max-lllC X-ray diffractometer developed by the Rigaku International Corporation Tokyo, Japan, and set to produce diffractions at a scanning rate of 2^0/min in the 2 to 50^0 at room temperature with a CuKa radiation set at 40kV and 20mA. The diffraction data (d-value and relative intensity) obtained were compared to that of the standard data of minerals from the mineral powder diffraction file ICDD, which contains and includes the standard data of more than 3000 minerals (Haque *and Roy,* 2019).

4. Results and Discussion

The results obtained from the geochemical analyses are presented in Table 1a and b.

For the area under study, the major oxide data (Table 1) show that (SiO_2; 58.10% for AY7 to 52.10% for UZ4 and UG4) and (Al_2O_3; 16.92% for UZ11 to 13.90% for UG4) predominate, followed by other oxides: Fe_2O_3, K_2O, MgO, CaO, TiO_2, Na_2O, P_2O_5, and MnO. There are traces of the residual oxides.

Table 1a. Major elements and chemical weathering indices of shale deposits sourced from Uzebba, Ugbenor, and Ayoguiri communities, Anambra basin, Nigeria.

Sample	SiO_2	Al_2O_3	Fe_2O_3	TiO_2	CaO	P_2O_5	K_2O	MnO	MgO	Na_2O
UZ 1	52.40	14.50	7.50	0.77	0.85	0.09	3.86	0.04	1.40	0.30
UZ 2	57.15	16.88	5.82	0.74	0.79	0.07	4.65	0.02	1.55	0.32
UZ 4	52.10	13.98	6.00	0.74	3.55	0.08	3.85	0.02	1.45	0.30
UZ 6	56.50	15.22	5.70	0.75	0.11	0.06	4.04	0.02	1.15	0.33
UZ 7	58.00	15.10	5.50	0.75	0.13	0.05	4.05	0.01	1.12	0.30
UZ 9	55.30	16.50	6.57	0.76	0.64	0.07	4.50	0.01	1.49	0.31
UZ 11	57.13	16.92	5.80	0.75	0.80	0.07	4.65	0.04	1.55	0.30
UG 4	52.10	13.90	6.05	0.79	3.55	0.07	3.80	0.03	1.45	0.31
UG 4B	56.50	15.27	5.65	0.77	0.11	0.06	4.04	0.01	1.16	0.31
UG 5	52.38	14.52	7.53	0.74	0.85	0.09	3.88	0.02	1.38	0.32
UG 7	57.16	16.87	5.80	0.76	0.79	0.07	4.65	0.02	1.55	0.32
AY 2	52.13	13.97	6.00	0.74	3.55	0.07	3.82	0.03	1.45	0.31
AY 4	56.50	15.27	5.65	0.77	0.11	0.06	4.04	0.01	1.16	0.31
AY 7	58.01	15.10	5.49	0.77	0.11	0.07	4.02	0.01	1.12	0.30
AY 8	55.31	16.49	6.59	0.76	0.63	0.07	4.51	0.01	1.49	0.31

Table 1b. Major elements and chemical weathering indices of shale deposits sourced from Uzebba, Ugbenor, and Ayoguiri communities, Anambra basin, Nigeria.

Sample	SiO_2/Al_2O_3	Fe_2O_3/K_2O	Al_2O_3 / TiO_2	K_2O/ Al_2O_3	CaO*	CIA	CIW	PIA	MIA
UZ 1	3.61	1.94	18.83	0.27	0.550	75.48	94.46	92.60	50.96
UZ 2	3.39	1.25	22.81	0.28	0.557	75.33	95.06	93.31	50.66
UZ 4	3.73	1.56	18.89	0.28	3.283	65.29	79.60	73.87	30.58
UZ 6	3.71	1.41	20.29	0.27	-0.090	78.05	98.45	97.77	56.10
UZ 7	3.84	1.36	20.13	0.27	-0.037	77.78	98.29	97.67	55.56
UZ 9	3.35	1.46	21.71	0.27	0.407	75.98	95.84	94.36	51.96
UZ 11	3.38	1.25	22.56	0.27	0.567	75.41	95.13	93.40	50.82
UG 4	3.75	1.59	17.59	0.27	3.317	65.18	79.31	73.58	30.36
UG 4B	3.70	1.40	19.83	0.26	-0.090	78.19	98.58	98.08	56.38
UG 5	3.61	1.94	19.62	0.27	0.550	75.35	94.35	92.44	50.70
UG 7	3.39	1.25	22.20	0.28	0.557	75.32	95.06	93.31	50.64
AY 2	3.73	1.57	18.88	0.27	3.317	65.23	79.39	73.68	30.46
AY 4	3.70	1.40	19.83	0.26	-0.090	78.19	98.58	98.08	56.38
AY 7	3.84	1.37	19.61	0.27	-0.123	78.25	98.84	98.43	56.50
AY 8	3.35	1.46	21.70	0.27	0.397	75.97	95.89	94.43	51.94

CIW – Chemical index of weathering, CIA – Chemical index of Alteration, PIA – plagioclase index of alteration, MIA – Mineral index of alteration

4.1 Major Elements

The SiO_2 content should be associated with the presence of quartz particles: the highest value for all samples refers to the higher sand fraction in particle size distribution analysis and higher quartz content in mineral composition. Alumina (Al_2O_3) reflects the presence of aluminosilicates. Iron (Fe_2O_3) is related to the presence of hematite while potassium (K_2O) is linked to the presence of k-feldspars (Nzeukou *et al.,* 2021).

Discussing the provenance of the shale samples since in situ weathering did not produce the majority of the shale deposits in the study area, geochemical signatures for clastic rocks were employed to determine the origin (Madharaju and Ramasamy, 2002; Armstrong-Altrin *et al*., 2004). The Al_2O_3/TiO_2 ratio grows from 3 to 8 for mafic igneous rocks, 8 to 21 for intermediate rocks, and 21 to 70 for felsic igneous rocks. These ratios have also been used to determine the composition of the source rock of clastic rocks (Ilevbare and Imasuen, 2020, Hayashi *et al.,* 1997). As calculated from Table 1b, the respective average ratios are as follows: 3.58, 1.07, 13.48, 0.27, and 0.871 for SiO_2/Al_2O_3, Fe_2O_3/K_2O, Al_2O_3/TiO_2, K_2O/Al_2O_3.

Decreasing SiO_2/Al_2O_3 ratio, (3.58), MgO content (low 1.36), and increasing Fe_2O_3 content, 6.11 (Table 1) may also indicate the residual weathered Fe–Mg minerals such as olivine and/or amphibole and pyroxene, which are inherited from moderately weathered granitoids.

Girty *et al.,* (1996) stated that sediments from mafic rocks have Al_2O_3/TiO_2 ratio <14 while sediments from felsic rocks ranged from 19-28. Comparing the major oxides, the bivariate plot of Titanium oxide and Alumina (Figure 6), indicates that the shale samples are from felsic source rock. However, the provenance discrimination plot (Figure 7) indicates that the data points plots in both the intermediate rock field and to felsic rock field.

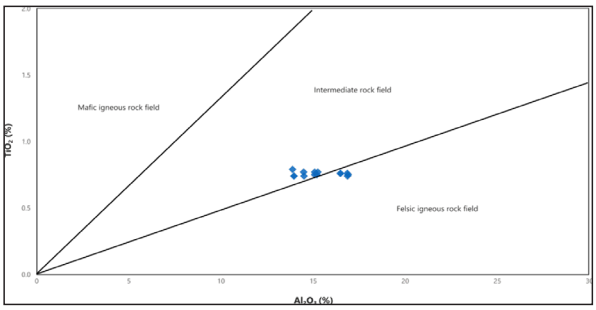

Figure 5. Titanium oxide versus Alumina for Provenance, (after Girty et al., 1996).

An insight into the paleoredox, source area weathering, and paleoclimate conditions for the shale indicates that the shale is of Continental oxic environment with prevailing oxidizing conditions (Figure 5), intensive chemical weathering (Figure 6), and a semi-arid paleoclimatic condition (Figure 7).

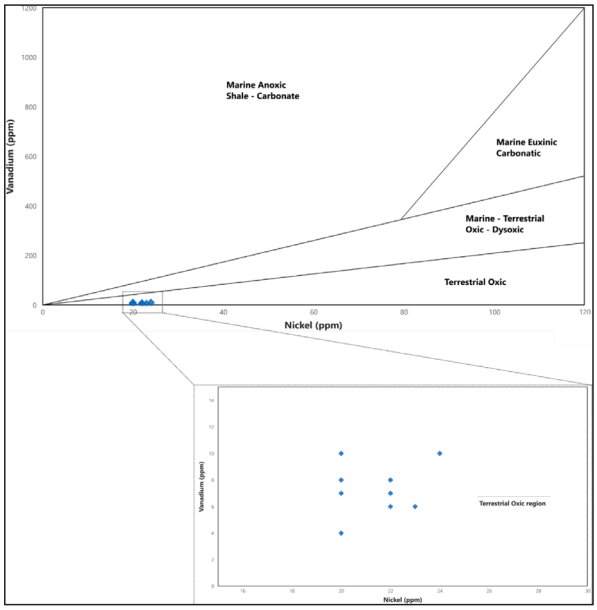

Figure 6. Vanadium versus Nickel for paleoredox discrimination, (after Girty et al., 1996).

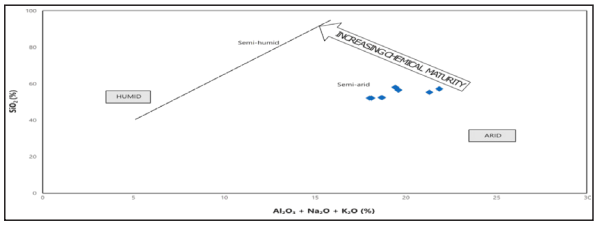

Figure 7. Silica versus Aluminina showing paleoclimate , (after Girty et al., 1996).

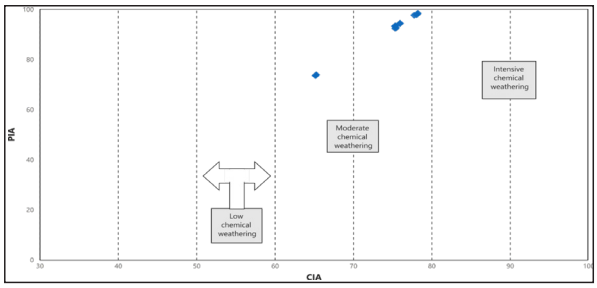

Figure 8. PIA versus CIA showing weathering conditions, (after Girty et al., 1996).

4.2 Trace Elements

The relative abundance of major oxides and trace elements in sediment is controlled by sedimentation rate, terrigenous influx, biogenic influx, hydrothermal input, diagenesis and, weathering (Leventhal, 1998; Schieber and Zimmerle, 1998). Their enrichments indicate a comprehension of their paleo-depositional and paleo redox setting, as well as the paleo-climate (Vine and Tourtelot, 1970). Therefore, the concentrations of these redox-sensitive elements (Table 2), were sensitive indicators of prevalence paleoconditions (Adegoke *et al.,* 2014). The concentration of vanadium (V), and nickel (Ni) as well as their ratios provide a means of deciding the degree of anoxia during deposition (Barwise, 1990; Bechtel *et al.,* 2001; Galarraga *et al.,* 2008). Vanadium is usually enriched in comparison with Nickel in anoxic marine environments (Peters and Moldowan, 1993).

According to Hatch and Levantal (1992) with Kimura and Wanatabe (2001), as well as Nagarajan *et al.,* (2007), Ni/Co ratio less than 2 ppm indicate an oxic environment, while ratios between 5 to 7 ppm indicate a dysoxic environment and a value greater than 7 ppm indicates a suboxic to anoxic environment. This study has a Ni/Co value of 1.80 ppm (Table 2) which again confirms an oxic environment. Again from this study, the Ni/Co ratio is below 5, which suggests an oxidizing condition for the Mamu shale.

Similarly, a V/Cr value less than 2 ppm indicates an oxic environment, while a value of 2 to 4.25 suggests a dysoxic environment, and that greater than 4.25 ppm indicates sub-oxic to anoxic conditions. From Table 2, these samples collected have a value much less than 2 (0.38ppm) which indicates oxidizing conditions. This again agrees with Akinyemi *et al.,* (2013) having a result of between 1.01 and 1.91. Olajubaje *et al.,* (2018) have V/Cr values which may indicate that relatively oxidizing conditions were also prevalent. Furthermore, the V/Cr ratios of the examined samples are below 2(1.142) and therefore indicate the oxic depositional setting.

The V/(V + Ni) value less than 0.46 suggests an oxic environment, while that of 0.46–0.60 indicates a dysoxic environment and 0.54-0.82 indicates a suboxic to anoxic condition, and a value less than 0.84 suggests an euxinic condition (Hatch and Levantal 1992). This study gives an average value of 0.26 ppm for V/V + Ni which again confirms an oxic environment.

Table 2. Trace elements of shale deposits sourced at Uzebba, Ugbenor and Ayoguiri communities, Anambra basin.

ppm

Sample	Ba	Cu	Zn	Cr	Ni	Co	V	Ni/Co	V/Ni	V/Cr	V/(V + Ni)
UZ 1	882	22	12	20	22	10	6	2.20	0.27	0.30	0.21
UZ 2	992	20	10	20	20	10	4	2.00	0.20	0.20	0.17
UZ 4	990	23	10	22	22	10	8	2.20	0.36	0.36	0.27
UZ 6	976	20	12	20	20	8	10	2.50	0.20	0.50	0.33
UZ 7	980	20	10	20	23	6	6	3.80	0.26	0.30	0.21
UZ 9	990	22	9	21	22	8	8	2.75	0.36	0.36	0.27
UZ 11	995	24	12	18	24	10	10	2.40	0.42	0.42	0.29
UG 4	894	22	10	20	20	8	7	2.50	0.35	0.35	0.26
UG 4B	986	20	8	19	20	8	8	2.50	0.40	0.42	0.29
UG 5	990	22	12	15	22	10	6	2.20	0.27	0.40	0.21
UG 7	994	20	10	22	24	10	10	2.40	0.42	0.45	0.29
AY 2	992	23	12	20	22	9	8	2.40	0.36	0.40	0.27
AY 4	995	22	12	18	20	10	10	2.00	0.50	0.50	0.33
AY 7	890	24	10	22	22	8	7	2.75	0.32	0.32	0.24
AY 8	880	20	12	22	20	10	10	2.00	0.50	0.45	0.33

UZ- Uzebba UG-Ugbenor AY- Ayoguiri

According to Hatch and Levantal (1992) with Kimura and Wanatabe (2001), as well as Nagarajan *et al.,* (2007), Ni/Co ratio less than 2 ppm indicate an oxic environment, while ratios between 5 to 7 ppm indicate a dysoxic environment and a value greater than 7 ppm indicates a suboxic to anoxic environment. This study has a Ni/Co value of 1.80 ppm (Table 2) which again confirms an oxic environment. Again from this study, the Ni/Co ratio is below 5, which suggests an oxidizing condition for the Mamu shale.

Similarly, a V/Cr value less than 2 ppm indicates an oxic environment, while a value of 2 to 4.25 suggests a dysoxic environment, and that greater than 4.25 ppm indicates sub-oxic to anoxic conditions. From Table 2, these samples collected have a value much less than 2 (0.38ppm) which indicates oxidizing conditions. This again agrees with Akinyemi *et al.,* (2013) having a result of between 1.01 and 1.91. Olajubaje *et al.,* (2018) have V/Cr values which may indicate that relatively oxidizing conditions were also prevalent. Furthermore, the V/Cr ratios of the examined samples are below 2(1.142) and therefore indicate the oxic depositional setting.

The V/(V + Ni) value less than 0.46 suggests an oxic environment, while that of 0.46–0.60 indicates a dysoxic environment and 0.54-0.82 indicates a suboxic to anoxic condition, and a value less than 0.84 suggests an euxinic condition Hatch and Levantal (1992) and Khoury (2014). This study gives an average value of 0.26 ppm for V/V + Ni which again confirms an oxic environment.

The correlation of alumina against the other trace elements (Figure 9) using the data set (Table 3) helps to delineate the shale type using the correlation coefficient classifies the shale to be predominately detrital shale, (Table 4) with the negatively correlated as authegenic and the positively correlated as detrital.

Table 3. The Correlation plot of Al_2O_3 against the trace elements.

Al_2O_3	Al	Ba	Cu	Zn	Cr	Ni	Co	V
14.50	3.84	882	22	12	20	22	10	6
16.88	4.47	992	20	10	20	20	10	4
13.98	3.70	990	23	10	22	22	10	8
15.22	4.03	976	20	12	20	20	8	10
15.10	4.00	980	20	10	20	23	6	6
16.50	4.37	990	22	9	21	22	8	8
16.92	4.48	995	24	12	18	24	10	10
13.90	3.68	894	22	10	20	20	8	7
15.27	4.04	986	20	8	19	20	8	8
14.52	3.84	990	22	12	15	22	10	6
16.87	4.47	994	20	10	22	24	10	10
13.97	3.70	992	23	12	20	22	9	8
15.27	4.04	995	22	12	18	20	10	10
15.10	4.00	890	24	10	22	22	8	7
16.49	4.37	880	20	12	22	20	10	10

Another important consideration in the use of trace elements in palaeo-redox determination is to examine whether they are detrital or authigenic in origin. Correlation values derived from cross plots of Al versus the trace elements (Figure 9) can determine if they are detrital or authigenic in origin. The shale sediments are predominantly of a detrital origin, (Table 4). This result is consistent with the pieces of evidence from the high weathering history recorded from the shale and with the mineralogical composition that reveals that the quartz has survived been weathered and has been transported through a fairly long distance. The correlation result of Alumina (Al_2O_3) versus Cu and Zn are both authegenic.

Table 4. Interpreted correlation result of the shale.

Al vs. TE	Corr. Coef.	Interpretation
Al vs. Ba	0.212	Detrital
Al vs. Cu	-0.321	Authigenic
Al vs. Zn	-0.110	Authigenic
Al vs. Cr	0.152	Detrital
Al vs. Ni	0.185	Detrital
Al vs. Co	0.213	Detrital
Al vs. V	0.257	Detrital

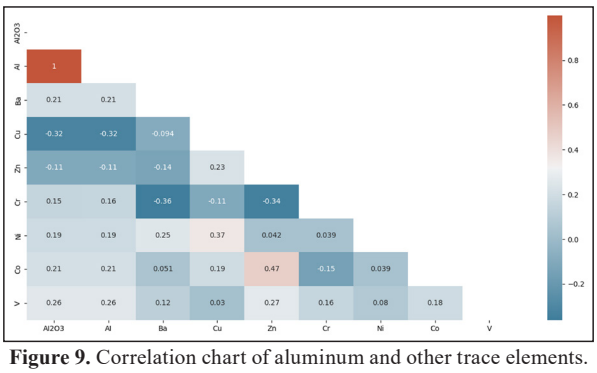

Figure 9. Correlation chart of aluminum and other trace elements.

In the diffractogram (Figure 10), for Ayoguiri shale, the quartz with six observed peaks had the highest peak of 90cps with 30° which was followed by calcite with 50cps/35° with three observed peaks. Other minerals in minor quantities and without prominent peaks are montmorillonite with four peaks and Figure fluorapatite with three observable peaks.

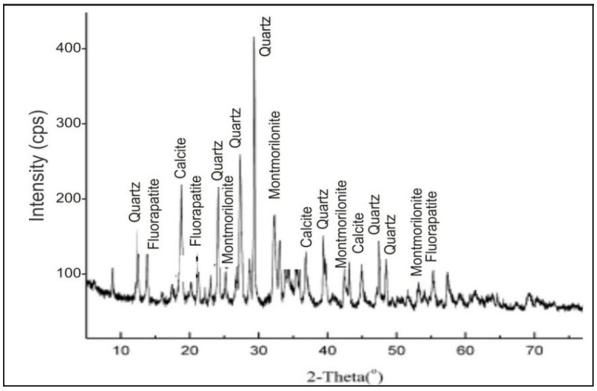

Figure 10. Diffractogram of Mamu shale in Ayoguiri community, Anambra Basin.

In Ugbenor shale, quartz has 6 observed peaks with 110cps/35° being the highest. This was followed by calcite with three observed peaks with the highest being 40cps/48°; also observed were fluorapatite and montmorillonite (Figure 11).

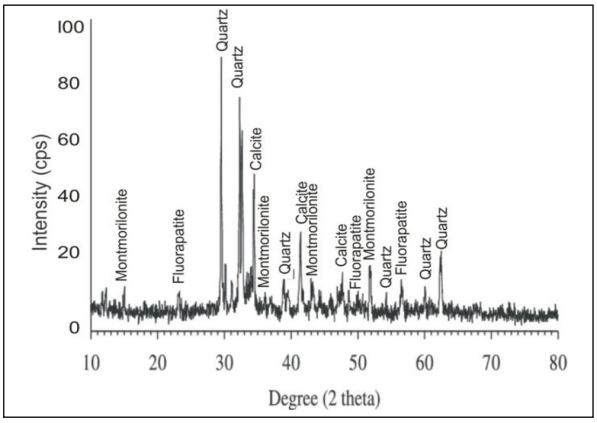

Figure 11. Diffractogram of Mamu shale in Ugbeno community, Anambra Basin.

In Uzebba shale, the quartz with seven observable peaks had 400cps/30° followed by calcite with 200cps/20°. With four observable peaks, montmorillonite also had a significant peak here in this sample with 180cps/32°. Fluorapatite had three observed peaks with no sharp peaks, (Figure 12).

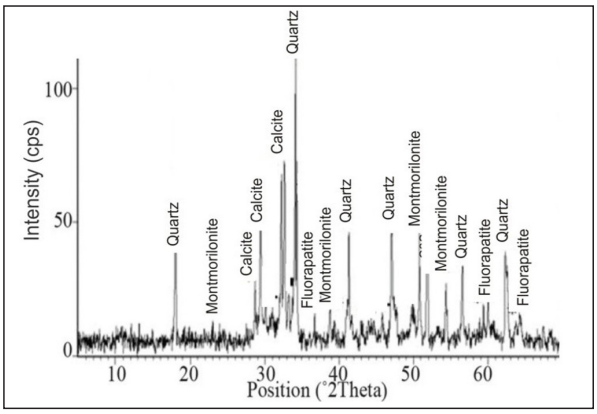

Figure 12. Diffractogram of Mamu shale in Uzebba community, Anambra Basin.

4.3 Chemical Weathering Index

Chemical weathering indices are often employed to quantify changes brought on by chemical weathering in different materials (Birkeland, 1999; Darmody et al., 2005; Ruxton, 1968; Harnois, 1988; Habboush and Jarrar, 2009). The indices are based on the idea that as leaching advances, the ratio between concentrations of mobile (e.g. SiO_2, CaO, MgO, and Na_2O) and immobile (e.g. Al_2O_3, Fe_2O3, and TiO_2) elements will progressively plummet. Calculating the Chemical Index of Alteration (CIA), where CIA = molar (Al_2O_3/[Al_2O_3+CaO+Na_2O+K_2O]) x 100, can help understand the extent of chemical weathering of the sediments' source rocks, according to Nesbitt and Young (1982). The CIA monitors the progressive transformation of potassium feldspars and plagioclase into clay minerals (Rahman and Suzuki, 2007). When Ca, Na, and K drop as weathering severity increases, (Duzgoren-Aydin *et al.,* 2002). The only difference between the CIA and the Chemical Index of Weathering (CIW) proposed by Harnois, (1988) is the omission of K_2O from the equation: CIW = molar (Al_2O_3 / (Al_2O_3+ CaO + Na_2O) x 100.

From the results of (Table 1), the Chemical Index of Alteration (CIA) gives an average value of 74.33% (65.18-78.25), while the Chemical Index of Weathering (CIW) has an average value of 93.12% (73.58-98.43). The Plagioclase index of alteration gives an average value of 91.00% (73.58-98.43) and the Mineralogical Index of Alteration measures 48.67% (30.36-56.50) on average.

According to McLennan, (1983), McLennan, (1993), and Mongelli *et al.,* (1996), the results of CIA and CIW are similar, with values of 50 for the unweathered upper continental crust and approximately 100 for heavily weathered materials. Low CIA values (i.e. 50 or less) also might reflect cool and/or arid conditions. Nesbitt and Young (1982) classified the CIA values as very slightly weathered (50 to 60), slightly weathered (60 to 70), moderately weathered (70 to 80), highly weathered (80 to 90), and extremely weathered (90 to100). This study (Table 1) indicates between slightly weathered and moderately weathered environments (65.18-78.25). For the CIA, weathering at the incipient stage, CIA (30-55), weathering at the intermediate stage, CIA (51-85), and weathering at the advanced stage CIA >85. An average value of 74.33 from this study implies that the weathering is at an intermediate stage.

Chemical Index of Weathering (CIW) values range from 50 for unweathered upper continental crust to roughly 100 for materials that have undergone substantial weathering, with the full elimination of alkali and alkaline-earth elements (McLennan *et al.,* (1983), McLennan (1993),. The CIW value of 93.12% (ave.) applies the shale has undergone substantial weathering.

To evaluate MIA values, it is helpful to consider the following ranges: incipient (0–20%), weak (20–40%), moderate (40–60%), and intense to extreme (60–100%) degree of weathering. The MIA of this study is 48.67 (range 30.36-56.50%) illustrates an environment with moderate weathering.

5. Conclusions

Based on the analysis of the geochemical discriminant, mineralogy and geochemical paleo redox indicators for the Maastrichtian shales of Mamu formation, Southern Nigeria the following conclusions may be drawn:

From the correlation results, the shale is of detrital origin, this explains also why the source area weathering indicated a substantial, intense to extreme chemical weathering of the phanerozoic shale.

The metallic oxide ratios indicated the provenance of the shale are of a felsic source rock in a semi-arid to arid paleoclimatic condition.

The paleoredox studies reveal that the shale was deposited in an oxic environment from the weathering indices (Ni/Co, V/Cr, and V/V+Ni) except for V/Ni which was deposited in a dysoxic - Oxic environment.

References

Adegoke, O. A., and Akande, O. A. (2014). Sedimentology and sequence stratigraphy of the Agbada Formation, Niger Delta: implications for hydrocarbon prospectivity. *Journal of African Earth Sciences, 138, 101-119*

Anakwuba, E.K., and Onyekwelu, C.U., (2010). Subsurface sequence stratigraphy and reservoir characterisation of southern part of Anambra basin, Nigeria. *AAPG search and discovery, Journal of Geological Science, Nnamdi Azikiwe Umiversity, 112(5):278-290*

Akinyemi, S. A., Adebayo, O. F., Ojo, O. A., Fadipe, O. A. and Gitari, W. M., (2013). "Mineralogy and geochemical appraisal of paleo-redox indicators in Maastrichtian outcrop shales of Mamu Formation, Anambra Basin, Nigeria", *Journal of Natural Sciences Research* 3(10): 48-64.

Al-Momani, T., Alqudah, M., Dwairi, M.E.A., 2020. Mineralogical and Geochemical Characterisation of Jarash Kaolitic Clay, Northern *Jordan. Jordan Journal of Earth and Environmental Sciences, 11(4): 272 – 287*

Armstrong-Altrin J.S., Lee Y.I, Verma S.P., Ramasamy S., (2004). Geochemistry of sandstones from the upper Miocene Kudankulam Formation, southern India: Implications for provenance, weathering, and tectonic setting. *Journal of Sedimentary Research*, 74(2): 285-297.

Barwise, A. J. G., (1990). Role of Nickel and vanadium in petroleum classification. *Energy fuels*, 4: 27-49.

Bechtel, A., Gratzer, R., and Sachsenhofer, R.F., (2001). Chemical characteristics of Upper Cretaceous (Turonian) jet of the Gosau Group of Gams/Hieflau (Styria, Austria). *International Journal of Coal Geology* 46: 27–49.

Bello, A., Heggland, R., Peacock, D. C. P., (2017). Pressure significance of gas chimneys. *Marine and petroleum geology, 86:402-407*

Birkeland, P.W., (1999). Soils and Geomorphology, Third edition. New York, Oxford University Press. 430 pp.

Bundy, W.M., (1993). The diverse industrial applications of kaolin. Kaolin Genesis and Utilization (Murray, H. H., Bundy, W., Harvey, C.,), Clay Minerals Society Special Publication 1, Boulder, 43-47.

Cao, J., Wu, M., Chan, Y., Hu, K., Bian, L.Z., Wang, L.G., Zhang, Y., (2012). Trace and rare earth elements geochemistry of Jurassic mudstones in the northern Qaidam Basin, Northwest China. *Chem. Erde, 72:245–252.*

Darmody, R.G., Thorn, C.E., Allen, C.E., (2005). Chemical weathering and boulder mantles, Kärkevagge, Swedish Lapland. *Geomorphology*, 67(1-2): 159–170

Duzgoren-Aydın, N.S., Aydın, A., Malpas, J., (2002). Re-assessment of chemical weathering indices: a case study on pyroclastic rocks of Hong Kong. https://doi.org/10.1016/S0013-7952(01)00073-4*Engineering Geology* https://doi.org/10.1016/S0013-7952(01)00073-463(1-2): 99-119.

Edegbai, A.J., Schwark, L., Oboh-Ikuenobe, F.E., (2019a). A review of the latest Cenomanian to Maastrichtian geological evolution of Nigeria and its stratigraphic and paleogeographic implications. *Journal of African Earth Sciences, 150, 823-837 https://doi.org/10.1016/j.jafrearsci.2018.10.007,*

Edegbai, A.J., Schwark, L., Oboh-Ikuenobe, F.E., (2019b). Campano-Maastrichtian paleoenvironment, paleotectonics and sediment provenance of Western Anambra Basin, Nigeria: Multi-proxy evidences from the Mamu Formation. *Journal of African Earth Science, 151:585-599 https://doi.org/10.1016/j.jafrearsci.2019.04.001.*

Egboka, J. C., and Emejulu, E. V., (2015). Palynology and palynofacies analysis of Ezeaku-1 well in Anambra Basin, southeastern Nigeria. *International Journal of Geosciences,* 6(8):825-837*. doi: 10.4236/ijg.2015.68067*

El-Hasan, T., Al-Malabeh, A., 2008. Geochemistry, mineralogy and Petrogenesis of El-Lajjoun Pleistocene Alkali Basalt of Central Jordan. *Jordan Journal of Earth and Environmental Sciences*, 1(2): 53-62.

Galarraga, F., Reategui, K., Martinez, M., Liamas J.F., and Marquez, G., (2008). V/Ni ratio as a parameter in paleoenvironmental characterization of non-mature medium crude oils from Latin American Basin. *Journal of Petroleum Science and Engineering*, 61: 9-14.

Girty, G.H., Ridge, D.L., Knaack, C., Johnson, D.D, A.I. Riyami, R.K., (1996). Provenance and depositional setting of Palaeozoic chert and argillite, Sierra Nevada, California. *Journal of Sediment Resolution*, 66 (1); 107-118.

Harnois, L., (1988). The C.I.W. index: a new chemical index of weathering. *Sedimentary Geology,* 55: 319–322

Hatch, J. R., and Leventhal, J.S., (1992). Relationship between inferred redox potential of the depositional environment and geochemistry of the Upper Pennsylvanian (Missourian) Stark Shale Member of the Dennis Limestone, Wabaunsee County, Kansas, U.S.A. *Chemical Geology*, 99: 65-82.

Habboush, M.A, Jarrar, G.H., 2009. Petrology and Geochemistry of the Metasediments of the Janub metamorphic suite, Southern Jordan: Implications for Geothermobarometry and Economic potential, *Jordan Journal of Earth and Environmental Sciences,* 2(1): 7-1

Haque, M., Roy, M.K., (2019). Sandstone-Shale Geochemistry of Miocene Surma Group in Bandarban Anticline, SE Bangladesh: Implications for Provenance, Weathering, and Tectonic Setting. *Earth Sciences*. 9(1) 38-51. *doi: 10.11648/j.earth.20200901.15*

Hayashi, K., Fujisawa, H., Holland, H., Ohmoto, H., (1997). Geochemistry of 1.9Ga Sedimentary rocks from Northern Eastern Labrador, Canada: *Geochimicaet Cosmochimica Acta*, 61(19): 4115-4137.

Heinnonem, J.S, Bohrson, W.A., Spera, F.J., Brown, G.A., Scruggs, M.A., Adams, J.V., (2020). Diagnosing open system magmatic processes using the magma chamber Simulator (MCS): Part II trace elements and *Isotopes. Contributions to Mineralogy and Petrology,* 175:105-126.

Ilevbare M, Imasuen, O.I., (2020). Sedimentology and maturity of Ajali Formation, Benin flank, Anambra Basin, Nigeria. *Ife Journal of Science*, 22(1): 123-135.

Ilevbare M, Omorogieva, O.M., (2020). Sedimentary Petrology, paleoclimatic and tectonic settings of Maastritchtian sediments, western flank of Anambra basin, Nigeria. *Nigeria Research Journal of Engineering and Environmental Sciences,* 5(2): 938-949.

Ilevbare M., and Omodolor, H.E., (2020). Ancient Depositional Environment, Mechanism of Deposition and Textural attributes of Ajali Formation, Western flank of Anambra basin, Nigeria. *Elsevier, Case studies in Chemical and environmental engineering,* 2: 1-8.

Khoury, H.N., 2014. Geochemistry of Surficial Uranium Deposits from Central Jordan. *Jordan Journal of Earth and Environmental Sciences*, 6(3): 11-22

Leventhal, J. S., (1998). Metal-rich black shales: formation, economic geology and environmental considerations. In Shales and Mudstones II, J. Schieber, W. Zimmerle, and P. Sethi, (Eds.), Stuttgart, E. Schweizerbart'sche Verlagsbuchhandlung, 255-282.

Madharaju J., Ramasamy S., (2002). Petrography and geochemistry of Late Maastrichtian - Early Paleocene sediments of Tiruchirapalli Cretaceous, Tamil Nadu - Paleoweathering and provenance implications. *Journal of the Geological Society of India*, 59:133-142.

Murray, H.H., Keller, W.D., 1993. Kaolin, kaolin and kaolin. In: Murray, H. H., Bondy, W. and Harvey, C. (Eds.), Kaolin Genesis and utilization. The Clay Mineral Society (Special Publication), Aurora, USA, (1).

Nagarajan, R., Madhavaraju, J., Nagendra1, R., Armstrong-Altrin, J. S., and Moutte, J., (2007). Geochemistry of Neoproterozoic shales of the Rabanpalli Formation, Bhima Basin, Northern Karnataka, southern India: implications for provenance and paleoredox conditions. *Revista Mexicana de Ciencias Geológicas*, 24(2): 150-160.

Nzeukou, N. A., Tsozué, D., Kagonbé, P. B., (2021). Clayey Soils from Boulgou (North Cameroon): Geotechnical, Mineralogical, Chemical Characteristics and Properties of Their Fired Products. *SN Applied Sciences*, 3(551): 22-37. https://doi.org/10.1007/s42452-021-04541-4.

Obaje, N.G., Wehner, H., Scheeder, G., Abubakar, M. B., and Jauro, A., (2004). Hydrocarbon prospectivity of Nigeria's inland basins: From the viewpoint of organic geochemistry and organic petrology. *AAPG Bull*., 88(3): 325- 353.

Ogungbesan, G. O., and Adedosu, T. A., (2020). Geochemical record for the depositional condition and the petroleum potential of the Late Cretaceous Mamu formation in the western flank of the Anambra basin, Nigeria. *Green energy and environment 5(1)83-96. https://doi.org/10.1016/j.gee.2019.01.008*

Okwara, I.C., (2020) Reservoir evaluation within the sequence stratigraphic framework of the Upper Cretaceous Anambra Basin, Nigeria. *3(5): 12-15*

Omietimi, E.J.??, *et al.,* (2021). Structural interpretation of the south-western flank of the Anambra Basin (Nigeria) using satellite-derived WGM 2012 gravity data *J. Afr. Earth Sci.* 5(7): *46-53.*

Peters, K. E. and Moldowan, J. M., (1993). The Biomarker Guide: Interpreting Molecular Fossils in Petroleum and Ancient Sediments. Englewood Cliffs, N.J., Prentice Hall, p. 363.

Schieber, J. and Zimmerle, W., (1998). Introduction and overview; the history and promise of shale research. In Shales and Mudstones I, J. Schieber, W. Zimmerle, and P. S. Sethi (Eds.), (pp. 1–10). E. Schweizerbart'scheVerlagsbuchhandlung Naegele u. Obermiller Stuttgart, Germany.

Tao, S., Xu, Y., Tang, D., Xu, Hao., Li, S., Chen, S., Liu, W., Cui, Y., and Gou, M., (2017). Geochemistry of the Shitoumei oil shale in the Santanghu basin, northwest China: implications for paleoclimate conditions, weathering, provenance and tectonic setting. *International journal of coal geology 184:42-56. https://doi.org/10.1016/j.coal.2017.11.007*

Tijani, M.N., Nton, M.E., Kitagawa, R., (2010). Textural and geochemical characteristics of the Ajali sandstone, Anambra basin, SE Nigeria: implication for its provenance. *Compt. Rendus Geoscience* 342: 136–150http://refhub.elsevier.com/S2405-8440(21)02213-1/sref85.

Vine, J. D. and Tourtelot, E. B., (1970). Geochemistry of black shale deposits a summary report. *Econ. Geol*., 65: 253-272.

JJEES

Jordan Journal of Earth and Environmental Sciences

JJEES (2023) 14 (4): 268-279
ISSN 1995-6681

Risk Perception Assessment for Sawmill workers in Benin Metropolis, Edo State, Southern Nigeria.

Chika F. Amaechi* and Akus K.Okoduwa

Department of Environmental Management and Toxicology, Faculty of Life Sciences, University of Benin, PMB 1154, Benin City, Nigeria.

Received March 1, 2023; Accepted July 9, 2023

Abstract

Sawmills are a common site especially in developing countries and studies suggest that this practice comes with attendant health risks. This study seeks to assess the risk perception of air quality around sawmills in Benin Metropolis, Edo State, Southern Nigeria. The study relied primarily on the administration of questionnaires. A total of 150 structured questionnaires were administered to workers in the three major sawmills in Benin City. Data analysis was done using Statistical Package for Social Science (SPSS) version 16.0. Statistical tools such as frequency, percentage, and Chi-square were also used to analyze relevant variables. 95% confidence level, a P<0.05 was considered statistically significant for the study. Results from the study revealed that the majority (82%) of respondents were males; the majority (30%) were between the ages of 51 and 60; and the majority (34%) had worked in sawmills for ten years or more. Findings from the study revealed that headache, catarrh, bronchitis and eye irritation were the most prevalent health risks amongst sawmill workers indicative of poor air quality. The study also revealed that though the air quality around sawmill is polluted sawmill workers have low adaptive capacity toward associated risks. Furthermore, other health risks reported by workers include asthma, chest pain, throat irritation, eczema, sneezing and coughs. The study concludes that sawmill workers in Benin City need more information about the dangers of inhaling polluted air as well as the need for adequate use of personal protective equipment.

Keywords: *Risk perception, Sawmill, Air quality, Health.*

1. Introduction

It is documented knowledge that the sawmill environment can cause health hazards for sawmill workers, and there is sufficient evidence that exposure to air pollution has negative effects on health (Faremi et al., 2014; Héroux et al., 2015; Raimi et al., 2018; Rückerl et al., 2011). Sawmill workers belong to a group of workers who are often exposed to many health risks in the workplace (Odibo et al., 2018). Natural and anthropogenic activities both contribute to air pollution around sawmill locations; however, anthropogenic activities such as emissions from sawmills and sawdust burning have contributed to an increase in air pollution (Odunaike et al., 2008, EPA South Australia, 2001). Health-related issues such as coughing, difficulty breathing, nasal irritations, throat irritations, itching of the eyes, sneezing, and asthma have been reported among sawmill workers (Raimi et al., 2020; Vallieres et al., 2015).

It has been reported that sawmill workers are exposed to a high level of wood dust and other air pollutants such as carbon (IV) oxide, oxides of nitrogen, and sulfur due to inadequate control measures, poor awareness of occupational hazards, and poor availability and use of protective equipment (Adeoye et al., 2014; Agu et al., 2016). Despite the potentially hazardous nature of the sawmill workplace, little attention has been given to the worker's health and safety in Benin City. It is therefore pertinent to carry out a risk perception assessment of air quality around sawmills to support or oppose existing literature.

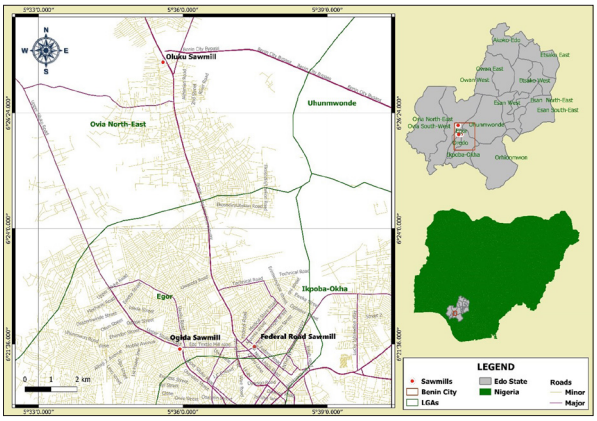

Figure 1. Location map showing the study area.

2. Materials and Methods

2.1. Study Area

The study was conducted in Benin City, the capital of Edo state, at latitude 6° 20' 5.95" N and longitude 5° 36' 13.49" E (Dimuna and Olotuah, 2020). Benin City is located in the southern region of Nigeria. It is the capital of Edo State, and in 2022, it boasted a population of 1,841,000, making it one of the largest cities in Nigeria. It is approximately 40 kilometers north of the Benin River and 320 kilometers by road east of Lagos State. The majority of the residents speak Bini language. The population is largely made up of Christians, Muslims, and traditional African worshippers.

The study was typically limited to three major sawmill sites because they host approximately 95% of wood milling

* Corresponding author e-mail: chika.amaechi@uniben.edu

in the metropolis. They are precisely Federal sawmill, Oluku sawmill and Ogida sawmill. Federal sawmill was established at Oredo Local Government Area which is 2 km North East from the center of the city. Ogida sawmill was established at Egor Local Government Area, which is 1.5 km north-east from the center of the city, and Oluku sawmill was established at Ovai North East Local Government Area which is 5 km north-east (Ediagbonya et al., 2013).

2.2 Data Type and Data Source

For the purpose of achieving the research aim, data were collected from primary field study. The primary data was collected by administering questionnaire at the three (3) study sites (Federal Sawmill, Ogida Sawmill, and Oluku Sawmill).

2.3 Method of Data Collection

Data were collected through the administration of a comprehensive and well-structured questionnaire. The questionnaire contained structured questions adopting the Likert scale method, whereby respondents answered on a scale of strongly agree (SD), agree (A), disagree (D), and strongly disagree (SD). The questionnaires were administered to workers at the various sawmills. The information obtained from the respondents was divided into two sections: section one included demographic characteristics (sex, age, period of work); section two included the certainty of air pollution, adaptive capacity, and health risks that are associated with sawmilling activities. The questionnaires were administered randomly to workers in the three selected sawmills; a total of 150 questionnaires were administered, and 150 were completed, giving a completion rate of 100 percent.

2.4 Method of Data Analysis

Data analysis for this study was done with Microsoft Excel 2018 and Statistical Package for Social Science (SPSS) version 16.0. Questionnaire survey data about the certainty of air pollution, adaptive capacity, and health risk were analyzed using descriptive statistics, which were used to obtain frequency and percentages. While chi square (X^2) techniques was used to test for relationship between certainty of air pollution, adaptive capacity and health risk within sawmill workers in the study site with Statistical Package for Social Science (SPSS) 16.0 version. Descriptive statistics like tables and figures were used in the study to describe the sociodemographic characteristics of the sampled sawmill workers and to examine risk perception. A five percent level of $p > 0.05$, there is no significant differences and when $p<0.05$, there is significant relationship. The gathered data were analyzed, and the results were presented using tables to draw conclusions in relation to the research.

3. Results

3.1 Demographic characteristics of respondent

Table 1 shows the gender distribution of the respondents. The trends observed show that the highest number of workers are male (82%), and the lowest number are female (18%). Using the chi square goodness of fit, there was a very high significant difference ($p< 0.001$) between the ages of respondents in the study area.

The trend also shows in Table 1 that respondents aged 18–20 years made up 4% of the 150 respondents. The highest was seen in respondents within the age range of 51–60 years, which makes up 30% of respondents, while the age of respondents from 41–50 years was 22.7%, those who fell between 31–40 years were 34.7%, and the age of respondents from 21–24 years was 10.7%, as seen in table 1. Using the chi-square goodness of fit, there was a very high significant difference ($p< 0.001$) between the ages of respondents in the study area.

The variation observed in the frequency counts of workers who have worked in sawmills, as seen in Table 1 shows that workers aged 10 years and older are the most numerous (34%), while workers aged 4 to 6 years are the least numerous (9.3%). Workers between 1 month and 2 years recorded 28.7%, workers between 2 and 4 years recorded 18%, and workers between 6 and 8 years recorded 10%. Using the chi square goodness of fit, there was a very high significant difference ($p<0.001$) between the years of working experience.

Table 1. Demographic characteristics of the respondent

		Egor LGA	Oredo LGA	Ovia Northeast LGA	Frequency	Percentage	
		Ogida Sawmill	Federal Sawmill	Oluku Sawmill	n=150	%	p-value
Sex	MALE	44	39	40	123[a]	82.0	p<0.01
	FEMALE	6	11	10	27[b]	18.0	
Age Range	18 -20	4	2	0	6[d]	4.0	
	21- 24	8	3	5	16[c]	10.7	
	25-30	4	2	6	12[c]	8.0	p<0.01
	31-40	9	19	9	37[b]	24.7	
	41-50	8	15	11	34[b]	22.7	
	51-60	17	9	19	45[a]	30.0	
Work Experience	1month to – 2 years	13	18	12	43[a]	28.7	
	2 – 4 years	8	11	8	27[b]	18.0	
	4-6 years	5	3	6	14[c]	9.3	p<0.01
	6-8 years	2	8	5	15[c]	10.0	
	10 years and above	22	10	19	51[a]	34.0	

No significant difference ($p > 0.05$), *$p < 0.05$ (significant difference) **$p < 0.01$ (highly significant difference)
***$p<0.001$ (very high significant difference)
Note: Similar letters (superscripts) indicate values that are not significantly different from each other ($P>0.05$)

3.1.2 Certainty of air pollution around sawmill

Table 2 shows the certainty of air pollution around the study area. This section consists of a total of eight (8) questions. The first question (Q1) was on the dusty environment around the sawmill. The highest frequency count of respondents who agreed on the dusty environment around sawmills was 72.7%, followed by respondents who strongly agreed with a percentage of 22%, respondents who disagreed with a percentage of 5.3%, and respondents who strongly disagreed that sawmill environments get dusty during working processes had a percentage of 0%. Using the chi square goodness of fit, there was a very high significant difference ($p<0.001$) between respondents on the dusty environment around sawmill.

The second question (Q2) was on the intensity of emission of dust during work hours. The highest frequency counts of respondents who agreed that the dust produced during work hours is intense had a percentage of 64.7%, followed by respondents who strongly agreed with a percentage of 22%, respondents who disagreed with a percentage of 13.3%, and respondents who strongly disagreed with a percentage of 0%. Using the chi square goodness of fit, there was a very high significant difference ($p<0.001$) between respondents on the intensity of dust produced during work hours.

The third question (Q3) was to ascertain if the sawdust stuck to the bodies of workers during working hours. The highest frequency counts of respondents who agreed that the sawdust stuck to their bodies during working periods had a percentage of 69.3%, followed by respondents who strongly agreed with a percentage of 23.3%, respondents who disagreed with a percentage of 7.3%, and respondents who strongly disagreed with a percentage of 0%. Using the chi square goodness of fit, there was a very high significant difference ($p<0.001$) between respondents on sawdust sticking to their bodies.

The fourth question (Q4) was to assess if workers were aware of the health implications of sawdust/particulate. The trend observed shows that 60% of respondents were aware that sawdust or other particles, when inhaled, cause health risks. Respondents who strongly agreed had a percentage of 30.7%; respondents who disagreed had a percentage of 9.3%; and respondents who strongly disagreed had a percentage of 0%. Using the chi square goodness of fit, there was a very high significant difference ($p<0.001$) between respondents on the health implications of inhaling sawdust or other particles from sawmill processes.

The fifth question (Q5) was enquiry on whether sawmill machines require diesel or fuel for operation. The highest frequency counts of respondents who agreed that sawmill machines require diesel or fuel to operate had a percentage of 76.7%, followed by respondents who strongly agreed with a percentage of 23.3%, and respondents who disagreed with a percentage of 0%. Using the chi square goodness of fit, there was a very high significant difference ($p<0.001$) between respondents.

The sixth question (Q6) was to assess if the sawmill machine or generator emits gases or smoke during operation. The highest frequency counts of respondents who agreed that sawmill machines emit smoke or gases during operation had a percentage of 76%, followed by respondents who strongly agreed with a percentage of 17.3%, respondents who disagreed with a percentage of 6.7%, and respondents who strongly disagreed with a percentage of 0%. Using the chi-square goodness of fit, there was a very high significant difference ($p<0.001$) between respondents on dust or gases emitted from sawmill machines or generators.

The seventh question (Q7) was to ascertain if the smoke or gases emitted during work hours are high. The highest frequency counts of respondents who agreed that the smoke or gases were high had a percentage of 44.7%, followed by respondents who strongly agreed with a percentage of 12.7%, respondents who disagreed with a percentage of 40.7%, and respondents who strongly disagreed with a percentage of 0%. Using the chi-square goodness of fit, there was a very high significant difference ($p<0.001$) between respondents on the high emission of smoke during work hours.

The eighth question (Q8) was to ascertain if temperature increased significantly around the work environment. The highest frequency counts of respondents who agreed that temperature increased during work had a percentage of 55.3%, followed by respondents who strongly agreed with a percentage of 12.7%, respondents who disagreed with a percentage of 32.7%, and respondents who strongly disagreed with a percentage of 0%. Using the chi-square goodness of fit, there was a very high significant difference ($p<0.001$) between respondents on increased temperature during work hours.

Table 2. Certainty of air pollution around sawmill.

Questions	Response	Egor LGA (Ogida Sawmill)	Oredo LGA (Federal Sawmill)	Ovia Northeast LGA (Oluku Sawmill)	Frequency n=150	Percentage %	p-value
Q1. The work environment gets dusty during working hours	SA	14	9	10	33[b]	22.0	p<0.01
	A	32	38	39	109[a]	72.7	
	D	4	3	1	8[c]	5.3	
	SD	0	0	0	0	0.0	
Q2. The quantity of dust particles produce during work hours is intense	SA	16	9	8	33[b]	22.0	p<0.01
	A	28	36	33	97[a]	64.7	
	D	6	5	9	20[b]	13.3	
	SD	0	0	0	0	0.0	
Q3. Particles/sawdust stick to the body during the working process	SA	15	11	9	35[b]	23.3	p<0.01
	A	31	39	34	104[a]	69.3	
	SD	4	0	7	11[c]	7.3	
	D	0	0	0	0	0.0	
Q4. Particles/sawdust when inhaled causes risk to health	SA	20	12	14	46[b]	30.7	p<0.01
	A	16	38	36	90[a]	60.0	
	D	14	0	0	14[c]	9.3	
	SD	0	0	0	0	0.0	
Q5. The sawmill machine requires diesel/fuel to operate	SA	15	11	9	35[b]	23.3	p<0.01
	A	35	39	41	115[a]	76.7	
	D	0	0	0	0	0.0	
	SD	0	0	0	0	0.0	
Q6. There is the release of smoke/gases during the operation of sawmill machines	SA	10	9	7	26[b]	17.3	p<0.01
	A	36	40	38	114[a]	76.0	
	D	4	1	5	10[c]	6.7	
	SD	0	0	0	0	0.0	
Q7. The degree of smoke released during the working period is high	SA	10	6	6	22[b]	14.7	p<0.01
	A	22	24	21	67[a]	44.7	
	D	18	20	23	61[a]	40.7	
	SD	0	0	0	0	0.0	
Q8. Temperature increases during work hours	SA	7	4	7	18[c]	12.0	p<0.01
	A	29	28	26	83[a]	55.3	
	D	14	18	17	49[b]	32.7	
	SD	0	0	0	0	0.0	

SA- Strongly Agree, A-Agree, D-Disagree, SD-Strongly Disagree, No significant difference (p> 0.05), *p < 0.05 (significant difference) **p < 0.01 (highly significant difference) ***p<0.001 (very high significant difference).

3.1.3 Adaptive capacity of sawmill workers

Table 3 shows the adaptive capacity of sawmill workers to protect themselves and improve their health while carrying out their daily activities. Question one (Q1) assessed workers' ability to afford personal protective equipment (PPE). The result shows that 66% of respondents agreed that they can afford to buy PPE, 17% strongly agreed, 17%. Disagreed, and 0% strongly disagreed. Using the chi-square goodness of fit, there was a very high significant difference (p<0.001) between respondents.

The result obtained from question two (Q2) shows that 68.7% agreed that sawmills as a wood processing industry can make PPE available for workers; 27.3% of the respondents strongly agreed to this, while 4% disagreed and 0% strongly disagreed. Using the chi square goodness of fit, there was a very high significant difference (p<0.001) between respondents.

The result obtained from question three (Q3) shows that 76% of respondents drink enough water to stay hydrated during working hours, 3% of respondents strongly agreed; 0.7% disagreed; and 0% strongly disagreed. Using the chi square goodness of fit, there was a very high significant difference (p<0.001) between respondents.

The result obtained from question four (Q4) shows that 77.3% of respondents take a shower and change into new clothes upon returning to their homes; 21.3% of respondents strongly agreed to taking their shower and changing into new clothes, while 1.3% disagreed and 0% strongly disagreed. Using the chi square goodness of fit, there was a very high significant difference (p<0.001) between respondents.

The result obtained from question five (Q5) shows that 61.3% of respondents eat fruits and supplements to improve their health; 3% of respondents strongly agreed to this, while

25.3% disagreed and 0%0 strongly disagreed. Using the chi square goodness of fit, there was a very high significant difference (p<0.001) between respondents.

The result of question six (Q6) shows that 69.3% of respondents think that air pollution is bad for health, 30.7% of respondents strongly agree, 0% of respondents don't agree, and 0% of respondents strongly disagree. Using the chi-square goodness of fit, there was a very high significant difference (p<0.001) between respondents.

Table 3. Adaptive capacity to air pollution

Questions	Response	Egor LGA (Ogida Sawmill)	Oredo LGA (Federal Sawmill)	Ovia Northeast LGA (Oluku Sawmill)	Frequency n=150	Percentage %	p-value
Q1. You have money to buy personal protective equipment to help reduce the risk of exposure to air pollutants	SA	10	6	10	26[b]	17.3	p<0.01
	A	34	37	28	99[a]	66	
	D	6	7	12	25[b]	16.7	
	SD	0	0	0	0	0	
Q2. The sawmill can help reduce the risk posed by coming in contact with air pollutants	SA	14	10	17	41[b]	27.3	p<0.01
	A	30	40	33	103[a]	68.7	
	SD	6	0	0	6[c]	4	
	D	0	0	0	0	0	
Q3. You drink enough water during the working period	SA	12	9	14	35[b]	23.3	p<0.01
	A	38	40	36	114[a]	76	
	D	0	1	0	1[c]	0.7	
	SD	0	0	0	0	0	
Q4. You take a shower and change into new cloths upon returning to your residence	SA	14	7	11	32[b]	21.3	p<0.01
	A	36	43	37	116[a]	77.3	
	D	0	0	2	2[c]	1.3	
	SD	0	0	0	0	0	
Q5. You eat fruits/ supplements to improve your health	SA	7	7	6	20[b]	13.3	p<0.01
	A	24	37	31	92[a]	61.3	
	D	19	6	13	38[b]	25.3	
	SD	0	0	0	0	0	
Q6. There is the negative impact of air pollution on health	SA	22	12	12	46[b]	30.7	p<0.01
	A	28	38	38	104[a]	69.3	
	D	0	0	0	0	0	
	SD	0	0	0	0	0	

SA- Strongly Agree, A-Agree, D-Disagree, SD-Strongly Disagree, No significant difference (p > 0.05), *p < 0.05 (significant difference) **p < 0.01 (highly significant difference) ***p<0.001 (very high significant difference)
Note: Similar letters (superscripts) indicate values that are not significantly different from each other (P>0.05)

3.1.4 Health risk perception of sawmill workers

Table 4 shows the variation observed in the frequency counts of the health risks experienced by sawmill workers. The highest frequency counts of respondents who agreed on having headache for question one (Q 1) had a percentage of 44%, followed by respondents who strongly agreed with a percentage of 24%, respondents who disagreed with a percentage of 32%, and respondents who strongly disagreed on having headache had a percentage of 0%. Using the chi-square goodness of fit, there was a very high significant difference (p<0.001) between respondents on having headache.

The highest frequency counts of respondents who agreed on having catarrh for question two (Q 2) had a percentage of 47.3%, followed by respondents who strongly agreed with a percentage of 35.3%, respondents who disagreed with a percentage of 17.3%, and respondents who strongly disagreed on having catarrh had a percentage of 0%. Using the chi-square goodness of fit, there was a very high significant difference (p<0.001) between respondents on had catarrh.

The highest frequency counts of respondents who agreed on having a cough for question three (Q 3) had a percentage of 35.3%, followed by respondents who strongly agreed with a percentage of 24%, respondents who disagreed with a high percentage of 40.7%, and respondents who strongly disagreed on having cough had a percentage of 0%. Using the chi square goodness of fit, there was a very high significant difference (p<0.001) between respondents on having cough.

The highest frequency counts of respondents who agreed on having chest pain for question four (Q 4) had a percentage of 30%, followed by respondents who strongly agreed with a percentage of 17.3%, Respondents who disagreed had a high percentage of 52.7%, while respondents who strongly disagreed on having chest pain had a percentage of 0%. Using the chi-square goodness of fit, there was a very high significant difference (p<0.001) between respondents having chest pain.

The highest frequency counts of respondents who strongly agreed on having a health challenge associated with bronchitis for question five (Q 5) had a percentage of 66%, followed by respondents who agreed with a percentage of 0.7%, respondents who disagreed with a high percentage of 30%, and respondents who strongly disagreed on having health challenges associated with coughing with a percentage of 3.3%. Using the chi square goodness of fit, there was a very high significant difference ($p<0.001$) between respondents on the health challenges associated with bronchitis.

The highest frequency counts of respondents who strongly agreed on having asthma for question six (Q 6) had a percentage of 7.3%, followed by respondents who agreed with a percentage of 4.7%. Respondents who disagreed had a high percentage of 82.7%, while respondents who strongly disagreed on having asthma had a percentage of 5.3%. Using the chi square goodness of fit, there was a very high significant difference ($p<0.001$) between respondents on having asthma.

The highest frequency counts of respondents who agreed on having eczema for question seven (Q 7) had a percentage of 23.3%, followed by respondents who strongly agreed with a percentage of 19.3%. Respondents who disagreed had a high percentage of 52%, while respondents who strongly disagreed on the skin disorder associated with eczema had a percentage of 5.3%. Using the chi-square goodness of fit, there was a very high significant difference ($p<0.001$) between respondents on had eczema.

The highest frequency counts of respondents who strongly agreed and agreed on having eye irritation for question eight (Q 8) were similar, with a percentage of 47.3%, followed by respondents who disagreed, who had a percentage of 5.3%, while respondents who strongly disagreed on having eye irritation had a percentage of 0%. Using the chi-square goodness of fit, there was a very high significant difference ($p<0.001$) between respondents on challenges of eye irritation.

The highest frequency counts of respondents who strongly agreed on having throat irritation for question nine (Q 9) had a percentage of 25.3%, respondents who agreed had a percentage of 24.7%, respondents who disagreed had a high percentage of 48%; and respondents who strongly disagreed on having throat irritation had a percentage of 2%. Using the chi-square goodness of fit, there was a very high significant difference ($p<0.001$) between respondents on had throat irritation.

The highest frequency counts of respondents who strongly agreed on having health challenges associated with sneezing for question ten (Q 10) had a percentage of 37.3%, respondents who agreed had a percentage of 27.3%, respondents who disagreed had a percentage of 33.3%; and respondents who strongly disagreed on having health challenges associated with sneezing had a percentage of 2%. Using the chi-square goodness of fit, there was a very high significant difference ($p<0.001$) between respondents on challenges of sneezing.

The frequency counts for question eleven (Q 11) of respondents who strongly agreed and also agreed on the incidence of cancer among sawmill workers were similar, with a percentage of 0%; respondents who disagreed had a percentage of 88.7%; and respondents who strongly disagreed on the incidence of cancer among sawmill workers had a percentage of 11.3%. Using the chi square goodness of fit, there was a very high significant difference ($p<0.001$) between respondents on the incidence of cancer among sawmill workers.

Table 4. Health risk reported by respondents.

Questions	Response	Egor LGA (Ogida Sawmill)	Oredo LGA (Federal Sawmill)	Ovia Northeast LGA (Oluku Sawmill)	Frequency n=150	Percentage %	p-value
Q1. Do you often have headache	SA	16	10	10	36[b]	24.0	
	A	16	25	25	66[a]	44.0	p<0.05
	D	18	15	15	48[b]	32.0	
	SD	0	0	0	0	0.0	
Q2. Do you often have catarrh	SA	23	15	15	53[b]	35.3	
	A	23	24	24	71[a]	47.3	p<0.01
	D	4	11	11	26[c]	17.3	
	SD	0	0	0	0	0.0	
Q3. Do you often have cough	SA	16	10	10	36[b]	24.0	
	A	19	17	17	53[a]	35.3	p<0.05
	D	15	23	23	61[a]	40.7	
	SD	0	0	0	0	0.0	
Q4. Do you often have often have chest pain	SA	14	6	6	26[c]	17.3	
	A	15	15	15	45[b]	30.0	p<0.01
	D	21	29	29	79[a]	52.7	
	SD	0	0	0	0	0.0	
Q5. Have you ever had bronchitis	SA	1	0	0	1[c]	0.7	
	A	1	49	49	99[a]	66.0	p<0.01
	D	43	1	1	45[b]	30.0	
	SD	5	0	0	5[c]	3.3	

Table 4. continuation: Health risk reported by respondents.

Questions	Response	Egor LGA (Ogida Sawmill)	Oredo LGA (Federal Sawmill)	Ovia Northeast LGA (Oluku Sawmill)	Frequency n=150	Percentage %	p-value
Q6. Have you ever had asthma	SA	7	2	2	11[b]	7.3	
	A	1	3	3	7[b]	4.7	p<0.01
	D	36	44	44	124[a]	82.7	
	SD	6	1	1	8[b]	5.3	
Q7. Do you often have Eczema	SA	13	8	8	29[b]	19.3	
	A	11	12	12	35[b]	23.3	p<0.01
	D	22	28	28	78[a]	52.0	
	SD	4	2	2	8[c]	5.3	
Q8. Do you often have eye irritation	SA	31	20	20	71[a]	47.3	
	A	17	27	27	71[a]	47.3	p<0.01
	D	2	3	3	8[b]	5.3	
	SD	0	0	0	0	0.0	
Q9. Do you often have throat irritation	SA	16	11	11	38[b]	25.3	
	A	7	15	15	37[b]	24.7	p<0.01
	D	26	23	23	72[a]	48.0	
	SD	1	1	1	3[c]	2.0	
Q10. Do you often have sneezing	SA	34	0	22	56[a]	37.3	
	A	15	0	26	41[b]	27.3	p<0.01
	D	1	47	2	50[a]	33.3	
	SD	0	3	0	3[c]	2.0	
Q11. Have sawmill workers ever had cancer	SA	0	0	0	0	0.0	
	A	0	0	0	0	0.0	p<0.01
	D	39	47	47	133[a]	88.7	
	SD	11	3	3	17	11.3	

SA- Strongly Agree, A-Agree, D-Disagree, SD-Strongly Disagree, No significant difference ($p > 0.05$), *$p < 0.05$ (significant difference) **$p < 0.01$ (highly significant difference)
***$p<0.001$ (very high significant difference) Note: Similar letters (superscripts) indicate values that are not significantly different from each other ($P>0.05$)

3.2 Discussion

The socio-demographic characteristics of the respondents showed that the majority of the respondents were males and this was not out of place considering the strenuous and dusty nature of the job. Similar male dominance was found among sawmill workers in Kwara State, Nigeria (Agbana et al., 2016). Most sawmill workers in this study are 31–40 years old, contrary to the results found by Sutcu and Semerci (2019). Additionally, thirty-four percent of the workforce has worked with the same sawmill for at least 10 years, similar to the report of Johnson and Umoren (2018), who discovered a high percentage (45.5%) of workers who have worked at the same sawmill for 10 years.

The results of this research supported earlier claims made by Adelagun et al. (2012) that sawmilling activities contribute to air pollution within the sawmill environment. Likewise, Olawuni and Okunola (2014), in their study carried out in Ile-Ife, Nigeria, ascertained that smoke is a major pollutant around sawmills and the second-most significant environmental issue in sawmills resulting from the burning of sawmill waste. Sawdust being burned every day sends smoke and ash into the air, which can be spread by the wind. This pollutes the air and makes the environment bad, and Masoudi et al. (2020) generally noted that the air we breathe is not pure. The results obtained from this study are in line with the study of Oguntoke et al. (2019) on the assessment of air pollution and health hazards associated with sawmills and municipal waste burning in Abeokuta Metropolis, Nigeria. As a result, we can see that effects like smoke disturbance, air pollution, and bad smell were ranked as almost certain in sawmill environment (Oguntok et al., 2019). Also, a lot of smoke is emitted into the air from the burning of wood and sawdust across the three sawmills. Wood and wood dust burning contribute smoke to the atmosphere, and this smoke produces dust and soot composed of tiny particles. Burnt wood produces gases and fine microscopic particles. These microscopic particles can get into the eyes and respiratory system, where they can cause health problems such as burning eyes, runny noses, and illnesses.

Akinbode and Owoeye (2019) stated that among the most frequent health risks faced by sawmill workers in Nigeria are occupational hazards brought on by inhaling wood dust, noise, and heat. Temperature has a lot to do with how close you are to heat sources, such as where sawdust is burned or where sawmill machines make heat. Temperature is a major factor that determines human comfort, work performance, and efficiency (Sütük and Semerci, 2019). Employees are less productive when the temperature in the room is too low or too high. In a study carried out by Sutcu and Semerci (2019)

on the health problems of sawmill workers in Turkey who process red pine, it was found that about 40% of respondents said they felt very hot during working hours.

Agu et al, (2016) in their study on health problems among sawmill workers in Abakaliki and workplace risk assessment, found that 85.3% of respondents were aware of PPE. However, only 39.5% of respondents use PPE, which shows that awareness doesn't mean use. During the walk-through survey, it was noticed that personal protective equipment (PPE) wasn't used very much in any of the sawmills visited. However, a lot of workers have enough money to buy PPE to protect themselves as a control measure. It was also found that employers can provide PPE and that workers know that the air pollution around sawmills can be bad for their health. A lot of workers always stay hydrated to boost their immune systems take a shower and change into new clothes to prevent skin diseases like eczema, while others take supplements to improve their health.

Adeoye et al. (2014) opined that workers don't use PPE because they can't afford it and that employers are responsible for giving workers PPE that is right for the risk involved and the conditions in which it will be used. There are a lot of particles in the air around sawmills, which could cause health problems. If workers don't take precautions, like wearing PPE, they are more likely to be vulnerable to health hazards.

The study reviews that the most common work-related hazards experienced by the sawmill workers were headache, catarrh, cough, chest pain, bronchitis, asthma, eczema, eye irritation, throat irritation, and sneezing. The lack of eye protection for the respondents may be the cause of eye irritation in the study group. This finding was similar to what was obtained by Agbana et al. (2016) in a related study done in Kwara state, where the study reported that one of the most common self-reported health problems by respondents was eye irritation. The findings of this research are in line with those of Aletan and Garba (2022) that health problems associated with sawmill workers include headaches and respiratory ailments, among others. Jagtap and Deshmukh (2018) found that conjunctivitis, rhinitis, hearing loss, acute respiratory infections, asthma, chronic bronchitis, and dermatitis were common illnesses among sawmill workers. In their research on occupational hazards and health problems among sawmill workers in Osun State, Nigeria, Adeoye et al. (2015) found that coughing, chest pain, and sneezing were among the most common symptoms.

From this research, there was no report of cancer among sawmill workers. However, sawmill workers in factories that process wood regularly come in contact with allergenic, immunotoxin, noxious, carcinogenic, and toxic substances that can be produced by wood dust, bacteria, and fungi that grow on timber, as reported by Mumuni (2015). After being exposed to these chemicals for a long time, people can get asthma, allergic rhinitis, bronchial hyperreactivity, contact dermatitis, allergic alveolitis, and cancer (Mumuni, 2015).

4.0 Conclusion

The study suggests that the air quality around sawmills is poor, this is indicative by the various associated health risks reported by the sawmill workers as well as correlative findings from previous studies. This study has shown that the air around sawmills is polluted and therefore impacts the health of workers. It further shows that the sawmill sites do not pay much attention to the provision and use of PPE, as they are generally not provided. It is imperative to adopt precautionary measures to reduce and or eliminate the incidence of these health risks. The study concludes that the sawmill workplace is not safe and poses a grave health risk to sawmill workers.

4.1 Recommendation

The recommendations from this study include:

I. The researchers of the study recommend that further studies be carried out using scientific instrumentation for air quality analysis to further buttress the findings of this study.

II. Workers in sawmills should be given the right personal protective equipment (PPE) and be mandated to wear them at all times during work hours.

III. Raise awareness about the health risks that pollutants pose to sawmill workers.

IV. Reduce air pollution from sawmills by creating monitoring and enforcement measures and regulations. Air quality monitoring should be carried out consistently to check air quality, and the enforcement agency should make sure sawmill workers adhere to the permissible limit of air pollution.

V. Appropriate measures should be implemented to eliminate waste burning in sawmills; controlled waste burning in incinerators can also be implemented to reduce pollutant emissions.

Acknowledgments

We wish to acknowledge Dr. Biose Ekene for his statistical expertise in presenting the results of this research.

References

Adelagun, R.O., Berezi, E.P., Akintunde, O.A. (2012). Air pollution in a sawmill industry: the Okobaba (Ebute-Meta, Lagos) experience. Journal of Sustainable Developmental and Environmental Protection 2(2): 29 - 36.

Adeoye, O.A., Adeomi, A.A., Abodunrin, O.L., Olugbenga-Bello, A., Abdulsalam, S.T. (2015). Awareness of occupational hazards and health problems among sawmill workers in Osun state, Nigeria. International Journal of Research and Review 2(1):1 - 14.

Adeoye, O. A., Adeomi, A. A., Israel, O. K., Temitayo-Oboh, A. O., Olarewaju, S. O. (2014). Wood dust particles: Environmental pollutant in Nigerian sawmill industries. Journal of Environmental and Occupational Health 3(2): 77 - 80.

Agbana, B.E., Joshua, A.O., Daikwo, M.A., Metiboba, L.O. (2016). Knowledge of occupational hazards among sawmill workers in Kwara state, Nigeria. Nigerian Postgraduate Medical Journal 23(1): 25.

Agu, A.P., Umeokonkwo, C.D., Nnabu, R.C. and Odusanya, O.O. (2016). Health problems among sawmill workers in Abakaliki and workplace risk assessment. Journal of Community Medicine and Primary Health Care 28(2): 1 - 10.

Akinbode, T., and Owoeye, J.O. (2019). Occupational Hazards and Safety of Sawmill Operators in Ogbese Ondo State, Nigeria. Sustainable Development Research 1(1): 24 – 24.

Aletan, O.E., and Garba, E.O. (2020). Environmental Implication of Sawmill Industries on Adjoining Residents in Kwara State, Nigeria. International Journal of Scientific Research in Multidisciplinary Studies 6(3): 28-31.

Dimuna, K.O., and Olotuah, A.O. (2020). Analysis of residents' satisfaction levels with housing and residential environment of six occupied housing Estates in Benin City, Edo State, Nigeria. Academic Journal of Interdisciplinary Studies 9(1): 179 - 179.

Ediagbonya, T.F., Tobin, A.E., Ukpebor, E.E. (2013). The level of suspended particulate matter in the wood industry (sawmills) in Benin City, Nigeria. Journal of Environmental Chemistry and Ecotoxicology 5(1): 1 - 6.

EPA South Australia. (2001). ''Operational guidelines for wood working'' draft document of the Australian Environmental Protection Agency, 1–3. http://www.epa.sa.gov.au/documents.php. (Dec. 8, 2021).

Faremi, F.A., Ogunfowokan, A.A., Mbada, C., Olatubi, M.I., Ogungbemi, A. V. (2014). Occupational hazard awareness and safety practices among Nigerian sawmill workers. International journal of medical science and public health 3(10):1244 - 1248.

Héroux, M.E., Anderson, H.R., Atkinson, R., Brunekreef, B., Cohen, A., Forastiere, F., Hurley, F., Katsouyanni, K., Krewski, D., Krzyzanowski, M., Künzli, N. (2015). Quantifying the health impacts of ambient air pollutants: recommendations of a WHO/Europe project. International journal of public health 60(5): 619 - 627.

Jagtap, A.A. and Deshmukh, J. (2018). Comparative study of morbidities in sawmills workers from central India: a cross-sectional study. International Journal of Community Medicine and Public Health 5(7): 2846 – 2852.

Johnson, O.E. and Umoren, Q.M., (2018). Occupational hazards and health problems reported by workers in a Sawmill in Uyo, Nigeria. Journal of Environmental and Occupational Health 7(2):17-24.

Masoudi, M., Ordibeheshti, F. and Rajai Poor, N. (2019). Status and prediction of nitrogen oxides in the air of Shiraz city, Iran. Jordan Journal of Earth and Environmental Sciences 10: 85-91

Mumuni, M. (2015). Respiratory Health Problems among Sawmill Workers at the Timber Market, Accra (Doctoral dissertation) University of Ghana.

Odibo A.A., 1Nwaogazie I.L., Achalu E.I., Ugbebor J.N. (2018). Assessment of Occupational Hazards in Sawmills: A Case Study. International Journal of Health, Safety and Environments 4 (2):203 – 217.

Odunaike, R.K., Laoye, J.A., Alausa, S.K., Ijeoma, G.C., Adelaja, A.D. (2008). Radiation emission characterization of waste dumpsites in the city of Ibadan in Oyo State of Nigeria. Research Journal of Environmental Toxicology 2(2): 100 – 103.

Oguntoke, O., Emoruwa, F.O., and Taiwo, M.A. (2019). Assessment of air pollution and health hazard associated with sawmill and municipal waste burning in Abeokuta Metropolis, Nigeria. Environmental Science and Pollution Research 26(32): 32708-32722.

Raimi, M.O., Adeolu, A.T., Enabulele, C.E., Awogbami, S.O. (2018). Assessment of Air Quality Indices and its Health Impacts in Ilorin Metropolis, Kwara State, Nigeria. Science Park Journals of Scientific Research and Impact 4(4): 60 - 74.

Raimi, M.O., Adio, Z., Emmanuel, O.O., Samson, T.K., Ajayi, B.S. and Ogunleye, T.J. (2020). Impact of sawmill industry on ambient air quality: A Case Study of Ilorin Metropolis, Kwara State, Nigeria. Energy and Earth Science 3(1): 2578 – 1359.

Rückerl, R., Schneider, A., Breitner, S., Cyrys, J. and Peters, A. (2011). Health effects of particulate air pollution: a review of epidemiological evidence. Inhalation toxicology 23(10): 555 - 592.

Sutcu, A., and Semerci, N.T. (2019). Occupational health problems of sawmill workers processing red pine in Turkey. Applied Ecology and Environmental Research 17(4): 7625 - 7639.

Vallieres, E., Pintos, J., Parent, M., Siemiatycki, J. (2015). Occupational exposure to wood dust and risk of lung cancer in two population-based case-control studies in Montreal, Canada. Environmental Health 14(1): 2 – 8.

Appendix

UNIVERSITY OF BENIN (UNIBEN)

RISK ASSESSMENT TOOL

SECTION ONE

Instruction: Please tick ☐ the most appropriate response for all the questions

Name of LGA…….
Name of Sawmill…….....
Date questionnaire was completed……..

BACKGROUND CHARACTERISTICS		
Q1	Sex of Respondent	Male ☐ Female ☐
Q2	Age range	18-20years…… ☐ 21-24 years ……... ☐ 25-30 years …… ☐ 31-40 years …… ☐ 41-50 years …… ☐ 50-60 years …… ☐
Q3	When did you start working at this sawmill	1- 5 months…….. ☐ 5months -1year…… ☐ 1 - 2 years…….. ☐ 2 - 4 years…… ☐ 4 - 6 years…… ☐ 6 - 8 years…… ☐ 10 years and above…… ☐

SECTION TWO (PART A, B, AND C)

QUESTIONNAIRE FOR CERTAINTY OF AIR POLLUTION, ADAPTIVE CAPACITY, AND HEALTH IMPLICATIONS ON EXPOSURE TO POLLUTANTS

PART A

Instruction: Please tick ☐ the most appropriate response for all the questions

S/N	CERTAINTY OF AIR POLLUTION AROUND THE SAWMILL	STRONGLY AGREE	AGREE	DISAGREE	STRONGLY DISAGREE
1	The work environment gets dusty during working hours				
2	The quantity of dust particles produced during work hours intense				
3	Particles/sawdust stick to the body during the working process				
4	Particles/sawdust when inhaled cause risk to health				
5	The sawmill machine requires diesel/fuel to operate				
6	There is the release of smoke/gases during the operation of sawmill machines				
7	The degree of smoke released during the working period is high				
8	Temperature increases during work hours				

PART B

Instruction: Please tick ☐ the most appropriate response for all the questions

S/N	ADAPTIVE CAPACITY TO AIR POLLUTION IN SAWMILL	STRONGLY AGREE	AGREE	DISAGREE	STRONGLY DISAGREE
1	You have money to buy personal protective equipment to help reduce the risk of exposure to air pollutants				
2	The sawmill can help reduce the risk posed by coming in contact with air pollutants				
3	You drink enough water during the working period				
4	You take a shower and change into new cloths upon returning to your residence				
5	You eat fruits/supplements to improve your health				
6	There are negative impacts of air pollution on health				

PART C

DO YOU EXPERIENCE ANY OF THESE HEALTH CHALLENGES?

Instruction: Please tick ☐ the most appropriate response for all the questions

S/N	HEALTH IMPLICATION	STRONGLY AGREE	AGREE	DISAGREE	STRONGLY DISAGREE
1	Headache				
2	Catarrh				
3	Cough				
4	Chest pain				
5	Respiratory problems				
6	Asthma				
7	Eczema				
8	Eye irritation				
9	Throat irritation				
10	Sneezing				

JJEES

JJEES (2023) 14 (4): 280-286
ISSN 1995-6681

Jordan Journal of Earth and Environmental Sciences

Remote Sensing and Aeromagnetic Study in Part of Sheet 244 Ado Ekiti Northeast for Groundwater Development, Nigeria

Hussain Olanrewaju Abubakar[1], Olusegun Omoniyi Ige[2], Saminu. Olatunji[3]

[1and3]*Department of Geophysics, Faculty of Physical Sciences, University of Ilorin, PMB 1515 Ilorin*
[2]*Department of Geology and Mineral Sciences, University of Ilorin, PMB 1515 Ilorin*

Received March 28, 2022; Accepted September 7, 2023

Abstract

The study area is located in the northern part of sheet 244 Ado Ekiti northeast of southwestern Nigeria to identify groundwater targets that could assist in improving the quality of life of rural communities. Airborne magnetic data, acquired from Nigerian Geological Survey Agency (NGSA), and the remote sensing data were interpreted to identify dykes, lineaments, and magnetic sources that could control groundwater occurrences. Data processing applied to the total magnetic intensity (TMI) includes residual magnetic intensity (RMI), reduction to the pole (RTP), first vertical derivative (FVD), vectorized first vertical derivative (VFVD), and analytical signal. Remote sensing data yielded five thematic maps, viz: geologic, land use, slope, elevation, and drainage density map. The length, and parallelism of magnetic lineaments in some parts of the area suggest emplacement under a tensional stress field along pre-existing zones of weakness. Lineaments extracted from the airborne magnetic data and satellite imagery data were superimposed on drainage lines to investigate the relative importance of structural features controlling the distribution of surface water and groundwater. In addition, the normalized difference vegetation index (NDVI), used in identifying areas of vegetation banding, enabled inferences of fracture zones and high moisture content in the soil. Integration of lineaments derived from aeromagnetic data and Landsat imagery together with the NDVI was able to identify the northern and central-eastern parts of the study area to be more prospective for groundwater occurrence, while the southern and south-western parts of the area are dry with no surface manifestation of groundwater.

Keywords: *Remote sensing, Aeromagnetic, Geology, Groundwater.*

1. Introduction

A typical use of Geophysics as a branch of geosciences is for hydrocarbon exploration typically at a depth greater than 1000 m. significant technological advances have been made in industries over the years, especially with seismic reflection techniques. In contrast, near-surface Geophysics for groundwater investigations is usually restricted to a depth less than 250 m below the surface and developments have not concentrated on one specific geophysical technique (Oluwatoyin and Ola-Buraimo 2022).

Water is a basic necessity of life which constitutes two-thirds of the whole body of human beings and coincidentally, that of the total earth mass. Underground water constitutes an important source of supplying drinking water. Virtually, every activity of man requires the use of water; whether domestically, industrially, in experiments in laboratories, or in any other forms of human daily activities. Wells drilled without proper geophysical and hydro-geological study often face failure challenges. In hard rock areas, groundwater is found in the cracks and fractures of the local rocks. Groundwater yield depends on the size of fractures and their interconnectivity. Groundwater generally occurs in rocks that are permeable enough to allow the accumulation and circulation along the geologic micro-structures. Generally, the information concerning the lithology, stratigraphic sequence, geologic structures, and hydro-geological characteristics of the subsurface materials can be provided through the application of the Electrical resistivity method (Koefoed, 1979). A large proportion (47%) of people in sub-Saharan Africa live without access to safe water sources in rural areas (Joint Monitoring Programme, 2008). The need for sustainable development and management of water resources, particularly groundwater resources, remains a major priority, especially within the context of climate variability, population growth, and pressures to increase food production (United Nations (UN), 2000).

2. Study Area

The area is located in the Northeastern part of Ekiti State, Southwestern Nigeria. It lies between geographic coordinates of Nothing 5^0 41' 40 "E and $5^0$43' 20" E and latitudes 7^0 31'50" N and 7° 62' 50" N (Figure 1). The topographic elevation in the area ranges from 345.0 to 375.0 m above mean sea level. The study covers an area extent of about 21000 km^2. The study area is located within the tropical rainforest of Southwestern Nigeria with dry and wet seasons. The wet season starts around mid-March and ends in October with an average annual rainfall of between 1500 mm and 2100 mm while the dry season starts around November and ends in March. Further, the average maximum temperature is about 33 °C (Ileoje, 1980).

* Corresponding author e-mail: abubakar.hussainolanrewaju3@gmail.com

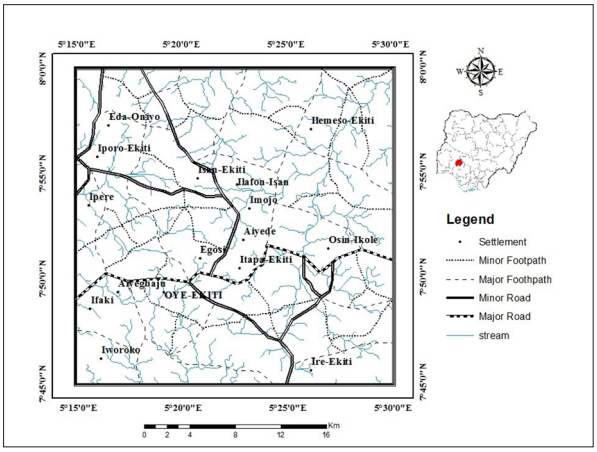

Figure 1. Location map of the study area.

3. Geology and Hydrogeology

The study area is underlain by rocks of the Precambrian basement complex of southwestern Nigeria (Rahman, 1976). It falls within three major lithostratigraphic units in which Gneiss and Granites are more pronounced. The Granitic rocks dominate the area (Figure 2). It is coarse-grained corresponding to the Precambrian age and is called Porphyritic Granite. The Granites occur as intrusive in low-lying outcrops within the Biotite Gneiss. Other rocks can be found in migmatite charnockite and other intrusive igneous rocks. In basement terrain, groundwater occurs in the weathered basement and the joints, fractures, or faults within the bedrock (Ademilua and Olorunfemi, 2000). The rock consists of Precambrian metasediments, Migmatites, Gneisses, Granites, and other intrusive igneous rock.

The Geomorphology of the study area, consisting of lowlands and extensively forested plain land, form high hills are prominent at Ire, Itapa, and Osin. Oye Ekiti has a low relief with the undulating surface formed as a result of differential weathering and erosion and the area is surrounded by hills which are moderate heights. Some of the hills are characterized by steep sides and deep valleys. It falls within the tropical rainforest zone of southwestern Nigeria. It has a tropical climate characterized by alternating dry and wet seasons. Rainfalls serve as the main source of groundwater replenishment (Akinola et al, 1986; Mohammed and Taufiq, 2022; Rzger Abdula et. al., 2021).

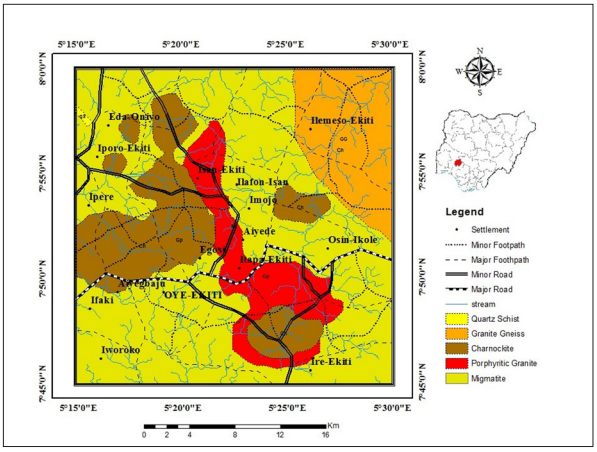

Figure 2. Geology map of the study area.

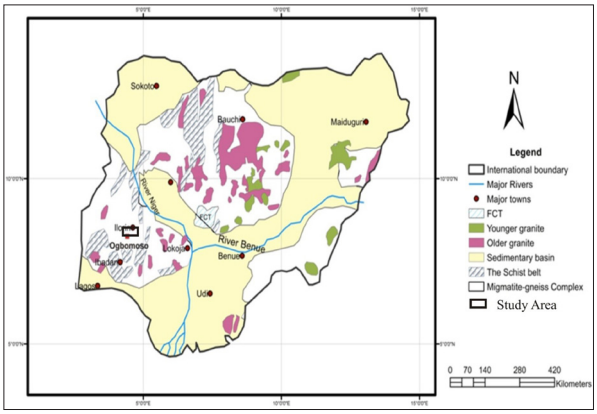

Figure 3. Geological Map of Nigeria showing the Study Area (Geological Survey of Nigeria, 2006).

4. Material and Methods

This study made use of both primary and secondary data. The primary data included Landsat 8 OLI and ASTER Digital Elevation Model. The secondary data included Lineament density maps and geological maps of the study area (Table 1). ArcGIS, Rockworks, ENVI, and PCI Geomatics Software were used for data processing.

Table 1. Data types and sources.

S/N	Data	Source	Scale
1	Landsat 8 OLI/TIRS	Glovis (http://glovis.usgs.gov)	30 m
2	ASTER DEM	Glovis (http://glovis.usgs.gov)	90m
3	Geological Map	Nigeria Geological Survey Agency	1:100,000
4	Soil Map	Center for World Food Studies (SOW-UV) (1997)	1:1,300,000
5	Topographical Map	Nigeria Geological Survey Agency (NGSA)	1:50,000

4.1 Method

The procedure adopted for this research comprised desk studies, fieldwork, and validation of findings. The steps involved are also presented in Figure 3. Desk studies involved the studying of literature and previous works on groundwater across Ekiti, Nigeria, and the world in general. Fieldwork involved geological mapping as well as a geophysical survey. While validation involves comparing the results of the outcomes of the GIS analysis with the geophysical survey.

To develop thematic maps of groundwater potential of the study area, lineament and land use/land cover maps were derived from the Landsat 8 OLI/TRS image using ENVI, PCI Geomatica, Rockworks, and ArcGIS software (Figure 3). Maximum likelihood classification (MLC) was used to produce the land use/land cover map of the study area. Elevation, slope, and drainage maps were produced with the spatial analyst tool and the Archydro tool of ArcGIS respectively. To derive the thematic maps from the secondary

data, hard copy maps (geology and soil) were scanned and imported into the ArcGIS software then georeferenced to the World Geodetic System (WGS 84) coordinate system.

The weighting of the thematic maps was carried out using the Analytical Hierarchical Process (AHP). The AHP calculates weights based on the consideration of each theme's influence on groundwater accumulation by the technique of pair-wise comparison to compare the influence of one criterion with another on a scale of 1 to 9. Thus, 1 denotes equal importance between a pair of criteria, 3 means moderately more important, 5 is strongly more important, 7 is very strongly more important, and 9 implies extremely more importance of one criterion to the other. Meanwhile, 2, 4, 6, and 8 were used as intermediate values (Nigerian College of Aviation, 1999). The scale for comparison was determined based on previous studies (Sarup et al., 2011).

Mapping of the groundwater potentials of the study area was done by the weighted index overlay method in the ArcGIS. Before the overlay operations, the next step after weighing the maps was to carry out reclassification. This was done by assigning the new weight values to the maps' sub-units (sub-criteria) computed from the AHP. The reclassify tool in the spatial analyst tool of ArcGIS was used for this task. The groundwater potential zones map of the study area was produced by overlaying all thematic layers using the weighted index overlay.

Groundwater Potential Zone Map (GWPZ) = $\sum_{i,j=1}^{8} WiXj$

Where; Wi = % weight for each thematic map, Xj= reclassified map

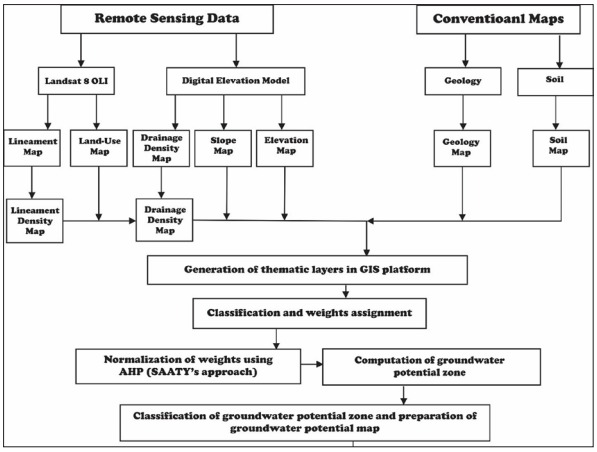

Figure 4. Flowchart for delineating groundwater potential in Oye-Ekiti and environs.

5. Result

5.1 Remote Sensing

5.1.1 Surface Lineament Analysis from DEM Image

Results obtained from DEM interpretation are discussed in other to demonstrate the effectiveness of remote sensing in lineament analysis for groundwater exploration study which is mostly to delineate zones that have groundwater potentials in the area of study. Figure 5 shows the digital elevation map of the study area, it can be seen that the area is characterized by high and low terrains. The mid-western part of the area has the highest elevation, this area consists of both charnockite and granite outcrops, occurring in the form of hills, boulders, ridges, and whaleback structures. This is responsible for the high elevation in the area. The low-elevation terrains on the other hand are characterized by migmatite and are mostly seen at the upper central and eastern part of the area.

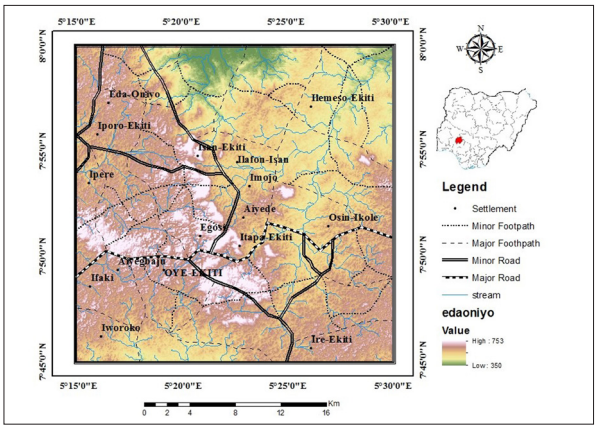

Figure 5. Digital Elevation Map of the study area.

Figure 6 shows the surface lineaments extracted from the DEM and imposed on the geologic map of the study area. It can be seen that lineaments are well distributed within the migmatites and granite gneiss in the study area, apart from the mid-western part of the area that is underlain by charnockite and granite, every other part has lineaments. The high concentrations of lineaments within the migmatite can be attributed to the polycyclic deformation that these rock types have gone through, creating a series of joints, faults, and fractures that can serve as openings for groundwater accumulation. This can also explain why the younger rocks have fewer lineaments within them, most especially in the mid-western part of the area.

Figure 7 shows the general orientation of the lineaments extracted from the Digital Elevation Model of the area of study which can be said to be closely related to tectonic activities such as fractures, faults, joints, etc. There is a huge concentration of lineaments in the NW-SE and the NE-SW directions, these fractures are favorable for groundwater locations (Olasehinde, 1999; Olasehinde et al., 1990; Obeidat and Awawdeh, 2021), other minor orientations include E-W, NNE-SSW, NNW-SSE, NEN-SWS, and ENW-WSW.

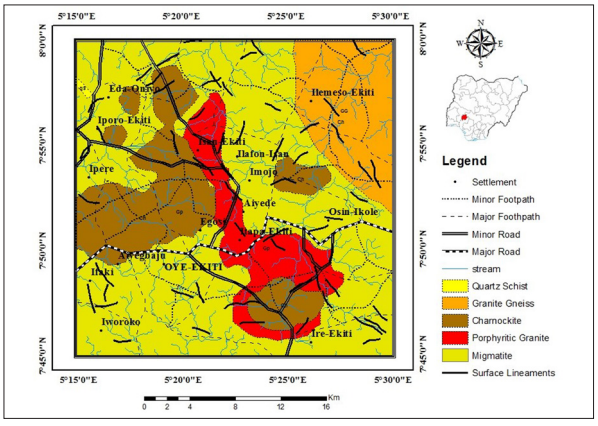

Figure 6. Extracted lineaments from DEM imposed on Geological Map of the area.

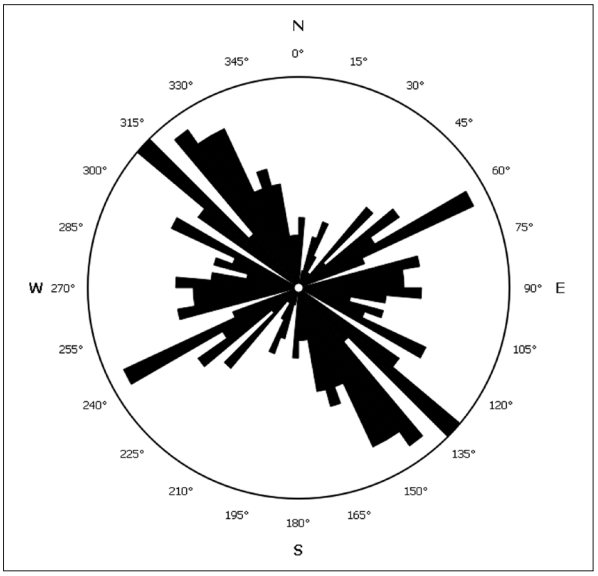

Figure 7. General orientation of Lineaments from DEM.

5.2 Aeromagnetic data Interpretation

An airborne magnetic survey is a supportive geophysical method for mapping subsurface bedrock geology (lithology) and structures due to variations in the magnetic susceptibility of rocks (Olasehinde and Raji, 2007). According to (Olasehinde and Ige, 2011), where the bedrock geology cannot be mapped due to thick jungle, swamp, deep weathering, or sand cover, aeromagnetic data can give information on the hidden geology using methods of inference that are similar to those used in photo geological interpretation (such as enhancement filters). One of the main goals for the use of magnetic data is to delineate geological structures and to some extent delineate lithology (Olasehinde and Ige, 2011) by gridding and applying enhancement tools.

Rocks of the study area showed different aeromagnetic responses that can be related to their lithology and tectonic activities that have resulted in the geological structures (e.g. folds, faults, and fractures) in the area. Linear features (geological structures) associated with the volcanic rocks are observed as moderately low and low magnetic signatures. The pink colors or characters in the presented figures are areas of high magnetic signature, whereas the blue characters represent areas of low magnetic signature.

5.2 Aeromagnetic data Interpretation

An airborne magnetic survey is a supportive geophysical method for mapping subsurface bedrock geology (lithology) and structures due to variations in the magnetic susceptibility of rocks (Olasehinde and Raji, 2007). According to (Olasehinde and Ige, 2011), where the bedrock geology cannot be mapped due to thick jungle, swamp, deep weathering, or sand cover, aeromagnetic data can give information on the hidden geology using methods of inference that are similar to those used in photo geological interpretation (such as enhancement filters). One of the main goals for the use of magnetic data is to delineate geological structures and to some extent delineate lithology (Olasehinde and Ige, 2011) by gridding and applying enhancement tools.

Rocks of the study area showed different aeromagnetic responses that can be related to their lithology and tectonic activities that have resulted in the geological structures (e.g. folds, faults, and fractures) in the area. Linear features (geological structures) associated with the volcanic rocks are observed as moderately low and low magnetic signatures. The pink colors or characters in the presented figures are areas of high magnetic signature, whereas the blue characters represent areas of low magnetic signature.

5.3 Subsurface Lineaments from First Vertical Derivative (1VD)

To observe the near-surface source magnetic features that are associated with geological structures, the first vertical derivative filter upwardly continued to 100 m was applied to the RTP grid. The 1VD filter helped decrease broad and more regional anomalies and rather enhanced local magnetic responses which are interpreted as structures in the area. Most of the structures delineated in the area coincided with already delineated structures in the Digital Elevation Model (DEM) map of the area. Prominent among these delineated structures is the northeast-southwest trending lineament at the eastern part of the map.

Figure 8 is a 1VD image of the study area upwardly continued to 100 m displaying near-surface source magnetic features that are associated with geological structures while Figure 9 is a vectorized map of the structures identified in Figure 8 imposed on the geological map of the area, while Figure 10 shows the orientation of the subsurface lineaments. The 1VD and Upward Continuation operators have helped attenuate broad, more regional anomalies and enhanced local, more delicate magnetic responses because of their sensitivity to shallow magnetic source bodies and contacts.

Assessment of the 1VD image of the area upwardly continued to 100 m (Figure 8) depicts a clear enhancement of observed structural features such as faults, folds, joints, and fractures. The general trends of the structures are in the NE-SW direction, while some others exist in the E-W and N-S directions, typical of the basement complex of Nigeria, it also corresponds with the observed structural trend observed on the field and on the DEM map. Unlike in the DEM map, there are more lineaments in the NE-SW directions. The majority of these structures may have been developed due to the various episodes of deformation that the migmatites have gone through, while others may be due to the stress developed during the emplacement of the granitoids. These structures may play openings for groundwater concentrations. These zones should be the sites of focus for groundwater exploration.

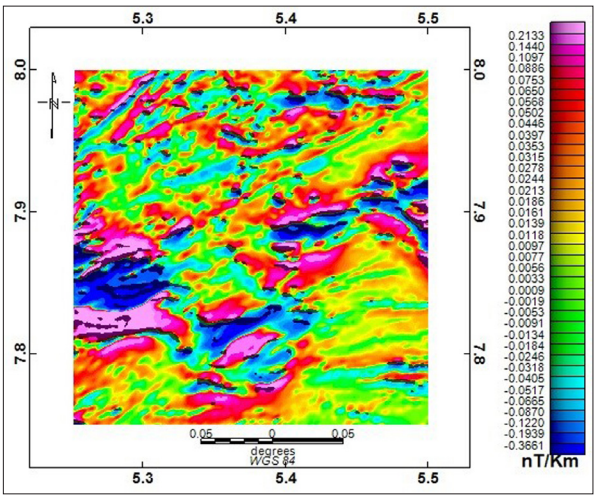

Figure 8. First Vertical Derivative (1VD) image of the study area.

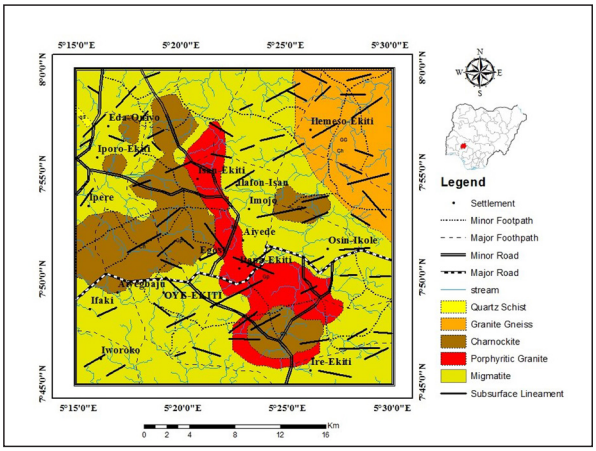

Figure 9. Lineaments from 1VD imposed on the geological map of the area.

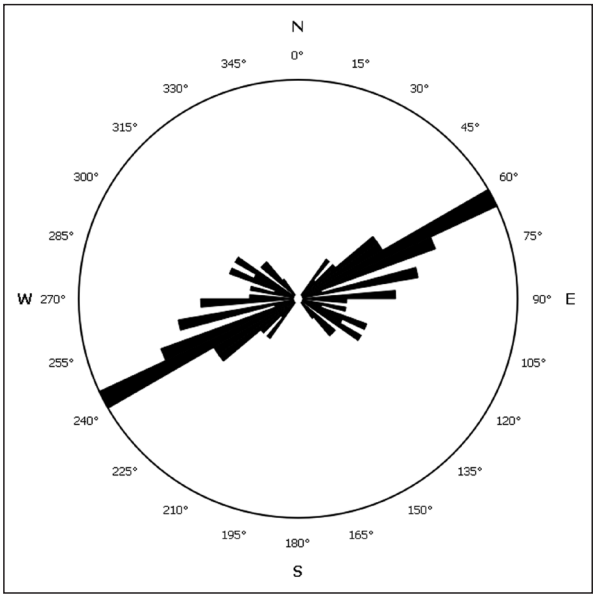

Figure 10. General orientation of Lineaments from 1VD.

Lineaments from both the DEM and IVD maps were combined and imposed on the geological map of the study area (Figure 11), to be able to separate areas of high groundwater potentials from low groundwater potentials. The lineaments were further used to produce the lineament density map of the study area (Figure 12) and subsequently the orientation of the combined surface and subsurface lineaments of the area (Figure 13). Figure 11 shows that the lineaments cut across every part of the area of study in various trends while figure 12 shows the areas of high lineament intersections of both the surface and subsurface lineaments. Areas like Eda-Oniyo, Ilemoso-Ekiti, Itapa-Ekiti, Isan Ekiti, Iworojo, Ire- Ekiti are located in an area having higher lineament intersections than the others, they can be classified as having higher groundwater potentials than the rest of the areas. Places like Aiyede, ipere, and Ifaki may not be well suited for groundwater exploration, the rest have medium groundwater potentials. Figure 13 shows the general orientation of the lineaments, it is obvious that the NE-SW orientation is the dominant trend in the area, which is a very good lineament direction for groundwater accumulation.

5.4 Combined surface and subsurface lineaments

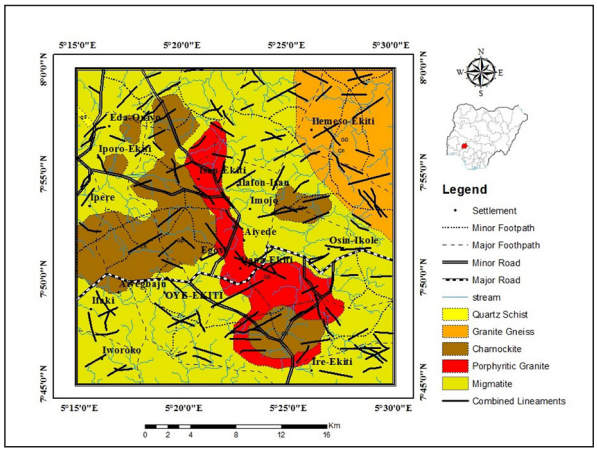

Figure 11. Lineaments from DEM and 1VD imposed on the geological map of the area.

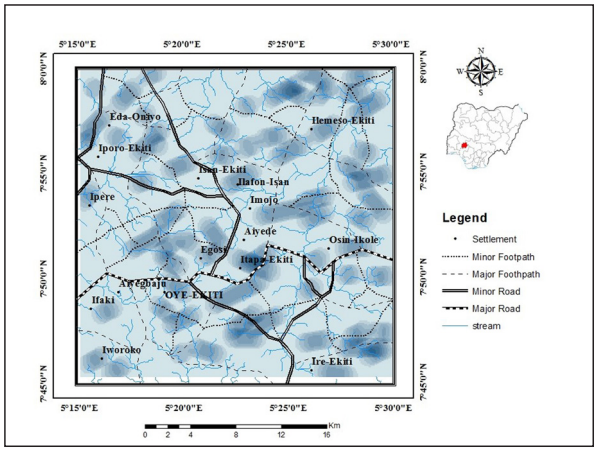

Figure 12. Lineaments density of the combined surface and subsurface lineaments map of the area.

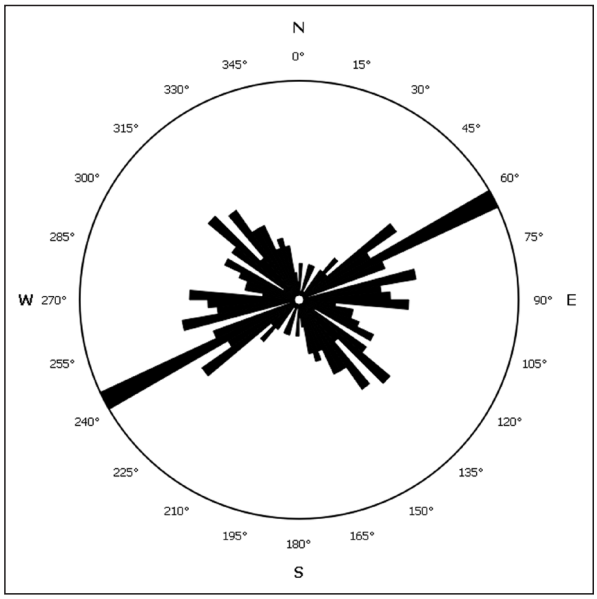

Figure 13. Orientation of the combined surface and subsurface lineaments map of the area.

5.5 Groundwater Potential Map

The various weights assigned to the thematic maps were used to produce the groundwater potential zones in the area of study. The groundwater potential of the study area is shown in Figure 14. The groundwater potential of the study area has been classified into five, namely: Very low, low, moderate, high, and very high. Very low groundwater potential area covers 1.4 km^2 (0.59 %) of the total area, low covers 72.18 km^2 (9.59 %), moderate covers 372.3 km^2 (49.44 %), high groundwater potential covers 272.12 km^2 (36.14 %), and very high groundwater potential covers 35 km^2 (4.64 %), as presented in Table 3.

From Figure 14, the western part of the area of study is dominated by very low to low groundwater potential while the southern part of the area of study is dominated by high and very high groundwater potential. Generally, low and moderate groundwater potential occupies the highest landmass in the area of study, this is to show that the basement complex terrain of Nigeria has a very low aquifer capability.

Places like Isan-Ekiti, Osin-Ikole, Imojo, and Ilafon-Isan all lie within the very low and low groundwater potential areas while Oye-Ekiti, Egosi, Itapa Ekiti, Eda Oniyo, Omu-Ekiti, Itagi, Iporo-Ekiti, etc. lie within moderate and high groundwater potential zone. Places like Ikole, Ire-Ekiti, Arigidi Omu-Ijalu, and Omu-Titun lie within the very high groundwater potential zone.

A closer look at figure 14 shows that areas of higher slope and high elevation values have low groundwater potential while places of high lineament density and low drainage density have high to very high groundwater potential. Also, geology played an important part in the groundwater potential of the study area as well and high and very high groundwater potential could be seen within the metamorphic rocks and very low to moderate within the igneous rocks. For land use, high and very high groundwater potential cuts across the farmland and forest more than the built-up, rivers, and rocky areas because forest and farmland enhance surface water infiltration into the subsurface.

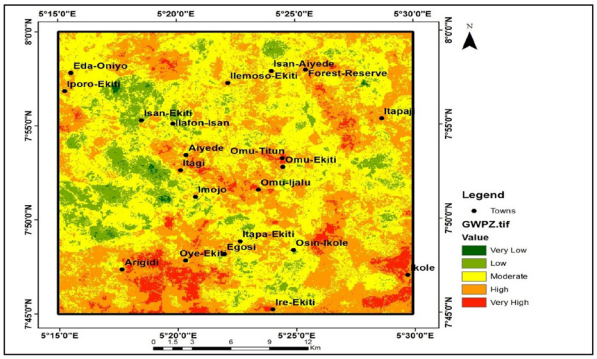

Figure 14. Groundwater Potential Map of the Study area.

6. Conclusion

From the analysis done the above results, Lineament density presents four dominant lineament orientations, N-S, E-W, NW-SE, and NE-SW, and these orientations are typical of the structures and deformation pattern within the basement complex of Nigeria. A lineament density map is a measure of the quantitative length of linear feature per unit area which can indirectly reveal the groundwater potentials as the presence of lineaments usually denotes a permeable zone. Lineament density values ranged from 0 to 2.52 km^2, areas with high lineament density are best for groundwater accumulation while areas with low lineaments are less favorable for groundwater accumulation as such, higher weights were assigned to high lineament values and low weights to low lineament values.

From the elevation map of the study low elevation values cover a total of 9.63 % while high elevation covers 7 % of the area. Intermediate values make up the remaining 83.46 %. Higher values were assigned to low elevation while lower values were assigned to high elevation.

The groundwater potential of the study area has been classified into five, namely: Very low, low, moderate, high, and very high. Very low groundwater potential area covers 1.4 km^2 (0.59 %) of the total area, low covers 72.18 km^2 (9.59 %), moderate covers 372.3 km^2 (49.44 %), high groundwater potential covers 272.12 km^2 (36.14 %), and very high groundwater potential covers 35 km^2 (4.64 %), the western part of the area of study is dominated with very low to low groundwater potential while the southern part of the area of study is dominated by high and very high groundwater potential. Generally, low and moderate groundwater potential occupies the highest landmass in the area of study, this is to show that the basement complex terrain of Nigeria has a very low aquifer capability.

References

Ademilua OL, Olorunfemi MO, Integration of hydrogeophysical and remote sensing data in the assessment of groundwater potentials of the basement complex terrain of Ekiti state, (2000), Journal of Emerging Trends in Engineering and Applied Sciences (JETEAS) 4(1): 77-83.

Akinola et al, General Review of the Geology of the Precambrian to Lower Palaeozoic Rocks of Northern Nigeria. (1986) Geology of Nigeria, Elizabethan Publishing Co, 19-47.

Ileoje The Occurrence and Exploration of Groundwater in Nigeria Basement Rocks, (1980), Journal of Mining and Geol. 36, 1:2 131-146.

Joint Monitoring Programme (JMP), Global Water Supply and Sanitation Report, Joint Monitoring Program, (2008), WHO/ UNICEF, World Health Organization, Geneva.

Koefoed, O. Geosounding Principles and Resistivity Sounding Measurements, (1979), Elsevier Science Publishing Company, Amsterdam International Journal of Geosciences, 5:8, 7: 31,

Mohammed Ibrahim and Taufiq Suleiman, Geoelectrical Study of Groundwater Potential at Waziri Umaru Federal Polytechnic's Gesse Campus BirninKebbi, Kebbi State, (2022), Nigeria. Jordan Journal of Earth and Environmental Sciences JJEES 13 (2): 82-8

Nigeria Geological Survey Agency (NGSA) (2006), Map of Nigeria showing Geological component.

Obeidat Mutawakil and Awawdeh Muheeb, Assessment of groundwater quality in the area surrounding Al- Zaatari Camp, Jordan, using cluster analysis and water quality index (WQI) (2021), Jordan Journal of Earth and Environmental Sciences, JEES 12 (3): 187-197

Olasehinde PI, An integrated geological and geophysical exploration for in the basement complex of west central Nigeria,

(1999), Water Resour 10:46–49

Olasehinde P.I., Pal P.C. and Annor A. E., Aeromagnetic Anomalies and Structural Lineament in the Nigerian Basement Complex, (1990), Journal of African Earth Sciences, 11(5), 351-355.

Olasehinde, P.I. and Raji, W.O., Geophysical studies of fractures of basement rocks at the University of Ilorin, Southwestern Nigeria: Application to groundwater exploration. (2007), Water Resources. https://www.researchgate.net/publication/308606723

Olasehinde, P. I. and Ige, O.O, Preliminary Assessment of Water Quality in Ayede-Ekiti, South western Nigeria, (2011), Journal of Geology and Mining Research, 3(6). 147-152.

Ologe Oluwatoyin and Ola-Buraimo A. Olatunji, Evaluation of Aquifer Characteristics within Birnin Kebbi Metropolis, Northwestern Nigeria Using Geoelectric Survey, (2022), Jordan Journal of Earth and Environmental Sciences JJEES 13 (1): 60-63

Rahman MA, Review of the basement geology of southwestern Nigeria. In: Kogbe CA (ed) Geology,(1976), Journal of Mining and Geology, 27-35

Reeves, C., Reford, S., and Millingan, PAirborne geophysics: old methods, new images, (1997), In A. Gubbins (Ed.), Proceedings of the Fourth Decennial International Conference on Mineral Exploration, 13-30.

Rzger Abdula, Sardar Fatah, Gardun Salih, Mohammed Mustafa, and Muhammed Al, Source rock evaluation of the Chia Gara Formation in the Bekhme-1 well, Harir District, Kurdistan Region, Iraq, (2021), Jordan Journal of Earth and Environmental Sciences, JJEES 12 (2): 106-112

Saminu O et al, The use of vertical electrical sounding (VES) for groundwater exploration around Nigerian College of Aviation, (1999), Austria Journal of Earth Sciences. 21 (4): 223.

Sarup, J. Takal, K. M., Mittal, S. K., Estimation of soil erosion and net sediment trapped of upper-helmand catchment in Kajaki reservoir using USLE model and remote sensing e GIS technique, (2011). International Journal of Advanced Engineering Research and Science, 4(2), 237056

United Nations (UN), United Nations Millennium Declaration, United Nations General Assembly, (2000), A/RES/55/2, United Nations, New York.

JJEES

JJEES (2023) 14 (4): 287-296
ISSN 1995-6681

Jordan Journal of Earth and Environmental Sciences

Mineralogy, Geochemistry and Petrogensis of Pleistocene Volcanism from Dear Al-kahef Basaltic Field (Harrat Al-Shaam), Northeast Jordan

Hassan Al-Fugha[1*] and Ahmad Al-Malabeh[2]

[1]Jordan University, Department of Applied Geology, Amman Jordan
[2]The Hashemite University, Department of Earth and Environmental Sciences, Zarka Jordan

Received October 29, 2022; Accepted July 3, 2023

Abstract

The northeast Jordan is part of the large intra-continental volcanic province of Harrat Al-Shaam (also written: Harrat Ash-Sham), which covers an area of about 50.000 km^2. In Jordan, the volcanic province covers an area of about 12.000 km^2. They are represented by basalt flows and tephra cones. Twenty-four basaltic rock samples were collected and covered about 25 km^2 area 7 km northeast of the village Dear Al-Kahef were studied. The petrographical data show that the samples are olivine-, plagioclase- and pyroxene-phyric basalt type. The geochemical investigation of the rocks shows that they are under-saturated regarding the silica content, which ranges between 46.00 and 49.86 wt.%. They are mainly alkali basalts and belong to the alkaline to sub-alkaline rocks series containing 2.26 to 4.55 wt. % alkali oxides. The geochemical parameters of these by the silica content (< 50 wt%) the high MgO content (>7 wt%), the Mg-number (0.60-0.65), and the high Ni contents lies between 100 to 170 ppm, and the high Cr content in the studied rocks range from 125 to 260 ppm. This magma shows low variable abundances of compatible and incompatible trace elements reflecting a homogenous source. Their Geochemical trend hints that the parental magma ascended rapidly, and underwent only limited fractional crystallization without crustal contamination. The primitive nature of the magma is reflected the distinct chemical similarity of the studied rocks suggests that they were derived from a single enriched and homogeneous mantle source, and initiated by a low degree of partial melting (4-13 %) of garnet peridotite at a depth >100 km.

Keywords: *Pleistocene Volcanism, Alkali Basalt, Harrat Al-Shaam, Northeast Jordan*

1. Introduction and Geologic setting

In general, alkali basalts are widespread on continental plates and are usually associated with continental rifting (Wilson, 1989; Al-Malabeh, et al., 2017). This is also the environment of the extended young volcanic fields near the western margin of the Arabian plate, which is separated from the African plate by the Red Sea Rift. Such volcanic fields occur in Yemen, close to the triple junction with the East African Rift and the Aden Ridge, and northwards in Saudi Arabia, Jordan, Syria, and Turkey. The occurrence in northeast Jordan is part of the large intra-continental volcanic province of Harrat Al-Shaam (also written: Harrat Ash-Sham), which covers an area of about 50.000 km^2 and extends continuously in NW-SE direction from the southern rim of the Damascus basin in Syria across Jordan into northwestern Saudi Arabia (Figure 1a). In Jordan, the volcanic province is known as the Jordanian Harrat and covers an area of about 12.000 km^2 (Figure 1b).

The extensive volcanism of the Jordanian Harrat occurred during faulting episodes and predominantly consisted of alkali basalts, basanites, and hawaiites (Barberi et al., 1979; Shaw, 2003; Al-Malabeh and Hamed, 2020). The volcanism of the Jordanian Harrat occurred over a relatively long time from the Early Miocene to the Holocene (Barberi et al., 1979 Kempe, and Al-Malabeh, 2013) with an age range from 0.2 to 18.5 Ma as determined by K-Ar dating (Siedner and Horowitz, 1974; Barberi et al., 1979; Moffat, 1988; Tarawneh et al., 2001). During late Cenozoic times, basaltic lavas erupted probably from vertical fissures and local vents along the Jordan rift, a mountain ridge in central and northeastern Jordan (Krienitz et al., 2006 Al-Malabeh and Kempe, 2009, Al-Malabeh, and Kempe, 2012; and Al-Fugha et al., 2012).

These magmas transported upper mantle xenoliths with a composition of spinel lherzolite to the surface. These xenoliths contain olivine, orthopyroxene, clinopyroxene, and spinel as typical for the upper mantle below continental plates, analogous to worldwide occurrences (Frey et al., 1978; Thompson et al., 1980; White and McKenzie, 1989; McGuire and Bohannon, 1989; Wilson, 1989).

Jordan is part of the Arabian plate, which is drifting to the NE towards the Tauros-Zagros compressional zone due to the aforementioned opening of the Red Sea. This process is accompanied by the development of the Dead Sea transform fault, which trends N-S with a net slip along it of about 105 km (Garfunkel, 1989; Al-Fugha, and Al-Malabeh, 2019, Weinstein et al., 2006; Abu-Mahfouz, et al., 2016), and the formation of the NW-SE striking Azraq-Sirhan Graben structure. volcanic rocks are situated on the east side of this major fault. In Northeastern Jordan basalts extend along the east side of the Al-Azraq-Wadi- Sirhan basin.

* Corresponding author e-mail: h.fugha@ju.edu.jo

Bender (1968) distinguished seven different phases of major volcanic activities in northeastern Jordan based on both field observation and bore-hole data. The total thickness of these flows reached about 350 m where the upper three phases are exposed at the surface between oil pump stations H5 (Al-Safawi) and H4 (Ruweished), in the central part of the Jordanian Harrat. K-Ar dating from Harrat Al-Shaam ranges from 0.05 to 40 Ma. A historical eruption in the 17th century was also recorded (Al-Malabeh, 2010; Tarawneh et al., 2000).

3. Study Area

The study area is located within the intraplate volcanic field of the Jordanian Harrat in Northeast Jordan; within the Mafraq government about 80 km northeast of Al-Mafraq city. It is located in Dear Al-Kahef village at 32° 15′ 570″ to 32° 15′ 580″ N and 36° 45′ 485″ to 36° 45′ 495″ E (Figure 1c). The basaltic flow is accessible through several asphaltic roads that already connect several towns.

The outcrop basaltic rock covered by 50 km^2 of basalt flows, was developed due to intermittent eruption from deep-seated faults form of 4 successive basaltic pahoehoe and aa (or a'a) flows with a total thickness of 40 m.

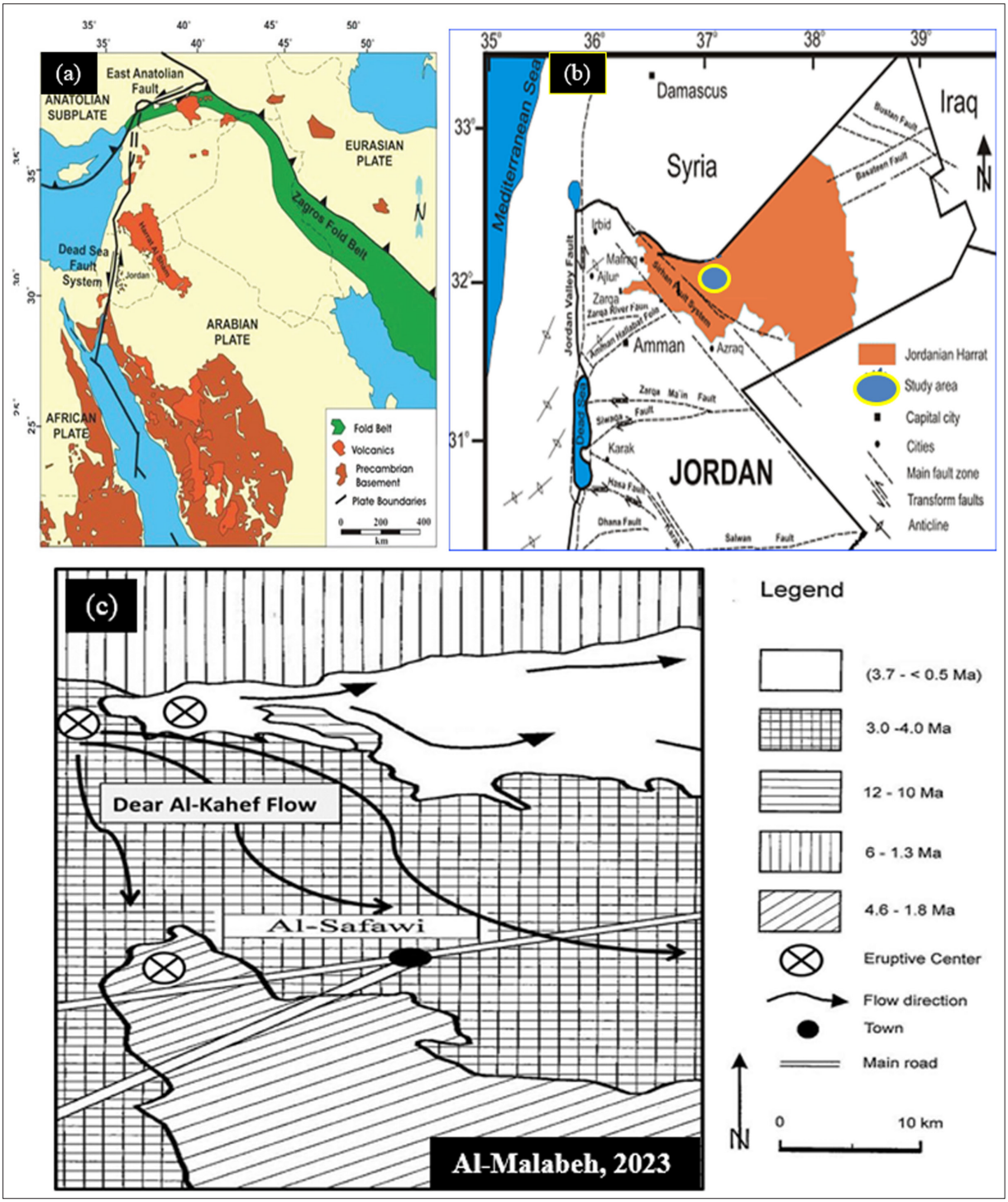

Figure 1. a. Location map of volcanic fields along the western Arabian plate (after Garfunkel, 1989; Camp Roobol, 1989 and Al-Malabeh, 1994). b. Tectonic setting of Jordanian Harrat and location of the study area (Modified after Al-Malabeh, 2009 (c). Geological map of Dear Al-Kahef basaltic field (Al-Malabeh this study).

3. Sampling and Analytical Techniques

Twenty-four representative rock samples were collected from the basalt flows. The samples were crushed and powdered using geochemical techniques. Major oxides and trace elements were analyzed on fused glass disks by using multi-channel XRF Spectrometry at the Department of Geology, University of Stuttgart, Germany. The powdered samples were dried at 110 C°. A total of 2 gm of the powder samples were mixed with 8 g of lithium tetra borate and fused in platinum crucibles over gas burners (1000˚C) for 1 h. Melts were poured into a mold creating 32 mm diameter glass disks. The loss on ignition (LOI) was determined by weight lost after melting at 1000 C°.

Thin sections of the basaltic rock samples were studied in transmitted light to determine the petrography.

4. Results

4.1 Mineralogy

The studied basaltic flows of northeast Jordan, which are mainly composed of basaltic flows, are black to grey in color and fine-grained. The melanocratic rocks typically show porphyritic to glomeroporphyritic texture and are characterized by olivine, clinopyroxene, and plagioclase phenocrysts embedded in a fine-grained groundmass that mainly consists of plagioclase, olivine, clinopyroxene, opaque minerals, and glass. The average modal composition of the basaltic rock samples studied is 54 vol.% plagioclase, 25 vol.% olivine, 17 vol.% clinopyroxene, and 4 vol.% accessory minerals. Plagioclase occurs as up to 5 mm long hypidiomorphic laths and fine crystals in the groundmass. The subhedral plagioclase laths are phenocrysts with extinction angles ranging from 26 to 30 degrees indicating a labradorite composition An 50 - An 60 by using the method described by Michel Levy color chart (Keer, 1977).

The olivines phenocrysts are unhedral to subhedral, fractured, mostly unaltered, and reach lengths of 4 mm. They are colorless to pale yellow. A few exceptions exhibit resorbed margins which can be partly or completely replaced by iddingsite. The olivine phenocrysts are typically Magnesian in the basalt with a forsterite component between 75 to 82 mol%.

The clinopyroxene phenocrysts are augite which is colorless or pale brown to pale green. The phenocrysts are 1 to 4 mm in length. The groundmass augite < 0.5 mm in size, shows prismatic crystals. Small amounts of this augite are affected by chloritzation where green chlorite is present along fractures and crystal rims. The accessory minerals include apatite as minute needles and opaque phases which were identified as magnetite and ilmenite

4.2 Geochemical

4.2.1. Major Oxides

Twenty-four samples of Pleistocene alkali basalts from northeastern Jordan have been analyzed for major, minor, and trace elements. The representative results are given in Table 1. The SiO_2 values range between 46.00 and 49.86 wt.% and average 47.63 wt%. They were plotted against alkalis in the (Irvine and Baragar, 1971 and Hamed et al., 2021) diagram of Figure 2. This diagram shows that all rock samples can be assigned to the alkaline to sub-alkaline suite.

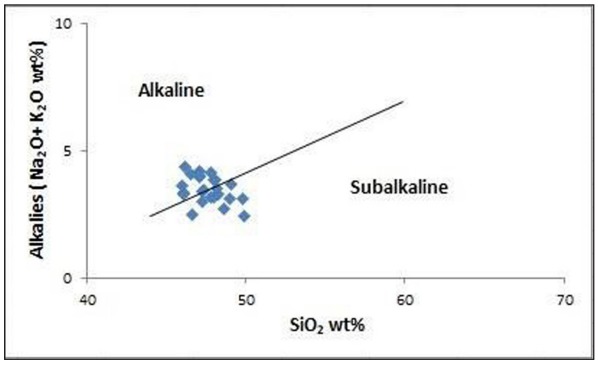

Figure 2. Alkalis Vs. SiO_2 for the studied samples (Divider is after Irvine and Baragar, 1971).

The AFM variation diagram of Figure 3 indicates that the compositions of the basaltic rocks from northeastern Jordan fall in the transition between calc-alkaline and tholeiitic fields (Irvine and Baragar 1971).

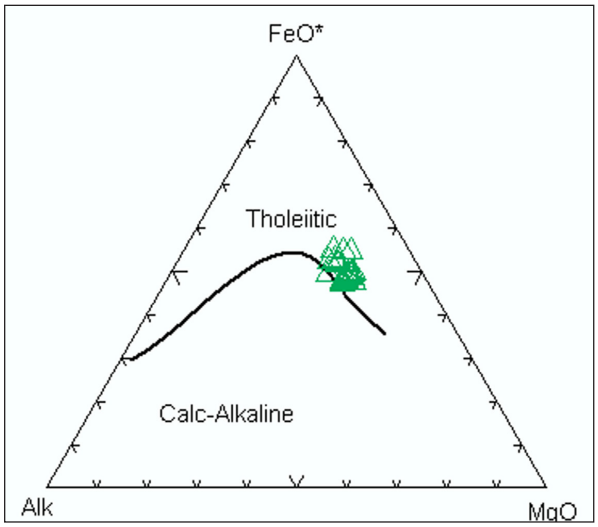

Figure 3. Discrimination (AFM) diagram plot alkalis-FeO-MgO for the studied samples (After Irvine and Baragar, 1971).

The data for Al_2O_3, P_2O_5, $FeO+Fe_2O_3$, and CaO scatter between 13.5 to 16.15 wt.%, average 14.69 wt% 0.01 to 0.50 wt.%, average 0.19 wt%; 10.16 to 14.02 wt.%, average 11.98 wt%; and 6.98 to 12.26 wt.%, average 9.78wt% respectively. A correlation with the determined SiO_2 content is only discernable for Al_2O_3. Figure 4 shows an increase of Al_2O_3 with decreasing SiO_2. The Mg number (Mg #; $Mg/Mg^{2+}+Fe^{2+}$) given in Table 1 ranges between 0.42 and 0.50. The determined major and minor element concentrations were also used to calculate the CIPW norm (Table 1).

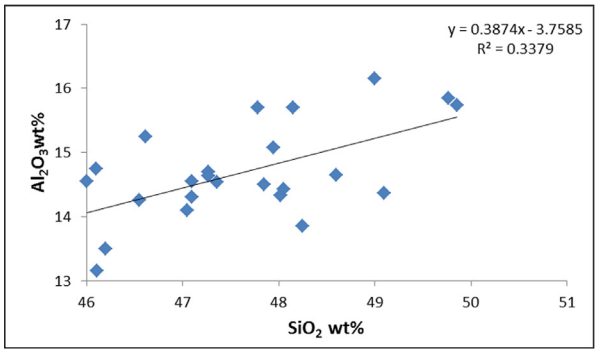

Figure 4. SiO_2 -Al_2O_3 correlation.

Normative anorthite (An) and albite (Ab) contents are high. According to the Ab-An-Or diagram of Figure 5, the majority of samples reflect the sodic affinity of the rocks. Normative apatite and nepheline contents are zero to 0.83% with an average of 0.29% and 4.2 to 0.07%, with an average of 1.14%, respectively Table 1. The latter content is, however, often zero.

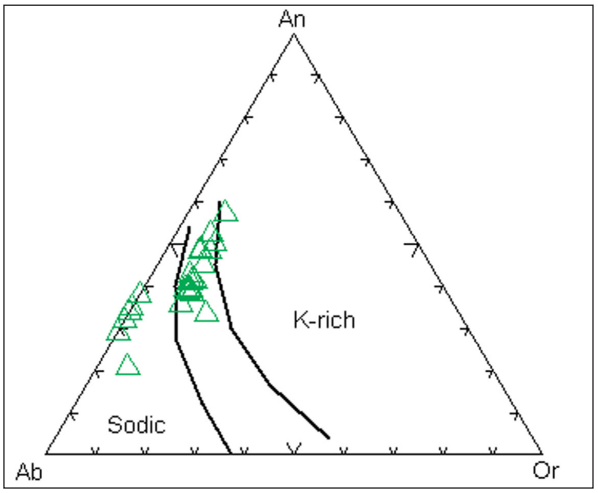

Figure 5. A triangular discrimination diagram plots Normative feldspar (Ab-An-Or) for the studied samples (after Irvine and Baragar 1971).

4.2.2. Trace Elements

The trace element data show relatively minor variation. Contents of Sr, Ba, Ni, and Cr range from 255 to 595 ppm, 360.63 ppm; 5 to 100 ppm; 100 to 170 ppm, and 125 to 260 ppm, respectively (Table 1). The concentrations of Rb, Nb, Y, and Sc are low scattering around between 2 to 12 ppm; 7 to 37 ppm; 18 to 29 ppm; and 11 to 26 ppm, respectively Table 1. A correlation of these trace-element contents with that of SiO_2 is not discernable.

5. Discussion

5.1 Bulk-rock compositions

The studied basalts are alkaline to sub-alkaline and often SiO_2-undersaturated. Very similar rock compositions were reported by (Al-Malabeh, 1994) from NE Jordan. Shaw (2003) already emphasized that the silica undersaturated magmas from NE Jordan with high MgO and $FeO+Fe_2O_3$ contents >7 wt% and >12 wt%, respectively, give evidence for the primary nature of these magmas. However, the Mg# ranging from 0.60 to 0.65 (Table 1), could point to little fractional crystallization and removal of olivine and pyroxene. Nickel and Cr varies between 100 to 170 ppm and 125 to 260 ppm, respectively. These concentrations also suggest some degree of olivine fractionation which tends to increase the incompatible trace element concentration in the studied basalts. The determined concentrations of Sr and Ba might, thus, represent a moderate enrichment in the melt phase. Despite the indication of little olivine fractionation, the magmas studied here and by other researchers (Steinitz, and Bartov 1992; Shaw, 2003 Al Fugha, 2006; Al-Malabeh, 2009; and Krienitz et al. 2006) from the Harrat Al-Shaam volcanic field in northeastern Jordan are relatively homogeneous over a wide area. This is in contrast to the rocks from this field in Syria. Krienitz et al. (2006) proposed the considerable crustal contamination of the continental intraplate lavas there because they show a wide variety of bulk-rock compositions and can be significantly enriched in SiO2. Furthermore, the Harrat Al-Shaam contains crustal nodules (Al-Malabeh, 2009). These lithics represent the lower crust and were brought from depths of 25 to 30 km (Al-Malabeh, 2003) by ascending alkali olivine basaltic and basanitic melts (Lustrino and Sharkov, 2006).

5.2 Crustal contamination

A few magmas can erupt without the effect of contamination (Thompson et al., 1980, Al-Malabeh, et al., 2004). The concentration of elements such as Sr, Rb, and K can be used to improve the understanding of the geochemistry and petrogenesis of magma. The comparable geochemical data deduced from the similar concentration of major elements, and mimicked by trace element ratios, e.g. K/Ba, and Ba/Rb, and the primitive nature of the magma, serve as evidence for a closed-system magma chamber for the studied volcanoes, and suggest that assimilation of upper crustal materials was minimal. The depletion and enrichment of the incompatible elements in the studied basalt were explained by partial melting rather than contamination.

5.3 Differentiation and fractionation of the studied magma

The parental magmas of the studied basaltic rocks are qualified as primary; silica content never exceeded 50 wt% and ranges between 46.00 to 49.86 wt.%.This matches the content below 50 wt% reported for primary magmas (Wilson, 1989 and Al-Malabeh, et al., 2004). MgO content in the investigated samples exceeds 7 wt% and ranges between 7 and 10 wt%, which is also compatible with the primary nature of the magma and argues for rapid ascent from the mantle with minimal fractionation. Consequently, the Mg#, which is considered one of the most important petrogenetic indicators for primary magmas, ranges in the studied rocks between 0.60 and 0.65. These values fit well with the values of 0.60 and 0.75 reported for primary magmas (Kesson, 1973, El-Hasan and Al-Malabeh, 2008). However, Wilson (1989) reported a value of > 0.6 for the distinction of primary magmas.

The Ni and Cr concentrations are good indicators for the fractionation of olivine and pyroxene. They also used fundamental criteria for determining the primary nature of magma. Ni content varies from 100 to 170 ppm. These values are consistent with the concentrations of Ni in primary magma (Green, 1980) The high Ni content matches well with the high MgO content of the rocks. Cr content in the studied rocks lies between 125 and 260. These values are intermediate between those reported for primary magmas of 142 ppm (Hughes, 1982). On the basis that Cr content may be considered as an index of fractionation, it would appear that the studied rocks were produced from limited fractionated magmas.

5.4 Identification of Inferred Mantle Source

A fundamental problem in understanding the magmatic process of development of the studied volcanoes centers on 1) the composition, mineralogy, and nature of the inferred source, and 2) the degree and mechanism of partial melting.

The primary melts of the Harrat Al-Shaam volcanic field were generally derived in the mantle below the crust as also evidenced by ultramafic xenoliths (Steinitz and Bartov 1992; Shaw et al 2003; Al-Fugha, 2006, Krienitz et al. 2006; and Al-Malabeh, 1994). Seismic and gravity data indicate that

the crust below this field is about 37 km thick (McBride et al., 1990; Sawaf et al., 1993). As the Arabian lithospheric mantle beneath the crust could be chemically and isotopically heterogeneous, various suggestions previously made from which part of the mantle the characterized primary melts, in principle, could be derived from transferred to the Jordanian part of the Harrat Al-Shaam volcanic field.

In general, primary alkali basaltic melts can be formed by a small degree of melting in the mantle at pressures above 13 kbar. At lower pressures, tholeiitic melts are formed (Mysen and Kushiro, 1977; Jaques, Green, 1980; Ibrahim, and Al-Malabeh, 2006).). Green (1970) reported that alkali basaltic melts can be derived at depths of 90 km (30 kbar) by about 5% partial melting and also by a higher degree of partial melting in the lithospheric mantle above (60 to 90 km). However, alkali basalts could also be differentiating of more primitive picritic partial melts (Al-Malabeh et al., 2002; Ozdemir et al., 2019). Based on this experimental information (Rooney et al., 2005), for instance, suggested that the recent basalts of the Ethiopian rift were produced by a small degree of partial melting of peridotite at mantle depths corresponding to pressures of 15 to 25 kbar. Thompson et al. (1980) also suggested that the Tertiary basalts from central France, which are similar in their mineralogy to those of northeastern Jordan, formed by partial melting of garnet lherzolite at 15 to 30 kbar pressure as evidenced by spinel lherzolite nodules. For the Harrat Al-Shaam volcanic field. Shaw (2003) proposed that the volcanic rocks have their source in the lower lithosphere and suggested that the alkali rocks were probably derived from a mixed lithospheric asthenosphere source. According to Al-Fugha 2006; Al-Fugha and Bany Yaseen 2019 and Bany Yaseen, 2019, proposed that the alkali basalts of the Tel-Remah, Atarous, and Jurf El Darawish volcanoes in NE and central Jordan were formed in a primitive upper mantle that has suffered partial melting at a temperature ranging between 930 to 1075°C and pressure around 15 to 25 kbar.

The Ti-richness of the studied alkali basalts could be attributed to low degrees of melting of a peridotite source (Shehata and Theodoros, 2011) and compatible with high MgO and $FeO+Fe_2O_3$ contents >7 wt% and >12 wt%, respectively. As the $FeO+Fe_2O_3$ contents show a scatter in a plot versus SiO_2 (Figure 6) this could reflect a variable degree of partial melting of a relatively homogenous source.

Traditionally, large volumes of basalts erupted in a continental environment over a longer time as in the Harrat Al-Shaam volcanic field are related to hot-spot volcanism, which is believed to be caused by an ascending mantle plume. For instance, this might be true for the Tertiary Snake River plain basalts in the northwestern United States of America. According to Shervais and Vetter (2009) the source for these basalts is the shallow mantle although some alkali basalts of this volcanic province might require pressures higher than 15 kbar for the source region. On the other hand, the mantle xenoliths in the various volcanic intraplate regions of the Arabian plate are broadly similar, including the ones studied here, suggesting that this Cenozoic volcanism with several centers might have the same base which can hardly be a single hot spot in the mantle. Shaw (2003) proposed that this volcanism may be the product of the melting of the upper mantle wedge that was fertilized already during the Pan-African subduction. Another reason for the fertilization of the mantle below the Arabian plate could be a delamination process with crustal material involved (Massonne and Fockenberg, 2012).

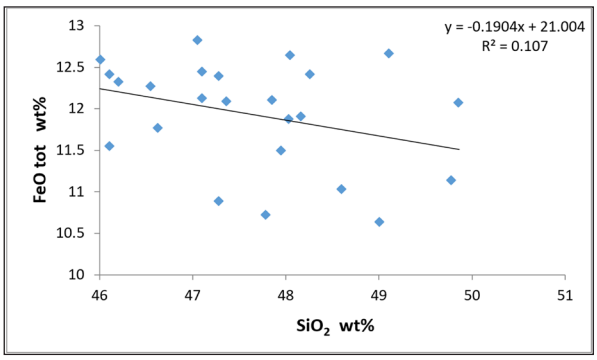

Figure 6. SiO_2-FeO tot correlation.

As the Arabian plate moved northwards colliding with Eurasia and forming the Taurus-Zagros mountain belt, significant crustal thickening occurred in the collisional zone in Tertiary or even earlier times. Such compression affected also areas south of this zone in the range of the fault-rich regions of Jordan, Syria, and Turkey. For instance, the region of the Golan Heights is a highly faulted and deformed plateau, which was subject to continuous deformation phases (Meiler, 2011). Thus, local crustal thickening could have taken place in the region of today's Harrat Al-Shaam volcanic field in the past resulting in eclogitization of the lower crust, especially when we consider a lower geothermal for this process than it is now, and its foundering into the mantle. The delaminated crust could have fertilized the mantle to cause the production of significant melt volumes in the fertilized mantle regions in late Cenozoic times to form the Harrat Al-Shaam volcanic field.

The inferred origin of the studied rocks is thought to be in the garnet peridotite zone of the mantle. This interpretation is based on the constancy of Y, which ranges from 18to 29 ppm; the high Zr/Y ratio; and the high TiO_2/Y ratio (Frey et al., 1978). The high Ni, Cr, and Co contents in the samples support that they were generated in a mantle of peridotite composition (Wilson, 1989, Smadi et al., 2018.). Moreover, the low Zr/Nb, Y/Nb, and high Y/Zr ratios may indicate the enriched nature of the garnet peridotite mantle source (Figure 7).

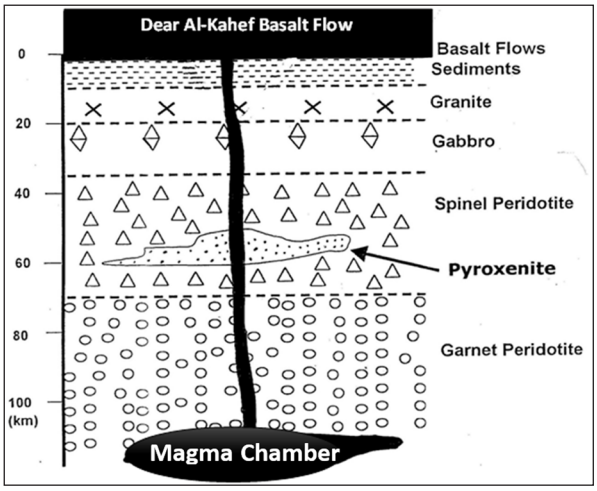

Figure 7. Schematic diagram of the studied basalt, crust, and mantle for the Jordanian Harrat and magma partial melting zone (Modified after Al-Malabeh, 2009).

6. Conclusions

The consideration of the bulk-rock chemical compositions of basalts from the Jordanian portion of the Jordanian Harrat at Dear Al-Kahef Basltic field supports the concept that:

The igneous rocks (basalt) can be derived from a garnt-lherzolite source in the upper mantle with a low degree of melting.

The distinct chemical similarity of the studied rocks suggests that they were derived from a single enriched and homogeneous mantle source, and initiated by a low degree of partial melting (4-13 %) of garnet peridotite at a depth >100 km.

The mantle region produced significant amounts of alkali basaltic melts because it was fertilized before either by Pan-African subduction or by crustal delamination in the Cenozoic as proposed here.

The melts reached the surface with very limited assimilation of crustal material.

A minor degree of olivine fractionation might have occurred for the studied rocks.

Table 1. Major, trace elements and CIPW norm data for Dear Al-Khaf basaltic rock.

Sample No.	1	2	3	4	5	6	7	8	9
SiO_2 Wt%	48.02	46.11	46.2	47.27	47.95	49	48.6	46.62	47.78
TiO_2	1.42	1.46	2.7	1.5	1.2	1.26	1.22	1.66	1.77
Al_2O_3	14.33	13.15	13.5	14.7	15.08	16.15	14.65	15.25	15.7
Fe_2O_3	2.95	2.95	4.15	3.00	2.70	2.77	2.72	3.16	3.27
FeO	8.93	8.6	8.18	7.88	8.80	7.86	8.32	8.6	7.46
MnO	0	0	0.01	0.04	0.01	-0.01	0.04	0.03	0
MgO	8.53	8.3	7.72	7.73	7.95	7.75	5.86	6.74	6.04
CaO	9.3	11.6	9.6	12.01	9.9	9.7	12.26	11.42	11.27
Na_2O	3.25	2.8	3.15	2.6	2.72	2.7	2.31	2.01	2.53
K_2O	0.6	0.53	1.2	0.42	0.45	0.44	0.42	0.48	0.66
P_2O_5	0.17	0.3	0.06	0.01	0.32	0.01	0.02	0.02	0.1
H_2O	1	0.78	0.5	0.7	0.87	0.82	0.63	0.76	0.7
Total	**99.7**	**98.77**	**99.17**	**100.06**	**100.15**	**100.64**	**99.25**	**98.95**	**99.48**
Mg#	0.63	0.63	0.64	0.64	0.64	0.64	0.60	0.60	0.61
CIPW Norms									
Or	4.2	3.97	7.98	3.25	3.35	3.35	3.3	3.54	4.64
Ab	25	18.16	20.58	21.9	24.45	24.15	20.9	18.35	22.75
An	21.3	20.34	17.72	19.92	26.25	26.45	26.97	30	28.15
Ne	1.5	3.35	3.53	0.28	0	0	0	0	0
Wo	8.93	14.14	11.61	13.34	7.92	8.21	13.3	10.45	10.9
En	5.3	8.54	7.65	7.85	9.9	12.03	11.5	11.16	9.25
Fs	2.62	4.25	2.58	4.26	6.62	8.22	8.52	6.7	4.72
Fo	10.67	8.2	7.66	5.85	4.79	2.9	1.72	3.55	3.6
Fa	6.16	4.54	2.9	9.49	3.48	2.08	1.35	2.25	1.9
Mt	4.06	4.12	5.9	4.17	3.72	3.81	3.75	4.4	4.55
It	2.64	2.7	5	2.78	2.2	2.3	2.22	3.1	3.25
Ap	0.4	0.71	0.18	0.05	0.75	0	0.05	0.02	0.2
Or	4.2	3.97	7.99	3.25	3.35	3.35	3.3	3.54	4.65
Trace elements in ppm									
Cr	145	150	125	219	130	250	120	128	260
Ni	155	160	137	102	110	100	100	100	135
Zn	90	239	86	595	75	75	140	75	65
Sc	20	17	19	25	28	15	20	17	20
Sr ppm	370	430	545	330	360	340	350	365	420
Rb	3	12	7	10	8	4	14	5	6
Ba	136	119	189	305	70	75	230	135	260
Nb	16	20	18	35	15	19	22	5	9
Zr	180	152	147	147	181	145	172	185	170
Y	20	23	21	20	18	21	22	20	18
Ce	39	65	60	50	40	55	60	41	20

Table 1. continue...

Sample No.	10	11	12	13	14	15	16	17	18
SiO_2 Wt%	48.05	48.25	47.1	47.85	46.55	47.1	47.05	48.15	46
TiO_2	1.42	1.37	1.7	1.45	1.62	1.45	1.5	1.45	1.8
Al_2O_3	14.43	13.85	14.3	14.5	14.26	14.55	14.1	15.7	14.55
Fe_2O_3	2.92	2.89	3.2	2.95	3.12	2.95	2.96	2.97	3.3
FeO	9.72	9.52	8.92	9.15	9.15	9.5	9.87	8.95	9.3
MnO	0.1	0.1	0.1	0.1	0.12	0.11	0.11	0.1	0.11
MgO	9.14	8.95	8.9	8.8	8.85	9.15	9.26	8.5	9.28
CaO	9.35	8.8	10.34	9.92	10.25	9.8	8.92	8.38	9.85
Na_2O	3.1	2.49	3.35	3.32	3.35	3.25	3.3	2.77	2.85
K_2O	0.77	0.77	0.85	0.8	0.75	0.71	0.75	0.76	0.75
P_2O_5	0.27	0.22	0.50	0.18	0.35	0.17	0.22	0.22	0.18
H_2O	0.3	0.37	0.25	0.27	0.82	0.32	0.28	0.35	0.8
Total	**100.67**	**98.68**	**100.61**	**100.39**	**100.29**	**100.16**	**99.42**	**99.4**	**99.87**
Mg#	0.63	0.63	0.64	0.63	0.63	0.63	0.63	0.63	0.64
CIPW Norms									
Or	4.66	4.72	5.18	4.78	4.55	4.29	4.47	4.64	4.51
Ab	25.06	26.98	20.44	22.5	19.78	21.19	24.17	23.91	20.05
An	21.85	18.9	20.24	21.2	20.5	21.91	20.59	27.17	23.67
Ne	0.26	1.06	3.8	2.7	4.2	3.01	1.76	0	1.94
Wo	8.5	9.01	10.7	10.31	10.8	9.8	8.5	4.63	9.21
En	4.89	5.17	6.52	6.03	6.43	5.71	4.9	10.08	5.54
Fs	2.62	2.81	3.02	3.14	3.13	3	2.63	3.37	2.53
Fo	11.7	11.29	10.2	10.24	10.16	11.2	12.05	7.14	11.58
Fa	7.3	7.07	5.41	6.08	5.71	6.72	7.57	4.17	6.18
Mt	3.85	3.81	4.21	3.86	4.14	3.92	3.94	3.93	4.42
It	2.35	2.3	2.85	2.4	2.72	2.44	2.5	2.44	3.09
Ap	0.37	0.27	0.83	0.15	0.56	0.14	0.28	0.27	0.15
Or	4.2	3.97	7.99	3.25	3.35	3.35	3.3	3.54	4.65
Trace elements in ppm									
Cr	147	133	132	147	201	132	152	218	132
Ni	158	159	155	157	155	152	152	155	139
Zn	99	95	95	95	100	85	85	80	80
Sc	23	21	25	12	13	17	16	17	13
Sr ppm	375	350	365	375	360	365	360	255	360
Rb	5	3	6	12	8	5	2	11	10
Ba	50	100	40	20	25	5	60	45	45
Nb	22	20	13	11	10	7	18	10	11
Zr	140	154	174	146	182	175	138	185	Rb
Y	18	21	20	22	19	20	23	19	20
Ce	27	20	30	18	45	38	41	30	20

Table 1. continue...

Sample No.	19	20	21	22	23	24
SiO_2 Wt%	46.1	49.86	49.77	47.27	47.36	49.1
TiO_2	2.02	1.27	1.45	1.37	1.48	1.44
Al_2O_3	14.74	15.73	15.84	14.63	14.53	14.36
Fe_2O_3	3.51	2.76	2.96	2.88	2.98	2.94
FeO	8.91	9.31	8.18	9.51	9.11	9.72
MnO	0.11	0.11	0.11	0.1	0.1	0.11
MgO	8.95	8.23	7.71	8.97	8.9	9.9
CaO	9.99	6.98	8.59	9.71	9.21	7.46
Na_2O	2.61	1.84	2.57	2.7	2.77	2.99
K_2O	0.68	0.57	0.57	0.68	0.66	0.71
P_2O_5	0.21	0.2	0.21	0.19	0.17	0.31
H_2O	0.92	1.94	1.22	0.81	0.93	0.82
Total	**99.85**	**99.9**	**100.28**	**99.92**	**99.4**	**101.1**
Mg#	0.64	0.61	0.63	0.63	0.64	0.65
CIPW Norms						
Or	0	4.39	0	0	0	0
Ab	4.26	3.55	3.48	4.2	4.04	4.38
An	21.83	16.11	21.1	23.3	23.97	25.53
Ne	25.27	32.23	28.81	24.7	24.33	22.21
Wo	0.07	0	0	0	0	0
En	8.78	o	4.28	8.44	7.67	4.32
Fs	5.42	17.99	18.71	5.41	7.53	10.9
Fo	2.21	12.59	9.84	2.94	3.81	5.57
Fa	11.19	0	0	11.13	9.63	8.7
Mt	5.41	0	0	7	5.51	4.89
It	4.72	3.71	3.89	3.82	3.99	3.83
Ap	3.51	2.13	2.47	2.29	2.52	2.36
Or	0.2	0.21	0.27	0.21	0.14	0.49
Trace elements in ppm						
Cr	137	215	135	135	135	152
Ni	75	85	90	85	80	80
Zn	140	147	135	145	143	145
Sc	26	25	22	11	17	21
Sr ppm	355	595	370	345	350	310
Rb	6	10	5	5	4	6
Ba	7	15	12	20	27	37
Nb	195	185	173	182	155	146
Zr	21	22	20	21	20	24
Y	23	19	41	26	37	43
Ce	27	20	30	18	45	38

Qz: Quartz, Or: Orthoclase, Ab: Albite, An: Anorthite, Ne: Nepheline, Wo: Wollastinite, En: Ensitite, Fs: Feroslite , Fo: Forsterite, Fa: Fayllite, Mt: Magnetite, It: Ilmenite, Ap: Apatite

Acknowledgments

The author is thankful to the laboratory of the University of Stuttgart, Germany for using geochemical techniques to analyze basaltic samples for major oxides and trace elements by using multi-channel XRF Spectrometry and thin section preparation and studies.

References

Abu-Mahfouz, I., Al-Malabeh, A. and Rababeh, S., (2016). Geo-engineering evaluation of Harrat Irbid basaltic rocks, Irbid District— North Jordan, Arab Journal of Geoscience, 9: 412 (5), 1-11.

Al-Fugha, H., (1995). Spinel-lherzolite xenoliths from Jabal Al-Qiranah basalt central Jordan. Mu'tah J. Res. Stud. Nat. Appl. Sci. Ser. 10, 1-14.

Al-Fugha, H., (1996). Basanites with mantle xenoliths from Jabal El-Dabusa in west central Jordan. Mu'tah J. Res. Stud. Nat. Appl. Sci. Ser. 11, 35-53.

Al-Fugha,H. and Al-Malabeh, A., (2019). Mineralogy, geochemistry and origin of Cretaceous chert from Wadi Al-Wala, Central Jordan. 51(1), 1-14.

Al-Fugha, H., El-Hasan, T., Al-Malabeh A., Hamaeideh Arwa,. and El-Mezayen, A. , (2012). Petrology, geochemistry and origin of felsic dyke swarms in Aqaba complex (Wadi Al-Yutum) - South Jordan. Arabian Journal of Geosciences, 6 (2) 31-54.

Al-Fugha, H. and Bany Yaseen, I. A. (2019). Petrography, Geochemistry and Petrogenesis of Pleistocene Basaltic Flow from Northwest Atarous Area, Central Jordan. International Journal of Geosciences, 10, 613-631.

Al-Malabeh, A. (1994) Geochemistry of Two Volcanic Cones from the Intra- continental plateau Basalt of Harra El-Jabban, NE-Jordan. In Basaltic Rocks of Various Tectonic Setting, Special Issue of the Geochemical Journal. 28, 542-558, Japan.

Al-Malabeh, A. (2003) Geochemistry and Volcanology of Jabal Al-Rufiyat, Strombolian Monogenic Volcano, Jordan. Dirasat, Jordan University, 30, 125-140.

Al-Malabeh, A. (2009). Cryptic Mantle Metasomatism: Evidences from Spinel Lherzolite Xenoliths/Al-Harida Volcano in Harrat Al-Shaam, Jordan. American Journal of Applied Sciences, 6, 2085-2092.

Al-Malabeh, A., (2010). Volcanic successions of the Jebal Remah volcano, Northeast Jordan. International Journal of Economic and Environment Geology, 1, 6-10.

Al-Malabeh, A. Hamed, R., 2020. Enrichment of radon (222Rn) concentration in Remah volcano, NE-Jordan. Iraqi Geological Journal 53(2B), 58-70.

Al-Malabeh, A., and Kempe, S., (2009) Petrolithology of Permian Melaphyre Lava of the Dieburger Straße Tunnel, Darmstadt, Germany. J. Neues Jahrbuch fuer Geologie und Palaeontologie, 252(2), 129-143.

Al-Malabeh, A. and Kempe, S., 2012. Hypogene Point Karstification along Wadi Sirhan Graben (Jordan).A Sign of Oilfield Degassing? Acta Carsologica, 41 (1), 35 – 45

Al-Malabeh, A., El-Hasan, T., Lataifeh, M. and O'Shea, M., 2002. Geochemical- and mineralogicalrelated magnetic characteristics of the Tertiary-Quaternary (Umm A-Qutein) basaltic Flows from the basaltic field of Harra El-Jabban, Northeast Jordan. Physica B-Physics of Condensed Matter, 321, 396-403.

Al-Malabeh, A., Al-Fugha, H. and El-Hasan, T. (2003) Volcanogenesis of Welded Tephra-Fall Pyroclastic Rocks in Jabal Aritain Volcano, Jordan. Abhath Al-Yarmouk. 12, 345-361.

Al-Malabeh, A., Al-Fugha, H. and El-Hasan, T. (2004) Petrology and Geochemistry of Late Precambrian Magmatic Rocks from Southern Jordan. Neues Jahrbuch fuer Geologie und Palaeontologie, 233 (3), 333-350.

Al-Malabeh, A., Al-Smadi, Z., Ala'li, J., (2017). Mineralogy, geochemistry and economic potential of zircon and associated minerals in dubaydib sandstone formation. Jordan. Iraqi Geological Journal 50, 1-11.

Al-Safarjalani, A., Nasir, S., Fockenberg, T. and Massonne, H-J, (2009). Chemical composition of an intermediate part of the lower crust beneath south-western Syria. Geochem. (Chem. Erde) 69, 359-375.

Banyyassin, I., (2019). Characterization of Mineralogy, Petrography, Geochemistry and Petrogenesis of Basaltic Outcrops in Jurf Ed Darawish Area, Central Jordan. Open Journal of Geology, Vol. 19, 9, 440-460.

Barberi, F., Capaldi, P., Gasperihi, G., Marinelli, G., Santacroce, R., Treuil, M. and Varet, J., (1979). Recent basaltic volcanism of Jordan and its implication on the geodynamic history of the Dead Sea Shear Zone. Acadevnia Nazionale. Deilincei, Att Del Convegilincei 47, Rome, 667-683.

Bender, F., (1968). Geologie von Jordanien. Beitrage zur Regionalen Geologie der Erde, Borntraeger, Berlin, Stuttgart, 7, 230 pp.

Bence, A. and Albee, A.L, (1968). Empirical correction factors for the electron microanalysis of silicates and oxides. Geology 76, 382-403.

Berman, R., (1988). Internally-consistent thermodynamic data for minerals in the system Na2O-K2O-CaO-MgO-FeO-Fe2O3-Al2O3-SiO2-TiO2-H2O-CO2. J. Petrol. 29, 445-522.

Brandelik, A. and Massonne, H-J., (2004). PTGIBBS - an EXCELTM Visual Basic program for computing and visualizing thermodynamic functions and equilibria of rock-forming minerals. Comp. Geoscience 30, 909-923.

Camp, V., and Roobol, M., (1989). The Arabian Continental Alkali Province: Part I Evolution of Harrat Rahat, Kingdom of Saudi Arabia.Geological Society of. America Bulletin,101, 71-95.

El-Hasan, T., and Al-Malabeh, A. (2008). Geochemistry, Mineralogy and Petrogenesis of El-Lajjoun Pleistocene Alkali Basalt of Central Jordan. Jordan Journal of Earth and Environmental Sciences, 1(2): 53-62.

Fediuk, F. and Al-Fugha, H., (1999). Dead Sea Region Fault - controlled chemistry of Cenozoic volcanics. Geolines 9, 29-34.

Frey, F., Green, D. and Roy, S., (1978). Integrated models of basalt Petrogenesis: a study of quartz tholeiites to olivine melilitites from southeastern Australia utilizing geochemical and experimental petrological data. J. Petrol.19, 463-513.

Garfunkel, Z. (1989). Tectonic setting of Phanerozoic magmatism in Israel. Isr. J. Earth Sci. 38, 51-74.

Green, D., (1970). A Review of experimental Evidence on the origin of basaltic and Nephelinitic Magma. Phys. Earth Planet. Int. 3, 221-235.

Al-Malabeh, and Hamed, (2020). Enrichment of radon (222Rn) concentration in Remah volcano, NE-Jordan. Iraq Geological Journal 53(2B), 58-70.

Hughes, C., (1982). Igneous petrology. 7 Development in petrology, 353 p., New York (Elsevier).

Ibrahim, K. and Al-Malabeh, A. (2006) Geochemistry and Volcanic Features of Harrat El Fahda, A young Volcanic Field in Northwest Arabia, Jordan. Journal of Asian Sciences. Vol. 127(2):127-154.

Jaques, A. and Green, D., (1980). Anhydrous melting of peridotite at 0-15 kbar pressure and the genesis of tholeiitic basalts. Contrib. Mineral. Petrol. 73, 287-310.

Irvine, T., and Barager, W., (1971). Aquide to the chemical classification of the common rock, Canadian Journal of Earth Science,8, 523-548.

Kesson, S., (1973). The primary geochemistry of the Monaro alkaline volcanics, Southern Australia-evidence for upper mantle heterogeneity. Contrib. Mineral. Petrol., 42, 93-108: Amsterdam.

Keer, P. (1977). Optical Mineralogy. 442p. John Wiley and Sons, New York.

Kempe, S. and Al-Malabeh, A., (2013). Desert Kites in Jordan and Saudi Arabia: Structural, Statistics and Function, A Google Earth Study. Quaternary International, 6, 1-21.

Krienitz, M-S., Haase, K., Mezger, K., Eckhardt, V., Shaikh-Mashail, M., (2006). Magma genesis and crustal contamination of continental intraplate lavas in Northwestern Syria. Contrib. Mineral. Petrol. 151, 698-716.

Lustrino, M., Sharkov, E., (2006). Neogene volcanic activity of western Syria and its relationship with Arabian plate kinematics. J. Geodyn. 42, 115–139.

Massonne, H-J., (1995). Experimental and petrogenetic study of UHPM, in Coleman, R., and Wang, X., eds., mah volcanic field (southern Ultrahigh pressure metamorphism: Cambridge, Cambridge Syria). J. Petrol. 48, 1513-1542. Univ. Press, p. 33-95.

Massonne, H-J., Fockenberg, T., (2012). Melting of metasedimentary rocks at ultrahigh pressure - insights from experiments and thermodynamic calculations. Lithosphere 4, 269-285.

McBride, J., Barazangi, M., Best, J., Al-Sad, D., Sawaf, T., Al-Tori, M., Gebran, A., (1990). Seismic reflection structure of intracratonic Palymyride fold-thrust belt and surrounding Arabian platform, Syria. Am. Ass. Petrol. Geol. Bull. 74, 238–259.

McGuire, A. and Bohannon, R., (1989). Timing of mantle upwelling: evidence for a passive origin of the Red Sea rift. J. Geophys. Res. 94B, 1677-1682.

Meiler, M., (2011). The deep geological structure of the Golan Heights and the evolution of the adjacent Dead Sea fault system. PhD Thesis, Tel-Aviv University, 167 pp.

Moffat, D. (1988). A Volcano Tectonic Analysis of the Cenozoic Continental Basalts of Northern Jordan: Implications for Hydrocarbon Prospectively in the Block B Area. Unpublished Report, University College of Swansea, Swansea.

Mysen, B. and Kushiro, R., (1977). Compositional variation of coexisting phases with degrees of melting of peridotite in the upper mantle. Am. Mineral. 62, 843-865.

Nasir, S., (1995). Mafic lower crustal xenoliths from the North-western part of the Arabian Plate. Eur. J. Mineral. 7, 217-230.

Rollinson, H. (1993). Using Geochemical Data: Evaluation, Presentation, Interpretation. Longman Scientific and Technical, England.

Rooney, T. Furma, T., Yirgu, G. and Ayalew, D., (2005). Structure of Ethiopian lithosphere: Xenolith evidence in the main Ethiopian Rift. Geochim. Cosmochim. Acta 69. 3889-3910.

Ozdemir, Y., Mercan, C., Oyan, V. and Ozdemir, A. (2019). Composition, Pressure, and Temperature of the Mantle Sources Region of Quaternary Nepheline- Basanitic Lavas in Bitlis Massif, Eastern Anatolia, Turkey: A Consequence of Melts from Arabian Lithospheric Mantle. Lithos, 328-329, 115-129.

Sawaf, T., Al-Saad, D., Gebran, A., Barazangi, M., Best, A., Chiamov, T., (1993). Stratigraphy and structure of eastern Syria across the Euphrates depression. Tectonophysics 230, 267–281.

Shaw, J., (2003). Geochemistry of Cenozoic volcanism and Arabian lithospheric mantle in Jordan. Ph.D. thesis, Royal Holloway University of London, 268 pp.

Shehata, A. and Theodoros, N., (2011). Alkali basalts from Burgenland, Austria petrological constraints on the origin of the westernmost magmatism in the Carpathian-Pannonian Region. Lithos 121, 176-188.

Shervais, J. and Vetter.S., (2009). High-K alkali basalts of the western Snake River plain: Abrupt transition from tholeitic to mildly alkaline plume-derived basalts, western Snake River plain, Idaho. J. Volc. Geotherm. Res. 188, 141-152.

Steinitz, G.,and Bartov, Y., (1992). The Miocene-Pleistocene history of the Dead Sea segment of the Rift in light of K-Ar ages of basalt, Israil.J. Earth, Sci.,40:199-208.

Siedner, G. and Horowitz, A., (1974). Radiometric ages of Late Cenozoic basalts from Northern Israel: Chronostratigraphic implications. Nature 250, 23-26.

Smadi, A., Al-Malabeh, A., and Odat, S., (2018). Characterization and origin of selected basaltic outcrops in Harrat Irbid (HI), northern Jordan. Jordan Journal of Earth and Environmental Sciences (JJEES), 9, 185-196.

Tarawneh, K., Ilani, S., Rabba, I., Harlavan, Y., Peltz, S., Ibrahim, K., Weinberger, R and Steinitz, G., (2000). K-Ar dating of the Harrat Ash Shaam basalts, northeast Jordan, Natural Resources Authority and Geological Survey of Israel, Report GSI 2/2000, 45p.

Thompson R. Gibson, I., Mariner, G., Nattey, D. and Morrison, M., (1980). Primary basalt magma genesis. Central France J. Petrol. 21,265-293

Van den Boom, G. and Sawan, O., (1966). Report on geological and petrological studies of the plateau basalts in NE-Jordan. Bundesanstalt für Geowissenschaften und Rohstoffe Hannover, 42p.

Weinstein, Y., Navon, O., Altherr, R. and Stein, M., (2006). The Role of lithospheric mantle heterogeneity in the Generation of Plio-Pleistocene alkali basaltic suites from NW Harrat Ash Shaam (Israel). J. Petrol. 47, 1017-10

White, R. and McKenzie, D., (1989). Magmatism at rift zone. The generation of volcanic continental margins and flood basalts. J. Geophys. Res. 94, 7685-7730.

Wilson, M., (1989). Igneous Petrogenesis, a global tectonic approach. Unwin, Hyman 2nd Ed., London, 466 p.

JJEES

JJEES (2023) 14 (4): 297-307
ISSN 1995-6681

Jordan Journal of Earth and Environmental Sciences

Trace Metals and TPH Assessment of Drill Cuttings from the Vicinity of the South-Bank Estuary Oil Facility in Forcados, Nigeria

Ohwoghere-Asuma, Oghenero*, Glory Ovwamuedo, Tony Irwin Akpoborie

Department of Geology, Delta State University Abraka, Nigeria

Received September 4, 2022; Accepted May 10, 2023

Abstract

Surficial soils in the Niger delta have been studied to be contaminated by activity of oil exploration and exploitation companies. The contaminated status of aquifer sediments below the static water levels is scarcely known and unavailable. As a result, drill cuttings collected from eleven dedicated shallow boreholes were screened for total petroleum hydrocarbon and selected trace metals. The results showed that sediments sampled at 0.5m (top), 3m (middle), and 7m (bottom) intervals returned total Petroleum hydrocarbon (TPH) concentrations in the order, 20.9-14,942mg/kg > 18.6-2,045mg/kg > (0-1,043.2mg/kg). The trace metals of Zn, Cu, Pb and Co loading is such that the top > middle> bottom, Cd, Mn and Ni loading in top > middle < bottom, Fe in top (40.83-450 mg/kg) > Middle (76.73- 560.45)> bottom (110-587.4), Cr in top (0.03-1.08) < middle (0.03-1.10) < bottom (0.01-1.15) and no significant change in the concentration of V across all depths. TPH and trace metal loading appeared to be higher and lower than the DPR-EGASPIN desirable limit. The concentrations of TPH in subsurface sediments in some areas indicated contamination of aquifer sediments at depth of 0.3 to 7m deep. There is a spatial variation of trace metals and TPH concentrations with depths, which suggests that contaminated of surficial soils over time remained continuous source of the deeper depths contamination. Factor analysis of trace metals and TPH suggests multiple sources of estuary sediment contamination, including geogenic sources of leaching and weathering of rocks enriched in these trace metals carried by flowing rivers and deposited in estuary sediments. Anthropogenic sources include oil spillage, gas flaring, and fossil fuel combustion near an oil facility.

Keywords: *Multivariate analysis; River Focardos, South bank, TPH, Trace metals*

1. Introduction

The Niger Delta region is an oil province that has been severely damaged by oil exploration and exploitation activities over the years. Oil spills have wreaked havoc on the ecology of the Niger Delta region's oil-producing communities. Several studies have documented the deleterious consequences of oil spills on the ecosystem, including (Celestine, 2003; Odeyemi and Ogunseitan 1985; Tolulope, 2004; Ipeaiyeda and Dawodu, 2008; Li, 2012; Ohwoghere-Asuma and Aweto, 2018) and others.

Soils contaminated with crude oil revealed elevated levels of organic matter and related organic nitrogen and carbon, as well as trace metals such as lead, iron, vanadium, nickel, chromium, and cadmium, as well as major ions such as sodium, potassium, and calcium, with the exception of magnesium (Tolulope,2004; Ohwoghere-Asuma and Aweto 2018). TPH and trace metal concentrations in soils and sediments are affected by the amount of crude oil spilled, the length of time it takes to clean up, and, most importantly, the capillary forces that contribute to residual TPH in the soil and biodegradation. TPH and trace metals are associated with petroleum contaminations (Ipeaiyeda and Dawodu, 2008; Khan and Kathi, 2014).

Several studies have identified trace metals and TPH in surficial soils across the Niger Delta and the source is adduced to the consequence of oil exploration and exploitation effects. Many of these studies are often limited to soil depths of 0 to 45cm deep (Ohwoghere-Asuma and Aweto, (2018), Iwegbue (2011), Udoetok, (2011) and Adewuyi, (2012), with the exception of Tse and Nwankwo (2013), whose soils depth of investigation was comparatively deeper than most surficial soils studied in the region. These depths are relatively too shallow considering the regional water table, which is between 0.3 and 7m below the ground surface (Ohwoghere-Asuma et al., 2017). The contamination of the surface soils may be source of contamination of the underlying soil layers. Studies on depths of 0.3 to 7m depths are significantly lacking in providing the contamination status of the aquifer materials, which constitute the groundwater. The aquifer sediments as well as the groundwater are therefore vulnerable to contamination from the surficial soils simply due to the static water level, which ranges from 0.5 to 1.5m in the Forcados area. Apart from this, the unconfined nature and the hydraulic conductivity of aquifers are capable of enabling contamination of coastal shallow aquifers.

It is often known that contaminants do not usually remain at the surficial soil surface but are subsequently transported downward into groundwater. Groundwater is actually the last destination for toxins that probably emerged from the surficial soils and unsaturated zones. In addition, the interaction between aquifer sediments and groundwater is

* Corresponding author e-mail: ohwonero@gmail.com

the major process through which toxins such as trace metals are introduced into groundwater. The health implications of drinking contaminated water are well known and would not be emphasized.

The status and source of TPH and trace metals in aquifer sediments at deeper depths in the vicinity of oil producing facility in the Niger Delta have received insufficient and little attention. Therefore, it very important to evaluate the contamination status of aquifer sediments beneath the environs of the south bank oil facility, a major oil processing facility in the Niger delta. Consequently, 12 dedicated boreholes were drilled to depth of 7m, one was a control, ditch-cutting samples of aquifer sediments were collected at interval of 0.5, 3 and 7m and analyzed for selected trace metals and TPH. The study is imperatively significant because the source of water for the rural dweller inhabiting the coastal areas of the Niger delta is mostly from shallow hand-dug wells. The contamination of the aquifers sediment invariably means contamination of groundwater through interaction of sediments and groundwater.

1.1 Geological and Hydrogeological setting

The Forcados River's South Bank is located on longitudes 05°20′16.18″N and 05° 20′14.32"N, and latitudes 05° 20′ 35.68"E and 05° 19′.8.18"E (Figure 1). It is close to the Atlantic Ocean and serves as a hydrogeological unit where the Forcados River discharges freshwater into the sea. It is a low-lying area with an elevation of less than 4 meters above sea level. Along the Forcados River's bank, the vegetation is predominantly mangrove swamp, which predominates over freshwater swamp. Creeks, marshes, and wetlands receive saline water from tidal inlets. These surface water bodies, as well as the Forcados River and its distributaries drain the area. An oil terminal, as well as other oil infrastructure such as a flow-station and oil wells is located in the region.

Geologically, the majority of the area (Figure 2) is made up of modern beach sands deposited by high-energy waves and tidal processes of the Niger River and the sea. In this coastal area, modern beach sands form the aquifers of the Benin Formation. The lithology is made up of thin layers of sand and clay deposits that alternate between 10m and 20m thick. Their deposition is caused by a series of repeated transgressions and regressions (Reijers, 2011), or by tidal forcing. The Benin Formation sits atop the hydrocarbon-rich Agbada Formation (Reijers, 2011). This Formation is composed of alternate deposits of sand and shale and is characterized by growth faults and sequence pinch outs. The Agbada Formation shale is of marine deposit and rich in organic matter, and thus serves as the primary source of hydrocarbon for the reservoirs. The Akata Formation is the base of the Niger delta stratigraphy. The Akata Formation is overly unconformably on the Cretaceous basement complex of igneous and metamorphic rocks.

Hydrogeologically, the water level is very close to the surface and varies with the seasons. The water level varies between 0.3m and 2m above the ground surface in most coastal regions of the Niger Delta (Ohwoghere-Asuma et al., 2023, Ohwoghere-Asuma et al., 2021). The Forcados region is the wettest region of the Niger delta, since it receives maximum amount of rainfall compared to other regions. It receives 3000-400mm of rainfall per year and most of the rainfall occurs in the months of May to September. It is during this period the aquifers are recharged by infiltration of precipitation.

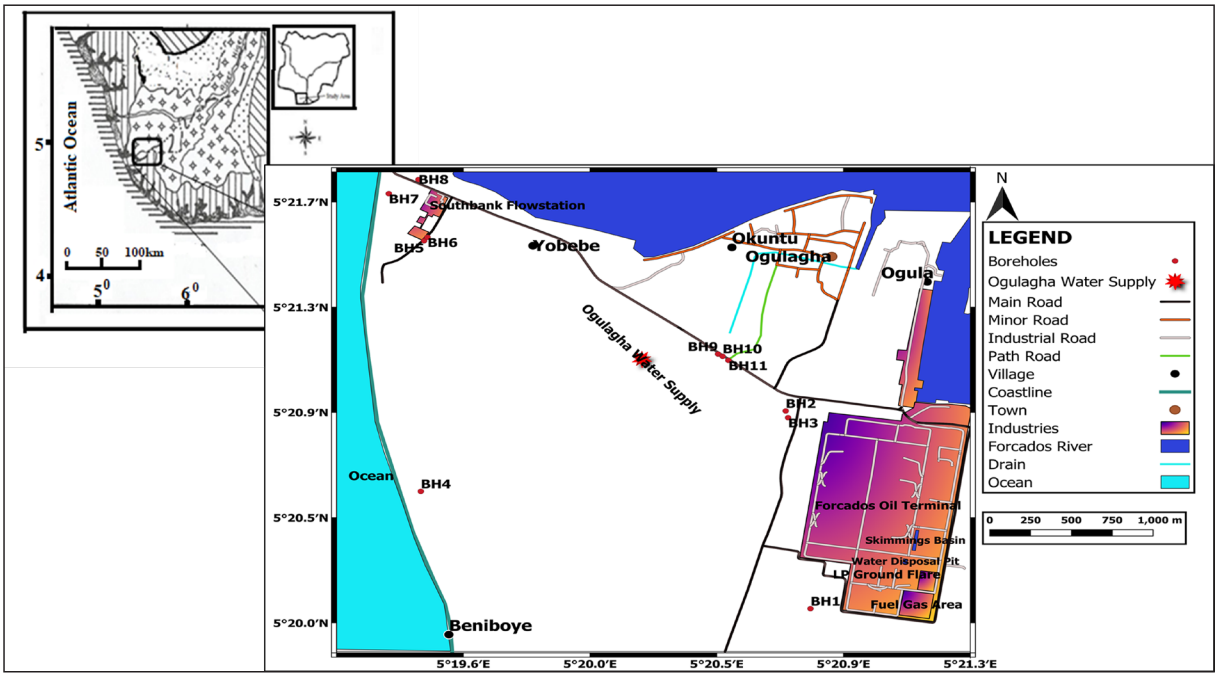

Figure 1. Map of South Bank of River Forcados and borehole locations.

The inundation of the high tide marks by saltwater and its subsequent infiltration into aquifers is another form of recharge that contribute to the salinity of the groundwater (Ohwoghere-Asuma, 2017). The beach and tidal deposits comprise the aquifers and clays are the aquicludes. The area is characterized by multilayer aquifers system arising from deposition of sands and clays, which alternates each other. The aquifers compose of unconsolidated sediments and therefore are quite prolific with high hydraulic conductivities. Groundwater is discharged into the sea and the Forcados estuary and the regional flow direction is from north to south, i.e., land to sea. The cone of depression, on the other hand, is caused by heavy groundwater pumping at the Forcados oil terminal (Figure 3). The interface between freshwater and saltwater is close to the ocean (Ohwoghere-Asuma et al., 2017b; Ohwoghere-Asuma et al.2023) and the aquifers are vulnerable to saltwater intrusion due to climate change, overextraction of groundwater, and sea level rise.

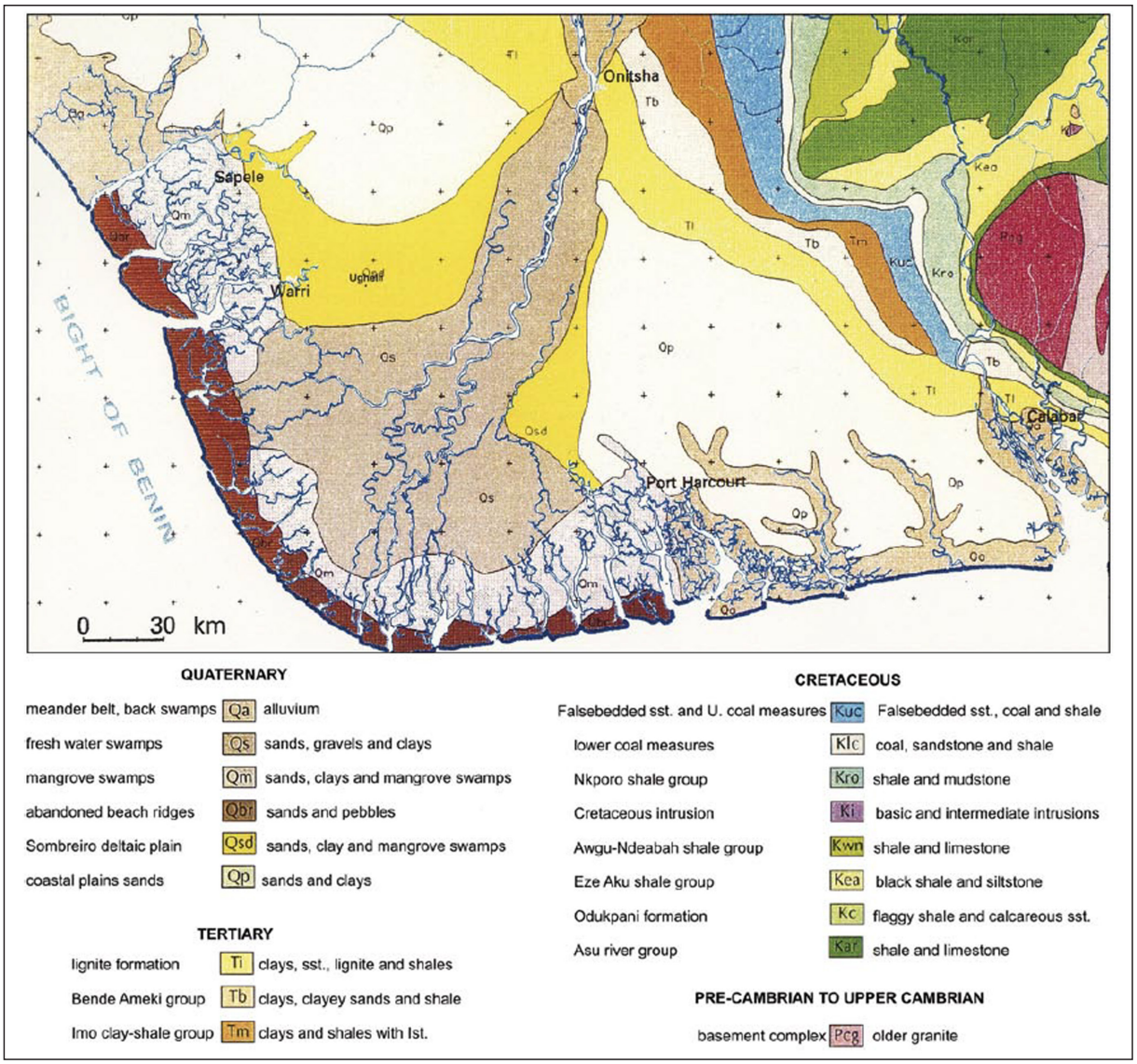

Figure 2. Geological Map of the Niger Delta (Reijers 2011).

2. Materials and methods

2.1 Sediment collection

The sediment samples were collected using a hand auger and a manual drilling rotational method to a depth of 7 meters. Eleven and control boreholes were drilled, with three samples collected at 0.5m, 3m and 7m intervals and labeled top, middle and bottom from each borehole. The depth of the aquifer has an impact on the sediment accumulation at these intervals. In addition, to confirm an earlier study (Atakpo, 2013) that found low resistivity petroleum plumes at 7m in the study region. In the field, plastic bags were used to store samples. The ends of the bags were tied together to keep the moisture content of the sediments stable. They were then brought to a laboratory to be tested for trace metals and TPH.

2.2 Laboratory analysis

The sediments were mixed in the following proportions: 1:2.5. The pH of both mixtures was then measured with a Beckman Zeromatic pH meter. The pH (KCl) of sediments was determined using a 0.1N potassium chloride solution, de-ionized water, and a pH (KCl) meter. The cation exchange capacity was determined using ammonium acetate and the procedure of Jackson (2003). The total organic carbon (TOC) was determined using the Walkley and Blackly technique. Organic carbon was oxidized in the presence of potassium dichromate (K2Cr2O7) acid in this method (Bremner, 1996). By converting carbon and hydrogen into carbon dioxide and water, organic nitrogen (ON) was determined (Bremner, 1996). The digestion of sediments for trace metal analysis was

done with a 4:1 solution of nitric and perchloric acid. Filtrates were recovered by drying and then eliminated with 5M HCL; the concentration of the resultant mixture was then decreased with 3M HCl. The filtrates were then determined by inductive coupling Plasma emission spectrometry for trace metals such as Fe^{2+}, $Pb_{2+,}$ $Cu^{2+,}$ $Zn^{2+,}$ $Cd^{2+,}$ $Mn^{2+,}$ $Co^{2+,}$ $Ni^{2+,}$ $Cr^{3+,}$ and V^{2+}

2.2.1 Laboratory analysis of TPH

TPH samples were collected in polypropylene sample bags and placed in 2-liter bottles that were carefully sealed with caps. In the field, samples were kept in an ice-filled cooler, and in the lab, they were kept at 4°C in the refrigerator. Pulverization was used to reduce the texture of the samples to a very fine texture while also removing foreign materials. Each sample weighed 10g and was kept in an amber glass bottle. To remove moisture, anhydrous sodium sulphate ($Na^{+}_{2}SO_{4}^{-}$) solution was added to the amber glass bottle containing the samples. The samples were extracted with a 30ml solution of dichloromethane (DCM); the glass bottle was carefully covered and placed on a mechanical shaker (LAWI, 2011), and it was violently shaken for several hours, precisely 5-6 hours at room temperature, before being allowed to settle.

2.2.2 Sample clean up

To clean up the sample, a column must be prepared. To prepare a column, the following steps were taken. Glass cotton was used to fill the column. A silica gel and DCM mixture is used to create the slurry, which is an anhydrous $Na^{+}_{2}SO_{4}^{-}$. Pentane was then poured into the column. The prepared column was filled with the sample extract and cyclohexane moisture. Pentane is used as a solvent to collect the extract in a beaker beneath the column. After removing all of the extract, the column was cleaned with DCM. The sample extract was removed and allowed to evaporate overnight at room temperature in a fume chamber (LAWI, 2011).

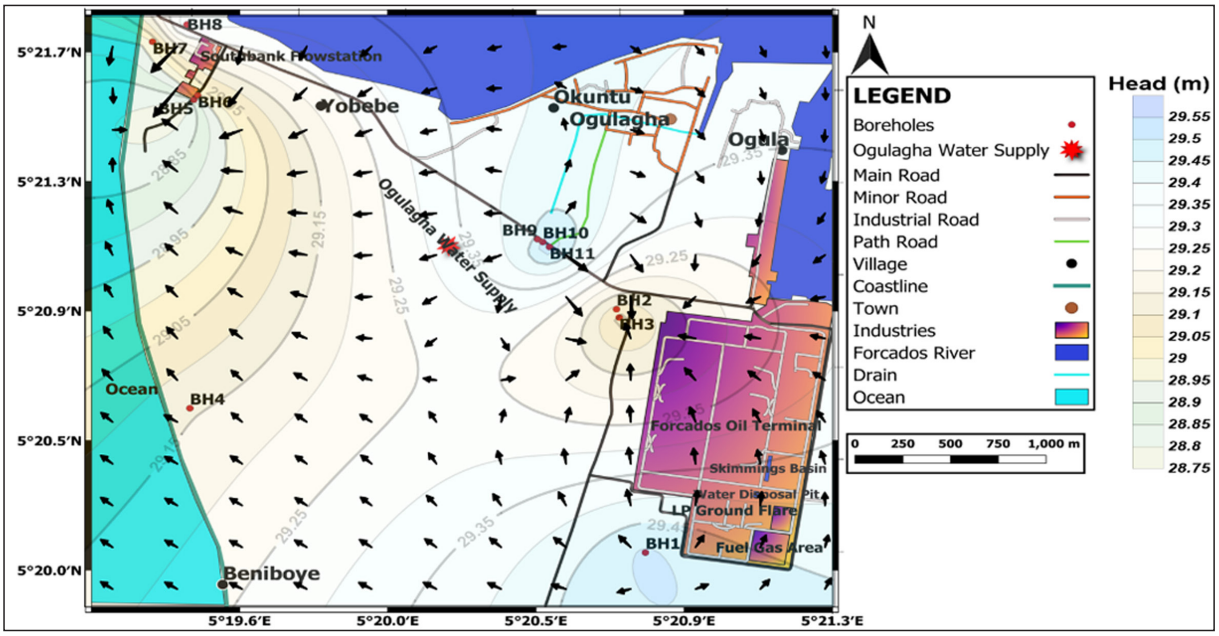

Figure 3. Groundwater flow direction at the South Bank of River Foracados.

2.2.3 Detection and separation apparatus

An Agilent 6890N Gas Chromatograph-Flame Ionization Detector (GC-FID) system was used to identify and separate chemicals in the samples (Cortes, 2012). The column was eluted using approximately 3µl of concentrated samples placed in the GC container. The micro-syringe component of the GC was cleaned several times before collecting material for analysis by injecting DCM and sample. Sample separation was enabled by injecting the sample into the column. The isolated chemicals were then detected using FID. The amount of TPH in each sample was determined using a specific Chromatogram in mg/kg.

2.2.4 Quality assurance and quality control (QA/QC)

According to (Adewuyi, 2012; Akporido, 2008), the quality of TPH extraction methods is determined not only by the amount of fat recovered, but also by the cost and duration of extraction, the ease of replication, and the degree of recovery of the component of interest. TPH component recovery is frequently accompanied by the loss of some of the most important components. TPH was determined by contaminating duplicate sediment samples with 2ml of liquid paraffin oil standard (Akporido, 2008).

2.3 Descriptive and multivariate analysis

Descriptive statistics were used to further process the sediment properties. The commonality between trace metals and TPH was determined with Pearson correlation and factor analysis using SPSS version 20 (IBM Corp., 2011).

3. Results and discussion

3.1 Physical Characteristics of Sediments

Table 1 displays the descriptive statistic of the results of laboratory analysis for sediments taken from 11 drilled boreholes. Soil pH promotes the retention and release of pollutants from shallow to deeper levels. The top sediments samples had a higher pH than the bottom sediments samples. Soil matrix pH_{KCl} ranges from 3.9 to 6.4, with a mean of 5.0. As a result, the sediments in the oil-spill areas were acidic, with mean values less than 6.0. Despite the deeper nature of the sediments collected, the pH values obtained are comparable to those found in typical Niger Delta soils (Ohwoghere-Asuma and Aweto, 2018). The acidity of the soil is caused by rainfall;

heavy rainfall likely accelerates the movement of soil elements from shallow to deeper depths. Electrical conductivity (EC) values in the top, middle, and bottom sediments samples from 124 to 6910s/cm, with a mean of 1168s/cm, and 101-6310s/cm, with a mean of 1332s/cm. These levels are much higher than at the control site, which is 19 kilometers away from the oil facility. Sediment EC indicates the presence of significant anions and cations. The presence of residual hydrocarbon components in the sediments is most likely responsible for the high EC value. The rise in EC could be attributed to the biodegradation of hydrocarbon plumes. Biodegraded hydrocarbon plumes are conductors, as opposed to un-degraded hydrocarbon plumes, which have a high resistance. Table 1 shows the total organic carbon (TOC) content of the sediments, with some variations. TOC and organic nitrogen make up total organic matter (TOM) (ON). These levels are lower than the TOC and ON specifications for a typical soil, which are 500% and 1%, respectively. In most cases, the TOC and ON content of soils damaged by oil spills remained low in these components, which is consistent with the findings of this investigation. The extremely high TOC and ON values of the top sediments, compared to lower values for deeper levels, clearly supports hydrocarbon plumes migrating downward and lateral from surface spillage to the underlying soil layers.

3.1.1 Exchangeable bases of Sediments

The concentrations of exchangeable bases such as sodium (Na^+), potassium (K^+), magnesium (Mg^{2+}), and calcium (Ca^{2+}) are shown in Table 1. The increment sequence is $K^+ > Na^+ > Mg^{2+} > Ca^{2+}$. The concentration of exchangeable bases varies significantly with depth. This clearly shows that the number of interchangeable bases increases as depth increases. The ionic concentration of Na^+ and K^+ ions decrease more with depth than Mg^{2+} and Ca^{2+} ions. The increased level of exchangeable bases was most likely caused by hydrocarbon pollution aided by rainfall-induced leaching, as evidenced by the decreasing trend in base metal concentrations. Base metals that were once present at the surface have migrated downward into the bottom sediments. The Niger Delta's exchangeable base concentrations are generally low, reflecting the nature of rainforest soil. This is most likely due to heavy rainfall in the Niger Delta, which contributes to extensive leaching of mobile basic cations from overlying and underlying soil strata. The values for effective cation exchange capacity (ECEC) are shown in Table 1. The readings are lower when compared to a typical soil. It also depicts sediments that are naturally deficient in ECEC. The ECEC at the top is significantly higher than the bottom. The decreasing pattern is primarily caused by the downward transport of hydrocarbon plumes, as well as infiltrating and percolating precipitation.

3.1.2 Spatial Distribution of trace metals

Table 1 shows the results of trace metals analysis content at the top, middle, and bottom sediments. The abundance of trace metals in the sediments is in the following sequence: Fe>Cu>Zn>Pb>Co>Mn>Ni>Cr>Cd>V. The Fe concentration in the top ranged from 40.83-540.4mg/kg with a mean of 342.4mg/kg, 76.73-560mg/kg with a mean of 387.58mg/kg (middle), and 110-587.4mg/kg with a mean of 407.064mg/kg (bottom). The concentrations of Fe were found to have a linear relationship with depth.

Table 1. Descriptive statistic and review of physical and chemical composition of sediments from the South bank of River Forcados.

Parameters n = 33	0.5m depth (Top)				3m depth(middle)				7m depth(bottom)			
	Min	Max	Mean	STDV	Min	Max	Mean	STDV	Min	Max	Mean	STDV
Zn	3.93	58	14.35	15.13	2.8	23.6	10.89	6.37	1.93	13.8	9.82	2.88
Cd	0.04	0.07	0.05	0.01	0.03	0.06	0.04	0.01	0.03	0.07	0.05	0.02
Cu	1.86	27.36	6.81	7.13	1.34	11.13	5.14	3.00	1.87	6.54	4.63	1.36
Pb	1.69	24.9	6.173	6.50	1.22	10.13	4.67	2.74	1.69	5.92	4.21	1.24
Mn	0.17	74.36	8.245	22.03	0.17	2.71	1.0	0.68	0.51	3.73	1.59	0.95
Co	1.58	23.26	2.59	1.99	1.14	9.46	4.37	2.55	1.58	5.53	3.94	1.15
Ni	0.56	6.24	2.59	1.99	0.56	3.9	1.97	1.037	0.56	31.2	5.25	8.71
Fe	40.83	540.4	342.4	198.82	76.73	560.45	387.58	168.33	110.0	587.4	407.06	150.87
Cr	0.03	1.08	0.352	0.45	0.03	1.1	0.27	0.41	0.01	1.15	0.28	0.43
V	0.00	0.02	0.007	0.01	0.00	0.02	0.01	0.01	0.00	0.02	0.01	0.01
TPH	20.9	14942	2026.3	4405.3	18.6	2045.2	475.76	650.15	0.00	1043.5	227.64	314.27
pH (Kcl)	4.2	6.43	5.18	0.73	4.1	5.9	4.87	0.60	3.9	5.7	4.85	0.63
pH (H_2O)	5	7.2	5.8	0.65	4.6	4.8	5.63	0.67	4.5	6.9	5.65	0.76
TOC	0.42	1.44	0.66	0.29	0.35	0.58	0.46	0.07	0.35	0.77	0.50	0.12
ON	0.04	0.13	0.06	0.03	0.04	0.06	0.05	0.08	0.04	0.08	0.05	0.01
Na	0.48	1.56	0.76	0.31	0.48	0.72	0.57	0.09	0.48	0.96	0.59	0.17
K	0.79	2.26	1.23	0.42	0.79	1.18	0.93	0.15	0.79	1.58	0.97	0.26
Mg	0.04	0.24	0.08	0.06	0.04	0.28	0.11	0.08	0.04	0.8	0.2	0.23
Ca	0.04	0.20	0.10	0.06	0.02	0.16	0.09	0.05	0.04	0.16	0.09	0.04
EA	0.01	0.03	0.01	0.01	0.01	0.04	0.02	0.06	0.01	0.1	0.03	0.03
ECEC	1.35	3.91	2.15	0.69	1.4	2.11	1.72	0.23	1.44	2.79	1.87	0.52
EC	124	6910	1168.5	2032.5	115	5330	1293.1	1965.2	101	6310	1332	2137.5

EA is exchangeable acidity, ECEC is effective cation exchange capacity, EC is electrical conductivity. Every parameter is in mg/kg except EC, which is μs/cm and pH

The high abundances of Fe in sediments highlighted the fact that sediments from unsaturated zones and the aquifer are naturally rich in Fe prior to crude oil spillage. The naturally Fe-rich aquifer sediments explained why most groundwater from shallow aquifers beneath the Niger Delta's coastal region is Fe characterized. The concentration of Cu content in the top has a minimum of 1.86mg/kg and a maximum of 27.36mg/kg with a mean value of 6.81mg/kg, the middle has a minimum of 1.34mg/kg and a maximum of 11.13mg/kg with a mean of 5.139mg/kg, and the bottom has a minimum of 1.87mg/kg, a maximum of 6.54mg/kg with a mean of 4.6354. These value ranges indicate a decrease in Cu concentrations from top to bottom. Zn concentrations ranged from 3.93-58mg/kg with a mean value of 14.35mg/kg for the top sediments, 2.8-23.6mg/kg with a mean value of 10.89 (middle), and 3.93-13.8mg/kg with a mean value of 9.819mg/kg for the bottom sediments (bottom). With increasing depth, the concentration of Zn decreases. Similarly, Pb concentration values ranged from 1.69-24.9mg/kg with a mean of 6.173mg/kg for the top, 1.22-10.13mg/kg with a mean of 4.666 and 1.69-5.92mg/kg for the bottom. Pb exhibited a decrease in concentration with depth that was not distinguishable from that of other trace metals. Mn showed a distinct decrease in concentration when compared to other trace metals, with values ranging from 0.17-74.36mg/kg and an average of 8.245mg/kg for the top, middle with values ranging from 0.17- 2.71mg/kg and an average of 0.9909mg/kg, and bottom sediments with values ranging from 0.51-3.73mg/kg and an average of 1.59mg/kg. Unlike the others, the concentration of Co in drill sediments increased with depth from top to middle and decreased at the bottom, with values ranging from 1.58mg/kg to 23.26mg/kg with an average of 2.586mg/kg, the middle value ranging from 1.14mg/kg to 9.46mg/kg with an average of 4.366mg/kg, and the bottom value ranging from 1.58mg/kg to 5.53mg/kg with an average of 3.93 mg/kg

Furthermore, the concentration of Ni in borehole sediments decreased and increased in the middle and bottom sediments, respectively. The top sediments had values ranging from 0.56–6.24mg/kg with a mean of 2.586mg/kg, the middle sediments had values ranging from 0.56–3.9mg/kg with a mean of 1.9654 mg/kg, and the bottom sediments had values ranging from 0.56mg/kg to 31.2mg/kg with a mean of 5.25mg/kg. Cr concentration differs from Ni concentration, with values ranging from 0.03-1.08mg/kg, with an average of 0.352mg/kg for the top, 0.03-1.1mg/kg, with an average of 0.27mg/kg for the middle, and 0.01-1.15mg/kg, with an average of 0.28mg/kg for the bottom. Cd concentration varies with depth in the same way that Cr does, with values ranging from 0.04mg/kg to 0.07mg/kg, with an average of 0.05 mg/kg for the top sediments, 0.03mg/kg and 0.06mg, with an average of 0.04 for the middle sediments. Bottom sediments values range from 0.03-0.07mg/kg, with an average of 0.07mg/kg. The concentration of V in the sediments is insignificant, with average values at different intervals less than 0.01mg/kg. Overall, trace metal concentrations are much lower than the EGASPIN (DPR-EGASPIN, 2002) intervention standard for contaminated soil. Trace metal concentrations in the sediments are lower than those reported for surficial depths by (Ohwoghere-Asuma and Aweto, 2018; Iwegbue and Nwaje, 2008); Emoyan, 2020; Onojake and Frank, 2013). The presence of elevated trace metal concentrations in the sediments clearly indicates trace metal contamination.

Our findings are consistent with a large number of studies involving the analysis of sediments and water (freshwater and saltwater) in the vicinity of oil facilities around the world. These studies have shown that trace metals are important constituents of crude oil and drilling fluids (Owamah, 2013; Krzyzanowski, 2012; Carls 1995; Kisic, 2009; Fu, 2014; Nie, 2010; Onojake, O. Frank, 2013). As a result, the presence of trace metals in sediments, water, and air from oil facilities was due to petroleum hydrocarbon contamination. Zn, Cd, Ni, V, and Mn have been reported in sediments from the Shengli oil field in China (Fu, 2014); detection of Cr, Ni, Pb, and Z in sediments from the Kachemak Bay Exxon Valdze was by (Carls 1995); Zn, Cu, Cd, and Pb (Ruelas-Inzunza et al. 2009). Local studies in the Niger Delta on trace metals constituents of sediments and water have also revealed their availability for oil exploration and exploitation. (Owamah, 2013) detected Cd, Cr, Cu, Fe, Ni, and Pb in sediments and water samples from oil-contaminated sites; Emoyan (2020) observed Cd, Cr, Ni, Cu, Zn, Mn, and Fe in sediments from a petroleum tank farm; (Iwegbue and Nwaje 2008) observed As, Cu, Cr, Cd, Fe, Pb, Ba, V from a crude oil-impacted site. In addition, consistent with our results is (Uwah, 2013), who detected Cd, Cr, Cu, Fe, Pb, Zn, Ni in sediments of the Qua Iboe Estuary and traced their source to oil contamination.

Furthermore, gas flaring has been identified as a source of trace metal pollutants in both the air and the subsurface. Trace metals are transported into the subsurface via precipitation infiltration and percolation. Another possible source of trace metals in the sediments analyzed is gas flaring near the south bank estuary. This submission is consistent with (Alani, 2020), and (Uyique and Enujekwu, 2017), they found high concentrations of Cr, Cd, Zn, Cu, Pb, Ni, and Fe in soils and water near oil production facilities. The concentration of trace metals in soils and plants decreases with distance from the flaring point (Anacletus, 2014). He discovered that the concentration of Fe, Zn, Pb, and Cd increases with proximity to the flaring point. Ahuchaogu (2019), (Nwankwo and Ogagarue, 2011) also revealed that Mn, Fe, Cr, Ni, Pb, Cu, and Cd were detected in soils and surface water near gas flaring facility.

3.1.3 Distribution of Total Petroleum Hydrocarbon in Sediments

Total petroleum hydrocarbon (TPH) analysis of sediments collected from different intervals of the eleven boreholes revealed values ranging from 20.9-14942.6mg/kg with an average of 2026.3mg/kg for the top sediments, 18.6-2045.2mg/kg with an average of 475.76mg/kg for the middle sediments, and bottom sediments characterized by no detection to 1043.5mg/kg with an average of 227.64mg/kg (Table 1). Except for a few boreholes in the middle and bottom where TPH was not detected. The lowest TPH concentration is far greater than the EGASPIN limit of 10mg/kg (2002). Similarly, these values are higher for sediments from (Osam, 2011; Osuji and Nwoye (2007), but similar to (Tse and

Nwankwo, 2013). Our findings are consistent with (Tolosa, 2005), they attributed high TPH concentrations in sediment from the BAPCO refinery to oil contamination; the same is also responsible for the increased TPH concentrations found in bottom sediments of the Arabian Gulf (Massou, 1996) and (Yanguo, 2013), they observed that oil contamination is responsible for high TPH concentrations in soils near the Songyuan oil field in northwest China.

TPH concentrations in top and bottom sediments were 14,943mg/kg and 1043mg/kg, respectively, indicating a recent spill from the flow station. These values differ from TPH in biodegrading sediments, which tend to decrease with depth (Mostagab et al., 2018; Margesin and Schinner, 1997). As a result, the decrease in TPH content with depth in sediments can be attributed to natural attenuation caused by microorganisms at these levels, particularly in top soil (Cozzarelli et al. 2001). TPH concentrations in the sediments were comparable to those found in soils contaminated by spillage (Tse and Nwankwo, 2013; Adeniyi and Afolabi, 2002; Toti et al.1998; Khan and Kathi, 20140 from other areas. The linear decrease in TPH with depths implied that the sediments were undergoing natural remediation decades after the spillage. The unsaturated zone is frequently regarded as posing a serious threat to groundwater as a sink through which contaminants are received from the top layer of soil and then advanced into aquifers below. The presence of TPH inside the unsaturated zones at 0.5m depth has remained a source of hydrocarbon contaminants to the underlying sequences for many years.

3.2 Multivariate Analysis

The outcome of the commonality between trace metals and TPH is shown in Table 2. As a result, trace metal variables obtained from laboratory analysis had a strong correlation with TPH; in fact, all trace metals have a positive correlation with TPH (Table 2), indicating the same source. The relationship is due to the fact that TPH is a major component of organic matter decomposition and trace metals are attached to organic matter-rich sediment, implying that trace metal adsorption by organic matter, which is a precursor for hydrocarbon. This relationship is explained by natural bioremediation of TPH, which states that as TPH concentrations decrease, trace metals decrease due to adsorption from petroleum (Atagana, 2011; Xiaolong, 2015).

Table 2. Pearson correlation matrix between trace metals and TPH.

Parameters	Zn	Cd	Cu	Pb	Mn	Co	Ni	Fe	Cr	V	TPH
Zn	1										
Cd	-.128 0.478	1									
Cu	1.00** .000	-.130 .469	1								
Pb	1.00** .000	-.134 0.458	1.00** .000	1							
Mn	.300 .869	.328 .620	.029 .874	.017 .927	1						
Co	1.00** .000	-.130 .471	1.00** .000	1.00** .000	.290 872	1					
Ni	-.099 .584	-.309 .080	-.098 .586	-.098 .589	-.048 .792	-.099 .584	1				
Fe	.199 .289	-151 .403	.193 .283	.190 .289	.155 .277	.193 .285	-.147 .415	1			
Cr	-.355* .041	-.077 .671	-.359* .041	-.118 .515	-.359* .040	.420* .015	-.352* .028	1			
V	-.009 .962	-.018 .921	-.002 .989	-.001 .995	-.179 .319	-.003 .986	-.121 .501	-.625* .000	.023 .897	1 .123	
TPH	.053 .770	.143 .429	.052 .774	.053 .770	-.061 .738	.052 .774	-.028 .879	.138 .444	.054 .767	.239 .181	1

(**Significant at 0.05; * significant at 0.01)

3.2.2 Factor analysis

The results of the laboratory analysis were factored using the SPSS statistical package, version 20, to determine the source of the variation in trace metal concentrations in drill sediments. Table 3 depicts a rotating factor matrix with five factors, the variable's loading on each component, and the percentage of data variance explained by each factor. The five variables explain 85.159 percent of the variation in trace metal concentrations and sediment properties (Table 3).

Factor 1

Factor 1 constituents explain 34.08% of the variance in the data and are distinguished by strong positive loading on Zn, Cu, Pb, and Co. The nearly perfect connection (Table 2) and the presence of positive values in this factor by these trace metals strongly suggest that they came from the same source. Those with negative values most likely indicate the origin of different sources or sinks in the sedimentary lithostratigraphy (Matini, 2011). This suggests that trace metals found in estuarine water and sediments come from multiple sources rather than a single source.

Trace metals may be derived from rivers draining large catchments of cities with industries, pesticides and fertilizers (El=Hasan and Al-Tarawneh 2020; Tarawneh et al., 2021), contaminated with petroleum hydrocarbon

spillage, wastewater discharge, and geochemical processes, according to a study report (Sun, 2018; Gavin and Stuart 1999; Matini, 2011; Cheng, 2015, Williams, 1978). Since the study area is within an oil facility located in an estuary, crude oil contamination and gas flaring are most likely not the only sources of trace metals in the sediments analyzed, but other geologic processes that deposit sediments eroded from the catchment into the estuary and their infiltration into the underlying aquifers.

Factor 2

The constituents of this factor account for around 20% of the explained data variability and show significant positive loading on Cd, TOC, and ON, where TOC and ON stand for total organic content and organic nitrogen, respectively, which combined to produce organic matter (OM). Cr's inclusion in this group only reflects Cd adsorption on surface soils enriched with TOC. The source is most likely related to the use of Cd-rich pesticides to control weeds at the south bank oil facility (Emoyan, et al., 2020), which has infiltrated and percolated into underlying aquifer. The higher levels of organic matter in this component, which is linked to Cd, indicate that trace metal adsorption mechanisms differ between trace metal species. The relationship between TOC, ON, and Cd suggests that OM complexing is occurring in the sediments.

Factor 3

This factor with positive Fe, Mn, and negative V loading accounts for 13.5% of overall data variability. The presence of Fe and Mn in this component indicates that it originated from a common source of the weathering of rocks rich in them. They can also be originated from dissolved organic soil materials rich in them. Both are significantly influenced by the oxidation-reduction reaction of sediments and the water interface (Moore, 1979). They are derived from the draining catchment rock and soil rich in them, mining, sewage input into the river, and discharge into the sea. The presence of V in this group with high negative loading suggests a different origin than the others, but its inclusion is related to its association with Fe-Mn oxy/hydroxides. V is derived from the combustion of fossil fuels, petrochemical and major chemical industries, as well as the draining of catchments, weathering of rock and soil enriched in ore into rivers and discharge into estuaries and oceans (Gustafsson, 2018). Bacterial biodegradation of hydrocarbon plumes in aquifer sediments has been shown to result in reductive dissolution of Fe and Mn (Borch et al., 2010). During respiration processes, the biodegradation reaction pathways use Fe and Mn as electron acceptors. The only difference between Fe and Mn in the biodegradation process is that Fe is consumed in greater quantities than Mn. This difference is also reflected in the correlated values and concentrations (Table 2). The presence of V in this factor explains the organic metallic nature of the element, which is important in the formation of petroleum. When the supply of Fe and Mn increases due to reductive dissolution, so does the supply of V.

Table 3. Varimax rotated factor-loading matrix for trace metals and soil physiochemical characteristics near south bank of River Forcados.

Variables (n=33)	Factor 1	Factor 2	Factor 3	Factor 4	Factor 5
Zn	0.990	-0.081	0.044	-0.093	0.019
Cd	-0.108	0.75	0.151	-0.254	0.140
Cu	0.990	-0.083	0.038	-0.094	0.017
Pb	0.990	-0.088	0.033	-0.094	0.020
Mn	0.060	0.392	0.408	-0.049	-0.226
Co	0.990	-0.083	0.038	-0.095	0.17
Ni	-0.029	-0.228	0.096	0.843	-0.020
Fe	0.124	-0.061	0.862	-0.278	-0.255
Cr	-0.290	0.085	-0.19	0.783	0.058
V	0.021	-0.006	-0.81	-0.053	0.198
TPH	0.053	0.098	-0.05	0.026	0.964
TOC	-0.105	0.956	-0.06	0.022	-0.001
ON	-0.112	0.930	-0.10	0.026	0.048
Variance Explained	34.076	19.989	13.489	9.440	8.165
Cum. % of variance	31.271	51.26	64.869	76.624	85.159

Factor 4

This factor, which has a positive Ni and Cr loading, accounts for 9.44% of overall data variability. Ni and Cr are related by their ability to be soluble and insoluble in soils and water, as well as their absorbance. They are related and included in this group because their adsorption on surface soil organic matter is enhanced by TOC, pH, clay content, and iron oxides (Estêvão, 2004; Chrostowski et al., 1991). This reflects the fact that Ni and Cr are frequently carried in insoluble or precipitate forms in runoff and deposited in estuarine sediments. Ni and Cr concentrations in shallow and deep groundwater aquifers are caused by the leaching of soluble and un-adsorbed forms from surface soil.

Factor 5

This variable accounts for 8.17% of total data variability and has a positive TPH loading. The presence of TPH with high correlated values indicates organic component of crude oil. Trace metal contamination in soil and groundwater aquifers has been linked to trace metals, but none have been identified in this component, which is surprising. The

nearly perfect correlation between TPH and trace metals, on the other hand, indicates that the two are inextricably linked (Table 2). Factor 5 explains why trace metals found in borehole sediments in this study are solely due to crude oil spills. The absence of trace metals in this factor can be attributed to their removal during TPH degradation via adsorption from petroleum plumes. This mechanism typically occurs when a migrating plume of petroleum hydrocarbons collides with oxygenated water in the aquifer, where they precipitate out of solution and migrate deeper into the aquifer than the petroleum plume.

4. Conclusions

Laboratory analysis of drilled sediments from 11 boreholes located within an oil facility terminal on the south bank of the Forcados River revealed distinct TPH concentrations beneath aquifer sediment underlying the vicinity of the oil facility. The discovery of abnormally high and low concentrations TPH in subsurface sediments in some areas in the studied site is attributable to its migration from the surficial to deeper depth. Variations in TPH concentrations over borehole depths revealed that pollution started at the surface and migrated below over time, passing through shallow to deeper depths.

Concentration value of the trace metal and TPH decreases vertically downward with depths. The results showed that the loading of trace metals was below the desirable limit except TPH, which is somewhat higher, than standard limit. This is suggestive of the fact that the groundwater at these depths has not been contaminated. Consequently, groundwater from such aquifer harness by hand-dug wells is safe for drinking

According to factor analysis, trace metals delineated in various depth intervals in the study have different pathways through which they are deposited in estuarine sediments. Since the study area is within an oil facility located in an estuary, crude oil contamination and gas flaring are most likely not the only source, but other geologic processes that deposit sediments eroded from the catchment into the estuary and their infiltration into the underlying aquifer. Some may have same geogenic source such as leaching and weathering of rocks and, other from anthropogenic activity including fossil fuel combustions.

References

Adewuyi, G.O (2012). Evaluation of total petroleum hydrocarbon and some related heavy metal in soil and groundwater of Ubeji settlement, Warri metropolis, Nigeria" Terrest. and Aqua. Environ. Toxico., 6(1), 61–65.

Adeniyi, A. A and Afolabi, J.A. (2002)..Determination of total petroleum hydrocarbons and heavy metals in soils within the vicinity of facilities handling refined petroleum products in Lagos metropolis. Environ. Intern., 28(1–2), 79–82.

Ahuchaogu, M., (2019). Effect of gas flaring on surface water in Mkpanak community of Akwa Ibom state Nigeria" Intern Journ. Engr. Resear Tech. 8(09), 1-5.

Akporido, (2008). Assessment of water, sediment and soil pollution arising from crude oil in the vicinity of Esi River western Niger Delta. Department of Chemistry, University of Ibadan, Nigeria. pp.198.

Alani, C. (2020), Impact of gas flaring and surface and groundwater; A case of the Anieze and Okwuibome areas of the Niger Delta, Nigeria" Environ. Monit Assessm 192(3), 166-178.

Al-Tarawaneh, K.,Eleyan I.,Alawan, R.,Sallam.S.,Hammad, S, (2021). Assessment of heavy metals concentration levels in surfaces soil in Baga'a area Jordan. Jordan Journal of Earth and Environmental Sciences, JJEES, 12, 4, 285-294.

Anacletus, F. (2014). Effect of gas flaring on some phytochemical and trace metal of fluted Pumpkin (Telferia occidentals)". Journ. Environ. Earth Sci, 4, (16), 1-5.

Atakpo, E.A. (2013), Resistivity imaging of crude oil spill in Ogulagha coastal community, Burutu L.G.A, Delta State, Nigeria". IJRRAS., 15 (1) 97–101.

Atagana,I.H.,(2011). Bioremediation of contaminated of crude oil and heavy metals in soil by phytoremediation using chromolaena odorata (L) King and H.E Robinson. Air, water and soil pollution, 215 216-271.

Borch, T., Kretzschmar, R., Kappler, A.,Van Cappellen, P., Ginder-Vogel, M.,Voegelin, A., and Campbell, K. (2010). Biogeochemical redox pprocesses and their impacts on contaminants dynamics. Environmental Science and Technology, 44 (1), 15-23. DOI: 10.1021/es9026248

Bremner, J.M. (1996). Nitrogen-total. In Methods of soil analysis, Part 3, Chemical methods. (Ed. D.L. Sparks), pp. 1085-1121. Nº 5. Soil Science Society of America Book Series. Soil Science Society of America, Inc. and American Society of Agronomy Inc., Madison, Wisconsin, USA.

Carls, E.G. (1995). Soil contamination by oil and gas drilling and production operations in Padre Island National Seashore, Texas, US. Jour. of Environ. Manage 45(3), 273-286.

Celestine, A. (2003). Hydrocarbon exploitation, environmental degradation and Poverty: The Niger Delta Experience. Diffuse Pollution'' Conference, Dublin.

Cheng, X. (2015). Assessment of heavy metal contamination in the sediments from the Yellow River Wetland National Nature Reserve (the Sanmenxia section), China" Environ. Sci. Pollut. Resear. 22, 586–8593.

Chrostowski. S.R e tal., (1991). The use of natural processes for the control of chromium migration" Remediat. 2 (3), 341–51. doi:10.1002/rem.3440010309.

Cortes JE, Suspes A, Roa S et al (2012). Total petroleum hydrocarbon by Gas Chromatography in Colombian waters and soil. Amer. Jour. of environ. Sci., 8(4): 396–402.

Cozzarelli., I.M., Bekins , B.A., Baedecker, M.J. (2001). Progressive of natural attenuation of natural attenuation processes at crude oil spill site: Geochemical evolution of the plume. Jour. of Contam. Hydrol., 53: 369–385.

DPR-EGASPIN (2002). Environmental Guidelines and Standards for the Petroleum Industry in Nigeria (EGASPIN), Department of Petroleum Resources Lagos, Nigeria.

El- Hasan,T and Al-Tarawaeh,A (2020).Heavy metal contamination and distribution within the urban soil cover in Mutah and Al-Mazar municipal area. Jordan Journal of Earth and Environmental Sciences, JJEES, 11(3):202-210.

Emoyan, O. (2020). Occurrence, Origin and Risk Assessment of Trace Metals Measured in Petroleum Tank-farm Impacted Soils" Soil and sediment contam; an interna Jour. 2-24, DOI: 10.1080/15320383.2020.1854677.

Estêvão, V.M. (2004). Nickel adsorption by soils in relation to pH, organic matter, and iron oxides: Soils and plants nutrition. Sci. Agric. (Piracicaba, Braz.) 61(21) ttps://doi.org/10.1590/S0103-90162004000200011.

Fu, J. (2014). Monitoring of non-destructive sampling strategies to assess the exposure of avian species in Jiangsu Province, China to heavy metals" Environ. Sci. Pollu Research 21(4), 2898–2906.

Gavin, B., Stuart, T. (1999). Source of heavy metals in sediments of the Port Jackson estuary, Austrl. Sci. Total Environ 227(2-3), 123-138).

Gustafsson J.P. (2019). Vanadium geochemistry in the biogeosphere-speciation solid-solution interaction and ecotoxicity. Applied geochemistry, 105, 1-25.

IBM Corp. Released 2011. IBM SPSS Statistics for Windows, Version 20.0. Armonk, NY: IBM Corp

Ipeaiyeda, A.R. Dawodu, M (2008). Heavy metals contamination of top soil and dispersion in the vicinities of reclaimed auto-repair workshops in Iwo, Nigeria. Bull. Chem. Soc. of Ethiopia 22(3): 339–348.

Iwegbue, C.M.A. (2011). Assessment of heavy metal speciation in soils impacted with crude oil in the Niger Delta, Nigeri". Chem Speci. and Bioavailab., 23(1), 7–15.

Iwegbue, C.M.A. and Nwaje, G.E (2008). Characteristics of level of total petroleum hydrocarbon in soil profile of automobile mechanic waste dumps". Intern. Jour. of soil Sci. 3 (1), 40–51.

Jackson, M.L (2003). Soil chemical analysis: An Advanced course, University of Wisconsm, USA (1958) pp56.

Kisic, I (2009). The effect of drilling fluids and crude oil on some chemical characteristics of soil and crops". Geoderma 149(3) 209 – 216.

Khan, A.B., Kathi, S. (2014). Evaluation of Heavy metal and total petroleum hydrocarbon contamination of roadside surface soil" Intern. Jour. of Environ. Sci. Tech., 11 2259–2270.

Krzyzanowski, J. (2012). Environmental pathways of potential impacts to human health from oil and gas development in northeast British Columbia, Canada, Environ Review 20(2), 122-134.

LAWI, (2011). Laboratory Analytical Work Instruction for the Determination of Total Petroleum Hydrocarbon in Soil/ Sediment/Sludge in Gas Chromatography". Published by Fugro (Nig.) Ltd, Pp.3

Li, J. (2012). Determination of total petroleum hydrocarbons (TPH) in agricultural soils near a petrochemical complex in Guangzhou, China. Environ. Monit. Assessm. 184(1): 281–287.

Margesin, R., Schinner, F. (1997). Bioremediation of diesel-oil-contaminated alpine soils at low temperatures. Appl. Microbiol. Biotech. 47, 462–468.

Massou, A.L. (1996). Bottom sediments of the Arabian Gulf-II. TPH and TOC contents as indicators of oil pollution and implications for the effect and fate of the Kuwait oil slick" Environ. Pollut., 93 (3), 271-284.

Matini, L. (2011). Heavy metals in soil on spoil heap of an abandoned lead ore treatment plant, SE Congo Brazzaville" Afr J Environ Sci Tech 5(2), 89–97.

Moorem. R. M. (1979). The behavior of dissolved organic material, iron and manganese in estuarine mixing. Geochem Cosmochima Acta, 43, 919–926.

Mostagab, H., Senosy, M., Rashed, A. and Salem, M. (2018). The Impact of Hydrocarbon Pollution on Soil Degradation Using GIS Techniques and Soil Characterization in Burgan Oil field, South Kuwait. Journal of Environmental Protection, 9, 699-719. doi: 10.4236/jep.2018.96044.

Nie, M. (2010). The interactive effects of petroleum-hydrocarbon spillage and plant rhizosphere on concentrations and distribution of heavy metals in sediments in the Yellow River Delta, China" Jour of Hazar, Mater 174(1) 156 –161.

Nwankwo, C.N., Ogagarue,O.O. (2011). Effect of gas flaring on surface and groundwater in delta state Nigeria" Journal. Geol. Mining Resear. 3(5) 131-130.

Odeyemi, O. Ogunseitan, O.A (1985). Petroleum Industry and its Pollution Potential in Nigeria. Oil and Petroleum Pollution, Elsevier Applied Science Publication. Ltd, England, 2: 223–229.

Ohwoghere-Asuma, O., and Aweto, K.E. (2018). Impact assessment of soil contaminated with crude oil spill in Otu-Jeremi, western Niger Delta. Jour. of Sci. and Environ. Manag. 23(3) 29–39.

Ohwoghere- Asuma, O., Chinyim, F.I.and Esi. O.E. (2017). Saltwater Intrusion appraisal of shallow aquifer in Burutu area of the western Niger Delta with 2D electrical resistivity tomography. J. Appl. Sc. Environ. Mange. 21 372-377. https// doi,org/10.4314/jasem.v21i2.19

Ohwoghere- Asuma O., (2017) 2D electrical resistivity imaging of the effect of tide on groundwater quality in Ogulagha estuary western Niger Delta, Scientia Africana, 16(2), 16-27.

Ohwoghere-Asuma, O. (2012). Investigation of Groundwater Quality and Evolution in an Estuary Environment: A Case Study of Burutu Island Western Niger Delta, Nigeria. Jour. of Environ. Hydrol. 22 (5), 1–14.

Ohwoghere-Asuma, O., Aweto, K.E, ovwamuedo,G.,and Ugbome, D (2023). Surficial survey of unstressed aquifers for saltwater- freshwater interaction using 2D Inverse resistivity model and saltwater markers in coastal areas of Ogheye in the Niger Delta Basin,Nigeria. Jordan Journal of Earth and Environmental Sciences, JJEES 14(3):195-202.

Ohwoghere-Asuma O., Oteng F.M, Ophori D., (2021). Simulation of saltwater intrusion into coastal aquifer of the Western Niger Delta. Advances in Science, Technology and Innovation; Proceeding of Mediterranean Geosciences Union Conference, Istanbul 1:149-158

Onojake,M.C., Frank, O. (2013). Assessment of heavy metals in a soil contaminated by oil spill: a case study in Nigeria". Chemand Ecol. 29(3),) 246 – 254.

Owamah, H.I. (2013). Heavy metals determination and assessment in a petroleum impacted River in the Niger Delta Region of Nigeria'. J. Petro. Environ. Biotech, 4(1), 1 – 4.

Osam, M.U., Wegwu, M.O., Uwakwe A.A., (2011). The Omoku old pipeline oil spill, total hydrocarbon content of affected soils and impact on the nutritive value of food crops. Arch. of Appl. Sci. Resear. 3(3): 514–521.

Reijers, T.J.A. (2011). Stratigraphy and sedimentology of the Niger dDelta. Geologos 17(3),133–162. https ://doi.org/10.2478/ v1011 8-011-0008-3.

Ruelas-Inzunza, J., Páez-Osuna,F., Zamora-Arellano,N., Amezcua-Martínez, F., Bojórquez-Leyva, H., (2009). Mercury in biota and surficial sediments from Coatzacoalcos estuary, Gulf of Mexico: distribution and seasonal variation" Water, Air, and Soil Pollut 197(1-4), 165-174.

Sun, W. (2018). Source identification, geochemical normalization and influence factors of heavy metals in Yangtze River estuary sediment' Environ. Pollut. 938-949.

Suji, L.C., Nwoye, J (2007). An appraisal of the impact of petroleum hydrocarbon on soil fertility: the Owaza experience" Afric. Jour. Agric. Resear., 2(7) 318–324.

Toti, M, Constantin, C., Dracea, M., Capitanu, V., Damian, M. (1998). Some Aspects Concerning the Oil Pollution and Brine in Romanian soils' Stinta sollului. Soil Sci. Jour. of the Romanian Nat. Soc. of Soil Sci., 1–2: 177–187.

Tolulope, A.O. (2004). Oil Exploration and Environmental Degradation: The Nigerian Experience. International Information Archives, International Society for Environmental Information Science, EIA04-039, 2: 387–393.

Tolosa, N. (2005). Aliphatic and aromatic hydrocarbons in marone biota and coastal sediments from the Gulf and the Gulf of Oman" Mar. Pollut. Bull., 50, 1619-163.

Tse, A., Nwankwo, A.C. (2013). An integrated geochemical and geoelectrical investigation of an ancient crude oil spill site in south east Port Harcourt, Southern Nigeria", Ife Jour. of Sci., 15(1) 125–133.

Udoetok, I.A. (2011). Associated Petroleum hydrocarbons and heavy Metals of an Oil spilled Site in the Niger Delta, Nigeria". Glob. Jour. of Pure and Appl. Sci., 17 (3), 261–265.

Uwah, I.O (2013). Evaluation of Status of heavy metals Pollution of Sediments in Qua-Iboe River Estuary and Associated Creeks,

South Eastern Nigeria". Environ and Pollut; 2(4), 110-122.

Uyique, L., Enujekwu, F.M. (2017). Physicochemical analysis of gas flaring impact on the environment of the host communities in the Niger Delta" Journal of Environ Pollu and Human Health 5(1), 22-29.

Williams, S.C. (1978). Source of heavy metals in sediments of the Hudson River estuary. Marine chemistry 6(3), 195-213.

Xiaolong, L., (2015). Spatial distribution and source of heavy metals and petroleum hydrocarbon in the sand flats of Shuangtaizi estuary Bohai sea of china" Marin. Pollut. Bull.95 (1), 503-512.

Yanguo, L. (2013). Total petroleum hydrocarbon distribution in soils and groundwater in Songyuan oil field north east China" Environ. Monit Assessm. 185, 9559-9569.

JJEES

Jordan Journal of Earth and Environmental Sciences

JJEES (2023) 14 (4): 308-317
ISSN 1995-6681

Amelioration of nano-Kaolinite deportation for heavy Pb(II)'s, Cd(II)'s, and Cu(II)'s ions from aquatic environments

Said Jeries Al Rabadi*[1], Mehaysen Al-Mahasneh[1], Akl M. Awwad[2]

[1] Chemical Engineering Department, Al-Balqa Applied University, Huson – Jordan
[2] Department of Nanomaterials, Royal Scientific Society, Amman, Jordan

Received November 30, 2022; Accepted June 13, 2023

Abstract

This study presents a novel solution for the chemical modification of Jerash natural kaolin clay (NC) after HCl leaching to obtain nano-Kaolinite (NK), for the investigations of the adsorption uptake of heavy Pb(II), Cd(II), and Cu(II)-ions onto modified NK from aqueous discharges, under the variation of pertinent constraints such as medium pH, adsorbent dosage, initial metal concentration, contact time, and temperature. Additionally, the BET analysis reveals an increase in the surface area and volume of the mesoporous structure after acid leaching of the natural KC. Thermodynamic analysis reveals negative values for (ΔG^o) and positive figures for (ΔH^o) and (ΔS^o), which accentuates that the adsorption process is spontaneous, random, and endothermic. The Langmuir and Freundlich Isotherms are the best-fit models to predict the adsorption data, the ultimate removal capacities were obtained as 250, 232.6, and 222.2 $mg/g_{adsorbent}$ for heavy Pb(II), Cd(II), and Cu(II)-ions, respectively, at initial metal concentration of 40 $mg/L_{solution}$, medium temperature of 303.15 K, and initial pH 5.5. By considering these merits of synthesizing a porous structure with intensive nucleation sites on the modified NK surface, a competent and low-prized adsorbent could be used for HM-ions remediation from an aqueous environment and the protection of public health.

Keywords: *Nano-Kaolinite; Adsorption Isotherms; Heavy Metals; Aquatic Environments; Public Health.*

1. Introduction

Heavy metals (HM) ions are common contaminants in the eco-system, thus, their sources and pathways are diverse from an-/ organic and chemicals, food and drug manufacturing, metal infrastructure, as well as anthropogenic activities in residential areas (Al-Rousan et al., 2012; Al Tarawneh, 2014; Tarawneh et al., 2021; Al-Mubaidin et al., 2022). HM accumulation with harmful levels in the aquatic streams and environments is a vital issue to be globally considered, which is subject to restrictions of their emissions by inter-/ national authorities due to slow degradation and high toxicity that leads to a massive impact on soil, water, and air. In developing countries like Jordan, which is suffering from poor aquatic resources, wastewater from industry and residential vicinities is recycled for other applications in agricultural activities like irrigation, animal farms, and bio-facilities. Intake of contaminated water and food products with HM-ions has essential health impacts, which leads to the disruption of numerous biological and biochemical processes inside the human body. Major HM-ions of potential hazards on the human health and environment are namely Lead [Pb(II)], Cadmium [Cd(II)], and Copper [Cu(II)], due to their physico-chemical characteristics, uses, and toxicity. In the middle east regime and specifically in Jordan, HM-ions remediation from aquatic streams is a vital challenge, which requires the implementation of feasible solutions to reduce the HM's concentrations and to maintain with safe and acceptable limitations in the environment.

One of the promising techniques that have been disclosed in literature are applying the natural KC deposits for the adsorption of HM-ions. This clay is naturally distributed with significant quantities in the district of Jerash – northern side of Jordan. Natural KC was investigated for adsorption of HM-ions in aqueous solutions in prior studies of (Wang et al., 2006; Sari et al., 2007; Aragão et al., 2014; El-Maghrabi and Mikhail, 2014, Jiang et al., 2010; Shahmohammadi-Kalalagh et al., 2011; Mustapha et al., 2019). Those techniques have shown crisp uptake of HM-ions from liquid discharges, since there is a relative low cation–exchange capacity and a small surface area of natural KC, (Al-Essa and Khalili, 2018). Else more, desorption of spent natural KC deposits were not feasible, consequently, further treatment processes of clays were foreseen to avoid the accumulation of HM-ions in environment. Consequently, a modification of the physio-chemical characteristics of KCs to ameliorate HM-ions uptake was a demand. In the study of Amer et al. 2010, KC was activated to Sodium polyphosphate-Kaolinite (NaPPK) clay powder, on the other hand, this technique is restricted to pH reading within acidic domain to perform effectively. In previous study by Awwad et al., 2021, KC was modified to $Fe(OH)_3$/kaolinite nanoplatelets. The reported adsorption capacity of Pb(II) ions from aqueous discharges was attributed to a specific surface area and main functional groups in the adsorbent surface, with few investigations of the applicability of this modified adsorbent to other harmful HM-ions.

* Corresponding author e-mail: said.alrabadi@bau.edu.jo

Whereas Alasadi et al., 2019 presented a novel technique applying NK as a natural adsorbent for the remediation of several toxic HM-ions like Cu(II), Ni(II) and Zn(II) from aquatic effluents. In this context, the uptake efficiency of the NK is restricted to the ratio of HM ions concentration in the wastewater stream. This finding has been highlighted in Abdallah, 2019. A thermal transformation and acid activation methods were applied to enhance kaolinite clay for the removal of Cu(II) and Zn(II) ions from wastewater discharges. The reported findings indicated that the ion exchange is the driving mechanism of HM-ions uptake with the constraint of identical molar concentrations, hence, a possibility that the HM-ions are being entrapped into the pores of modified kaolinite clays cannot be ruled out. In this context, Unuabonah et al. (2008) have revealed the application of Polyvinyl alcohol-modified (PVA) Kaolinite clay to move Pb(II) and Cd(II) ions from aqueous effluents. However, when the spent adsorbents were recycled with acidic solutions to be subsequently used for the re-adsorption of the concerned HM-ions, less adsorption capacity was obtained, this is attributed to the acid treatment employed for re-generation desorption that may dispute the active sites available for the adsorption of these HM-ions. An analog finding was obtained by Adebowale et al. (2005), Adewuyi et al. (2019), and Chukwuemeka-Okorie et al. (2018) for the re-generation of Phosphate, Amine, and calcined Corncob-modified Kaolinite, respectively, and adsorption of HM-ions form aqueous effluents of wastewater. These techniques have implied physical pre-treatment to improve the physio-chemical characteristics of natural KC. Meanwhile, Gougazeh (2018) has applied a pre-treatment of chemical leaching by Sodium dithionite ($Na_2S_2O_4$) to increase the active sites on the surface of natural KC for the adsorption of Iron and Titanium contaminants from wastewater. Whereas David et al. (2020) implemented thermal and hydrothermal alkaline modification of Enugu KC for the Pb(II) removal from wastewater, their findings showed that the uptake efficiency of the modified KC was improved in comparison to the raw KC due to the increasing the specific pore volume of adsorbent particles. However, this modification approach led to a weak alteration to the KC matrix, since residual ions remain on the active sites of the modified adsorbent, therefore menial re-generation is foreseen. In this context, combined approaches of physical and chemical treatment were apparently applied for the modification of natural kaolinite for enhancing the uptake efficiency of HM-ions from wastewater, as a coincidence Nigeria kaolinite clay was modified by natural Ammonium oxalate and sodium hydroxide (Lawal et al., 2020), calcined sawdust-kaolinite composite (Ogbu et al., 2019), and three kinds of attapulgite clays (Huang et al., 2020) for the remediation of HM-ions from wastewater. From one side, the activation stage was approached by hydrothermal reactions, which contributed to the alternation of the adsorbent surface into needle-like and granular structures, to ensure a better re-generation process and a prolongated cycle-life of the adsorbent. On the other side, it has been indicated that menial adsorption capacity was obtained due to limited nucleation sites of the adsorbent surface. In a recent study by Al Rabadi and Awwad (2021), a novel approach was presented for the modification of nano-Kaolinite/ Silica oxides composites (nKSOC), for potential immobilization of HM-ions from aqueous solutions, where physical pretreatment and chemical methodologies were combined prior to the implementation of the adsorption stage. In this context, their methodology was effective and further adopted in the current investigations. Up to the authors' knowledge, few studies were conducted on the modification of Jerash KC and its application as an adsorbent for the treatment of contaminated wastewater streams with HM-ions. The potential of the modified NK as an effective adsorbent, for removing the three hazardous HM-ions; Pb(II), Cd(II), and Cu(II), from aqueous ecosystems, is accentuated thoroughly in these experimental investigations.

2. Methods

As a result of the modification strategy, the natural KC underwent physical pre-treatment through size reduction and adsorbent washing. After that, chemical stripping was done to remove contaminants from the adsorbent surface. Finally, washing, gradient drying, and size reduction were used to create a fine powder made of high-purity NK.

2.1 Materials

Sources for the anticipated HM-ion pollutants were provided by the Taufkirchen, Germany-based Sigma-Aldrich company as highly concentrated salt solutions of lead nitrate [$Pb(NO_3)_2$], cadmium nitrate [$Cd(NO_3)_2$], and copper nitrate [$Cu(NO_3)_2$]. The necessary chemicals, including sodium hydroxide (NaOH) and hydrochloric acid (HCl), were purchased from Merck in Darmstadt, Germany. From the Jerash district, KC samples were gathered. Whereas liquid nitrogen (LIN) was delivered locally by a special firm for technical gases. In the experimental study, de-ionized and distilled wastewater were used for washing and solution preparation.

2.2 Treatment methodology of raw KC

The collected and natural samples of Jerash KC were firstly subject to size reduction by being mechanically crushed and sieved with mesh No. 350, the corresponding fine powder has an average pellet size in the macro-range of less than 5μm. The specific surface area and pore volume were determined using the Brunauer-Emmett-Teller (BET) methodology. The sample's adsorption isotherm was measured using Micrometric 2020 and LIN adsorption at 77 K. Before characterization, a 0.3±0.001 g clay sample had been ground up, dried at 423.15 K, and then degassed for 6 h underneath a vacuum. For the HM-ions' adsorption experimentation, a sample of 500±0.01 g of the fine powder was washed with de-ionized water several times to remove any soluble substances, then it was mixed with an HCl solution of concentration 35 % (w/w), the suspended-pellet clay mixture was subject to mechanical stirring for a foreseen time interval of 6 hours. After that, the suspension was incubated overnight at the foreseen surrounding temperature. Following the incubation stage, a red-yellow emulsion was obtained, which was decanted and filtered to separate the emulsified solids, as filter cake to be washed again for few times to remove any traces of acid. The wet filter cake was treated with NaOH solution of a concentration of 20 %

(w/w) under continuous mechanical stirring for a period of 4 hours. Proceeding with the upstream steps of decantation, filtration, and washing the white filter cake with de-ionized water, the wet and kaolinite cake was placed in the dry oven, with gradient warming of 1 K/ 1 minute for the first hour, then baked under steady drying with 353.15 K hot air for additional 4 hours, then gradual cooling of oven content for further one hour. Finally, the dry solids obtained were subject to XRF chemical analysis and optical imaging by Scanning electron microscope (SEM) for the investigation of the appropriateness of the treated nano-Kaolinite pellets for the HM-ions uptake experimentation. SEM is a microscopic technique, which is capable of imaging at significantly higher resolutions than optical microscopes. A portable pH meter from Mettler Toledo was used during the experiment, and the anticipated pH measurement was monitored by adding a buffer solution of either HNO_3 or NaOH with 0.01 M for each. Different temperatures were foreseen for the current investigations: 293.15, 303.15, and 313.15 K. The concentration of the HM-ions supernatants was analyzed with Spectrometer (ICPS-7510).

2.3 Adsorption of HM-ions

The experimentation proceeded in the following manner for the investigation of HM-ions adsorption onto the treated NK: in glass flasks of 250 ml containing 0.5±0.001 g of adsorbent mass and 20 ml of prepared HM-ions solutions with diverse concentrations ranging between 5 to 120 mg/L were mixed, the balance was filled with distilled water, the foreseen HM-ions concentrations were consistent with prior investigations (Aragão et al., 2014; Alasadi et al., 2019; Awwad el al., 2021; Al Rabadi and Awwad, 2021), to simulate a contamination scenario of aqueous solution with HM-ions. The mixtures were shaken with a rotational speed of about 200 rpm until an equilibrium is established by monitoring the temperature at 303.15 K in a water shaker bath, this procedure was repeated for different contact time intervals. Then, the solid phase was separated from the liquid phase by centrifugation at a speed of 2000 rpm for 10 min intervals, then dried according to the procedure described in the above section. The structure and the composition of the separated nano pellets were analyzed by XRD and SEM approaches. For forecasting the size of nano-pellets smaller than 60 nm, the Debye-Scherr equation was used to determine the domain size of the purified nano-pellets based on the width of the XRD peaks (Kurapati and Srivastava, 2018). After equilibrium is being established, the remaining concentrations of HM-ions were analyzed by a Spectrometer (ICPS-7510) and further approved by back titration methods for HM- salts precipitation. The assessment criteria for the absorption of HM-ions, Pb(II), Cd(II), and Cu(II) onto NK were evaluated by the removal efficiency - equation (1), and uptake capacity – equation (2):

$$R\,\% = \frac{C_o - C_e}{C_o}\ x\ 100\% \quad (1)$$

$$q_e = \frac{C_0 - C_e}{m/V} \quad (2)$$

Where, C_o (mg/L) is the initial concentration of HM-ions, C_e (mg/L) is the equilibrium concentration in aqueous solution. m is the NK mass, V is the solution volume in liter, q_e is the uptake of the adsorbed HM-ion per gram of adsorbent ($mg/g_{adsorbent}$) and R% represents the removal percentage of HM-ions.

3. Results and discussion

The results for the characteristic modification of NK adsorbent and the assessment criteria under the alteration of the pertinent limitations for the absorption capability of HM-ions, Pb(II), Cd(II), and Cu(II) onto NK will be highlighted.

3.1 Characteristics of modified NK adsorbent

Figure (1) displays the results of the XRD examination for both the untreated NK and natural KC. The major peaks for SiO_2 and Al_2O_3 were found at 2Theta of 20.7° and the second at 26.7°, respectively. Subsequent peaks were found for various oxides. It is demonstrated that the raw clay deposits are mostly constituted of KC and traces of other metal oxides. It was discovered that the clay's peak intensity slightly decreased after HCl treatment. This is because the acid treatment caused a structural disturbance that alters the clay's matrix structure. While a few peaks were apparently obtained for the modified NK at 2Theta of 12.26°, 20.82, 24.91, and 26.46, primarily referring to SiO_3/Al_2O_3 and traces of other oxides. Both XRDs accentuate that different analyses were obtained for both adsorbent's samples before and after modification, highlighting the necessity of the pre-treatment process for the alternation of the characteristics of the adsorbent, this virtue was also confirmed in previous studies (Al Rabadi and Awwad, 2021; Awwad et al., 2021 and Mustapha et al., 2019). Following the observations by Ogbu et al., 2019; Lawal et al., 2020 and Huang et al., 2020, the presence of soluble metal oxides in the raw KC would have an adverse effect on the modification process of the adsorbent, since these soluble metal oxides offer additional nucleation sites for the precipitation of the HM's pollutants, their presence in the raw sample would have an amplified impact on the sorbent's modification process. As a result, the microporosity increases, and the reforming structure of NK adsorbent would ameliorate the uptake capacity towards HM-ion.

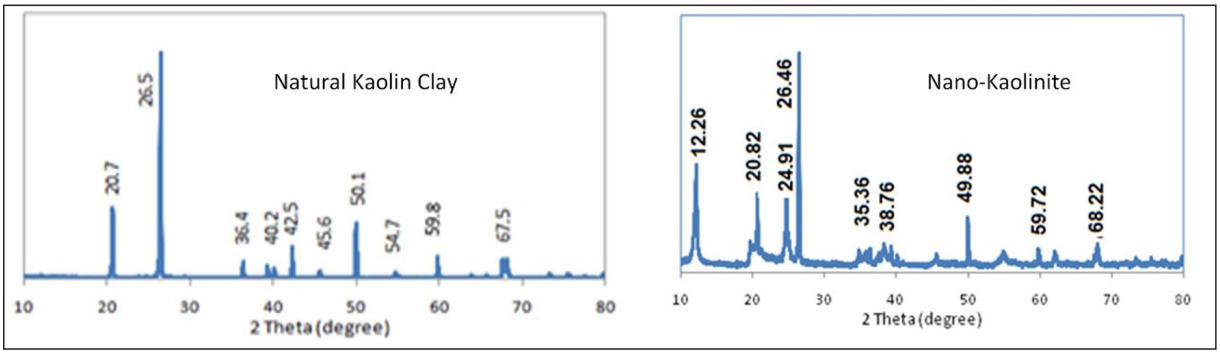

Figure 1. XRD of KC clay and the modified NK adsorbent.

Mineralogical characterization studies of the obtained Jerash KC, have shown that the main constituents are Kaolin (Wang et al., 2006; Sari et al., 2007; Aragão et al., 2014; El-Maghrabi and Mikhail, 2014; Jiang et al., 2010; Shahmohammadi-Kalalagh et al., 2011; Al-Essa and Khalili, 2018). The composition of SiO_2 and Al_2O_3 in raw and modified samples is the primary accomplishment. Table (1) summarizes the chemical composition of the modified NK as well as the Jerash KC. After chemical processing, the treated NK's composition was altered to include more than 88% metal oxides and 10% Kaolin, which is different from the composition of the raw KC deposits. According to El-Maghrabi and Mikhail (2014), the relevant composition with the altered oxide ratio warrants a moderate to high SiO_2/ Al_2O_3 ratio with a factor of 3. The BET analysis reveals that the obtained surface area are 1.289 and 3.142 $m^2/g_{adsorbent}$ for KC and NK adsorbent, respectively, while pore volume was altered from the figure of 0.0064 to 0.155 $cm^3/ g_{adsorbent}$ for KC and NK adsorbent, respectively. These BET findings emphasize that HCl leaching of KC led to two advantages. Firstly, the surface structure of NK adsorbent has been converted into modified NK without the treatment of any of the other mineral's oxides like TiO_2, as was reported by Mahandrimanana (2020). On the other hand, the porous structure volume was developed, hence, creating more numbers and pore volumes on the surface of NK adsorbent, which in turn could be more adequate for the deportation of HM-ions out of the aquatic environments, this finding was highlighted in the investigations of Bkour et al. (2016) and Panda et al. (2010).

Table 1. Textural characteristics for natural KC and modified NK adsorbent according to XRD and BET analyses.

Metal ions	Natural KC [% w/w]	Modified NK [% w/w]
SiO_2	59.67	67.45
Al_2O_3	19.13	22.12
Fe_2O_3	4.65	4.89
TiO_2	1.09	NIL
K_2O	1.32	NIL
MgO	1.53	NIL
CaO	1.64	NIL
Miscell.	10.97	5.54
BET		
Surface area [$m^2/g_{adsorbent}$]	1.289	3.142
Pore volume [$cm^3/ g_{adsorbent}$]	0.0064	0.155

Additional evidence of the NK adsorbent's deformation was provided by the SEM imaging of the modified NK, Figure (2). As a result of impurities such as precipitated oxides, which constitute nearly the whole surface of the KC, being leached with HCl treatment, the surface of the NK adsorbent became purified. The mesoporous structure infers plate-like and thin slit-shaped holes from the NK adsorbent surface. According to the Debye-Scherr equation, the modified NK has a target diameter of 24 nm, which is less than the normal nano-pellet size of 60 nm, as can be observed from the SEM. The key considerations influencing the absorption process are the well-developed porous structure, microporosity, and textural characteristics of the NK adsorbent, implying intense nucleation sites for the migration of HM-ions onto the adsorbents out of an aquatic environment (Hameed et al., 2007; Mojoudi et al., 2019; Somyanonthanakun et al., 2023).

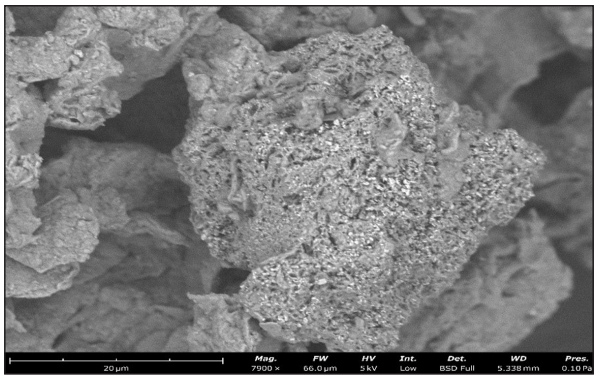

Figure 2. SEM imaging of modified NK adsorbent.

3.2 pH Influence

The alternation of uptake capacity of HM-ions into NK adsorbent with initial pH variation is shown in Figure (3), the investigations of varying the initial pH were performed under a constant temperature of 303 K and an initial HM-ions concentration of 40 $mg/L_{solution}$. The initial pH reading was studied within the range of highly acidic medium (pH = 2) to neutral (pH = 7). The removal percentage of HM-ions from the aqueous solutions increases exponentially with increasing pH in the range from 2.0 to 5.5 to establish a maximum and then decreases under neutral conditions for all the investigated HM-ions. Maximum removal was obtained of 91.9%, 86.3%, and 78.4% for Pb(II), Cd(II), and Cu(II) ions, respectively, within a slightly acidic medium in the pH range of 5.5 – 6. This finding is consistent with prior studies (Wang et al., 2006; Sari et al., 2007; Unuabonah et al., 2008; Al-Essa and Khalili, 2018; David et al., 2020), where the maximum uptake capacity of HM-ions was obtained at initial pH in the range of 5.5 – 6. This finding could be attributed to excess (H^+) concentration in the acidic solution being investigated. Due to the soluble metal oxides, there is an electrostatic competition between the positively charged (H^+) and HM-ions, towards the negatively charged sites of the adsorbent surface. Eventually increasing the initial pH will stimulate (H^+) concentration in an aqueous solution, and the competition between the positively charged HM-ions to be attracted on the negatively charges sites on NK adsorbent surface will increase, hence then HM-ions are the dominating species due to the higher electro-charges, which will attract to the surface of NK due to the driving mechanism of Coulomb interactions (Al-Zboon et al., 2011; Khaleque et al., 2020). Following this finding, an initial pH reading of 5.5 was set as a default value for the proceeding investigations.

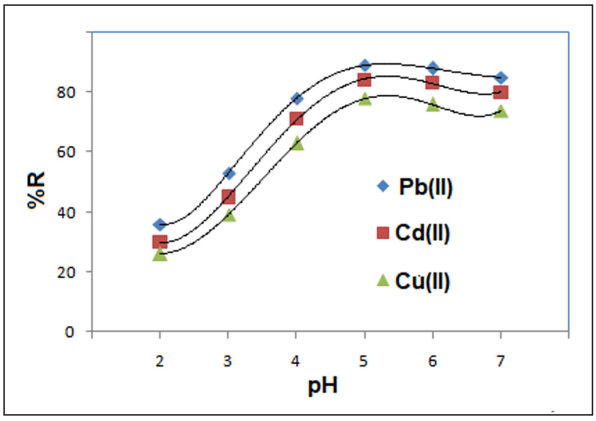

Figure 3. Adsorption removal efficiency of HM-ions onto NK vs. initial pH variation with C_o = 40 mg/$L_{solution}$, 303.15 K.

3.3 Adsorbent dosage Influence

Figure (4) shows the NK dosing for determining the impact on the percentage of HM-ions that are removed from aqueous solutions when the adsorbent dosage is varied from 0.1 to 1.0 $g_{adsorbent}/L_{solution}$, pH is 5.5, and medium temperature of 303.15 K. Adsorbent dosage was changed from 0.1 to 0.5 $g_{adsorbent}/L_{solution}$ to increase the uptake capacity. This established a maximum removal capacity of HM-ions from the aqueous medium at about 0.5 $g_{adsorbent}/L_{solution}$, and for adsorbent dosages higher than this value, there was almost no change in the uptake capacity towards HM-ions. Increased adsorbent dosage may have the effect of increasing the number of nucleation sites available on the adsorbent surface for interaction with free HM-ions in solution. Consequently, the more nucleation sites mean a higher driving force for HM-ions adsorption, a further competition is established adversely between the negatively charged sites towards fewer HM-ions concentration in the aqueous media, thus less removal percentage is accomplished for the HM-ions from the aqueous streams.

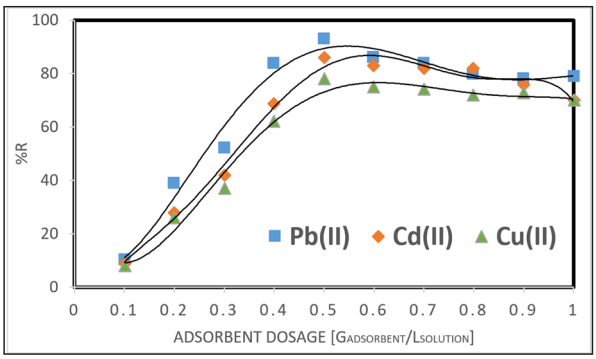

Figure 4. Adsorption removal efficiency of HM-ions onto NK vs. adsorbent dosage variation in the range from 0.1 to 1.0 $g_{adsorbent}/L_{solution}$ with C_o = 40 mg/$L_{solution}$, 303.15 K, and initial pH = 5.5.

3.4 Contact time influence

Figure (5) depicts the behavior of the HM-ion adsorption onto NK with a modification in contact time, at a constant temperature of 303.15 K, an initial HM-ion concentration of 40 mg/$L_{solution}$, and a pH value of 5.5. For all the investigation HM-ions anticipated, it was found that the immobilization of HM-ions rises with increasing contact duration, reaching a maximum after 60 minutes of contact time. When a final contact time of 120 minutes was established, the removal percentage remained unchangeable until the experiment was terminated. The conclusion is that Within the contact time of 60 minutes prior to reaching the adsorption equilibrium, HM-ions are successfully taken up from aqueous solutions. By default, this contact duration was noted as being long enough for HM-ions to adsorb onto NK and was considered in the studies that followed.

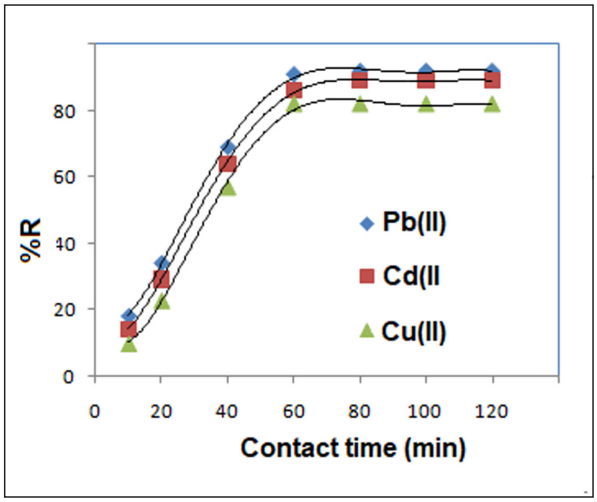

Figure 5. Adsorption removal efficiency of HM-ions onto NK adsorbent vs. contact time variation with C_o = 40 mg/$L_{solution}$, 303.15 K, and initial pH = 5.5.

3.5 HM solubility and temperature Influence

The trend of the HM solubility as a function of temperature for all the investigated HM nitrates salts is presented in Figure (6), the data were outlined from Sigma-Aldrich Chemie (2022). Obviously, the solubility of the nitrate salts indicates an increase within the foreseen range of the investigated temperature. Accordingly, the reported values for HM solubility imply that at a predefined temperature, a higher concentration of free Cu(II) ions are available in the aqueous media compared to Cd(II) and Pb(II) ions, respectively. This means that HM solubility is recorded in the following order Cu(II) > Cd(II) > Pb(II).

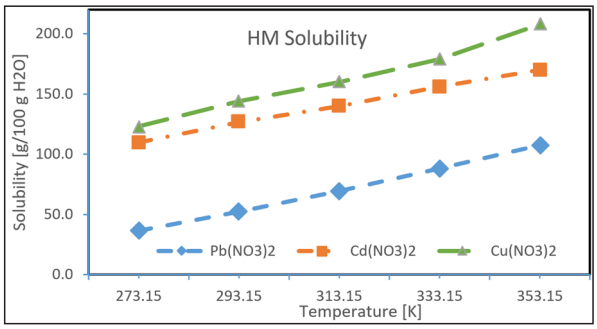

Figure 6. HM solubility vs. temperature (Sigma-Aldrich Chemie, 2022).

The temperature influence on the adsorption process of HM-ions is illustrated in Figure (7), where the uptake capacity of HM-ions from aqueous media (q_e) was plotted as a function of temperature. It can be deduced that the immobilization of HM-ions onto modified NK from aqueous solution is enhanced upon increasing temperature, for an initial metal ion concentration of 40 mg/$L_{solution}$ and pH reading of 5.5. The removal efficiency has been promoted from 135 to 184.4 mg/$g_{adsorbent}$, 128 to 168.7.4 mg/$g_{adsorbent}$, and 113.7 to 158.2mg/$g_{adsorbent}$ for HM-ions of Pb(II), Cd(II), and

Cu(II), respectively, within the investigated temperature range of 293 to 313 K. This finding is consistent with previous studies (Jiang et al., 2010; Shahmohammadi-Kalalagh et al., 2011; Ogbu et al., 2019), where it was stated that the HM-ions removal achieves better effectiveness with higher temperatures. The variation of the uptake capacity of HM-ions on modified NK was found in the order Pb(II) > Cd(II) > Cu(II), this fact is explained by the higher solubility of Cu(II) ions with respect to Cd(II) and Pb(II) ions, hence Cu(II) ions have a higher affinity towards aqueous media than that of Cd(II) and Pb(II) ions, respectively. Consequently, the lower uptake capacity was obtained of Cu(II) ions onto modified NK compared to that of Cd(II) and Pb(II) ions, respectively.

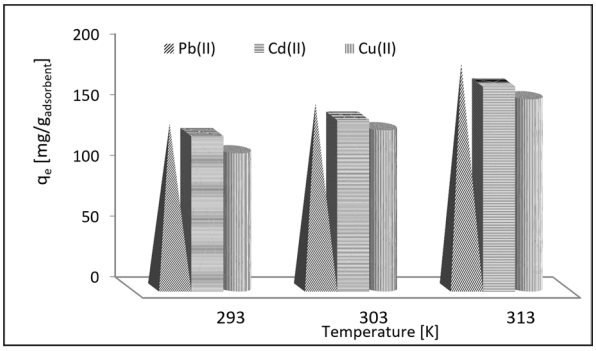

Figure 7. Temperature effect on adsorption capacity of HM-ions onto modified NK adsorbent.

As may be inferred from Figures 6 and 7, elevated temperatures are associated with high solubility figures of the HM, which results in the incorporation of increased concentrations of soluble HM-ions into the aqueous medium. The randomization is then encouraged by the warming of the aqueous medium, increasing the probability that HM-ions will come into closer contact with the nucleation sites on the NK's surface and so increasing the NK adsorbent's capacity for uptake.

3.6 Modelling of Adsorption Isotherms

Adsorption isotherms are the most practical way to describe data for HM-ions removal onto modified NK (Amer et al., 2010; Adewuyi et al., 2019; Alasadi et al., 2019; Al-Essa and Khalili, 2018; Chukwuemeka-Okorie et al., 2018; David et al., 2020; Lawal et al., 2020. To process the experimental data for the removal of Pb(II), Cd(II), and Cu(II) ions onto modified NK, Freundlich and Langmuir adsorption isotherm models were used. Mono-layer adsorption on a homogeneous surface with a finite number of adsorption sites is the basis of the Langmuir model (Langmuir, 1918). As a result, the Langmuir isotherm's linearized form is changed:

$$\frac{C_e}{q_e} = \frac{C_e}{q_{max}} + \frac{1}{K_L \cdot q_{max}} \quad (3)$$

Where q_{max} is the maximum adsorption capacity (in mg/$g_{adsorbent}$) and K_L is a constant relating to the Langmuir energy of adsorption. A linearized plot is obtained by plotting the right side of equation (3) as a function of (C_e) for the HM-ions of Pb(II), Cd(II), and Cu(II). The slope and intercept of the linear plot of (C_e/q_e) vs. (C_e) in Figure (8) were used to analytically calculate the values of the Langmuir parameters, q_{max} and K_L. The Langmuir isotherm model adequately fits the experimental results of the adsorption of HM-ions onto modified NK from aqueous environments.

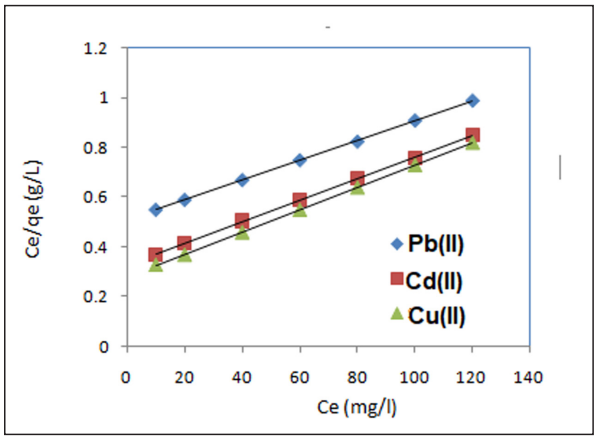

Figure 8. Experimental and model data of C_e/q_e vs. C_e according to Langmuir Isotherm.

The nonlinear function that frequently appears in the adsorption process, according to Freundlich Isotherm (Freundlich and Hellen, 1939), follows the exponential function. The following equation is rearranged for linearization fitting of the experimental adsorption data using the natural logarithm of the exponential form:

$$lnq_e = lnK_F + \frac{1}{n} \cdot lnC_e \quad (4)$$

where K_F is the Freundlich constant and (n) is a function of the strength of adsorption; higher n figures indicate even higher adsorption capacity. The adsorption is linear when (n) equals unity. For (n) figures smaller than unity, adsorption is a chemical process; as a result, enough energy must be provided to force HM-ion exchange with other metal ions onto the adsorbent surface. If (n) figure is higher than 1, then the adsorption process is governed by spontaneous Coulomb interactions acting as the main driving forces behind the electrostatic attractions of positively charged HM-ions to the negative nucleation surface sites. The Freundlich Isotherm prediction of the experimental adsorption data is shown in Figure (9). The intercept of the linearized Freundlich Isotherm's data with the ordinate line is an inherent way to determine (K_F) by charting the term (ln q_e) as a function of the (ln C_e). As opposed to this, the (n) parameter is obtained from the inverse slope of the linearized data fitting. Evidently, the Freundlich Isotherm accurately reproduces the experimental adsorption data for the phenomenon of HM-ions deporting onto modified NK from aqueous environments.

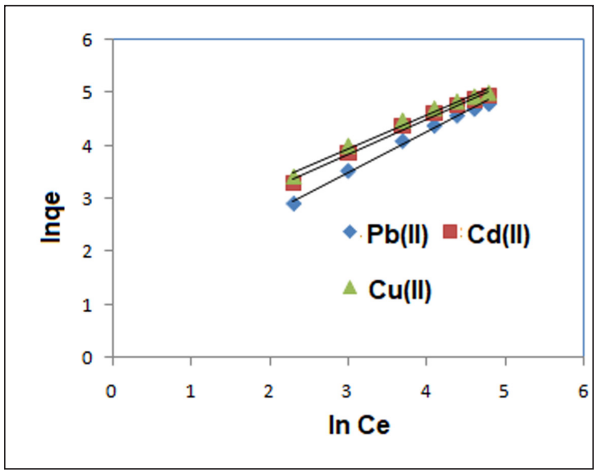

Figure 9. Experimental and model data of (ln q_e) vs. (ln C_e) according to Freundlich Isotherm.

The thermodynamic parameters for the Langmuir and Freundlich isotherms are listed in Table (2). The HM ions of Pb(II), Cd(II), and Cu(II) have an affinity to attract onto modified NK because the magnitude (n) is greater than unity. For HM-ions of Pb(II), Cd(II), and Cu(II), the variation of the maximum absorption capacity of HM-ions on modified NK was determined to be 250.0, 232.6, and 222.2 mg/$g_{adsorbent}$, respectively. This anticipated result is explained by the metal's solubility in aqueous media. Under unchanging adsorption conditions of a medium temperature of 303.15 K, a pH reading of 5.5, and an initial HM-ion concentration of 40 mg/$L_{solution}$, the adsorption experimental data are accurately reproduced to a large extent, according to obtained regression coefficient (R^2) figures by both models of Langmuir and Freundlich Isotherms.

Table 2. Adsorption isotherms' parameters by Langmuir and Freundlich.

HM-ion	Langmuir			Freundlich		
	q_{max}	K_L	R^2	n	K_F	R^2
	[mg/g]	[L/mg]	[-]	[-]	[(mg/g).(L/mg)^n]	[-]
Pb(II)	250.0	4.3	0.999	1.20	0.7655	0.994
Cd(II)	232.6	4.3	0.999	1.84	0.6610	0.989
Cu(II)	222.2	4.5	0.999	2.05	0.6310	0.985

3.7 Thermodynamic Analysis

The following analysis is done on the thermodynamic behavior of HM-ions of Pb(II), Cd(II), and Cu(II) adsorption onto modified NK adsorbent. Following Tran (2022), the relationship, which combines between the equilibrium constant and change in the Gibbs-Helmholtz energy (ΔG^o) of the adsorption process, can be described as:

$$\Delta G^o = \Delta H^o - T \cdot \Delta S^o = R \cdot T \cdot ln\, K_a, \text{ with } K_a = \frac{q_e}{C_e} \quad (5)$$

where C_e is the equilibrium concentration of remaining HM-ions (mg/$L_{solution}$) in solution, and K_a is the thermodynamic equilibrium constant ($L_{solution}$/g). The Van't Hoff equation was used to calculate the specific enthalpy change, ΔH^o[kJ/mol], and specific entropy change, ΔS^o[J/mol/K] (Amer et al., 2010; Jiang et al., 2010, El-Maghrabi and Mikhail, 2014). After being rearranged, equation (5) is then solved for K_a:

$$logK_a = \frac{1}{2.303 \cdot R} \cdot \left(\Delta S^o - \frac{\Delta H^o}{T}\right) \quad (6)$$

where R is the gas constant [8.314 J/ (mol. K)] and T is the absolute temperature (K). The adsorption energies (ΔS^o and ΔH^o) were analytically assessed from the slope and intercept of a linearized data plot of (log K_a) as a function (1/T), following the methodology by Alasadi et al. (2019), Al-Essa and Khalili (2018), David et al. (2020), Awwad et al. (2021), and Al Rabadi and Awwad (2021). At three anticipated temperatures, 293, 303, and 313 K, under analog conditions with an initial HM-ions concentration of 40 mg/$L_{solution}$ and pH of 5.5 reading, the adsorption energies and the pertinent thermodynamic parameters were measured. Table (3) lists the findings for K_a, ΔG^o, $\Delta H^o$and ΔS^o. According to Wang et al. (2006), Sari et al. (2007), and Shahmohammadi-Kalalagh et al. (2011), the adsorption process is endothermic and is generally favored at higher temperatures. This is indicated by the positive figures of (ΔH^o), (ΔS^o), and the decrease in (ΔG^o) with rising temperature. Negative figures of (ΔG^o) indicate the HM-ions adsorption onto modified NK adsorbent is instinctive. This could be attributed to the activation of more nucleation sites on the surface of the modified NK adsorbent. Because the HM-ions are readily soluble in aqueous environments, endothermic adsorption may be explained (Alasadi et al., 2019; Khaleque et al., 2020). While the HM-ions require energy to be absorbed on the modified NK absorbent surface, the necessary energy must balance the dehydration energy provided by the (H^+) ions in the aqueous medium so that the HM-ions can attract to the adsorbent surface. According to Aguado et al. (2009), and Tran (2022) the range of (ΔG^o) for physical adsorption is between -20 and 0 (kJ/mol). The resulting (ΔG^o) was within the range of -3.79 to -5.48 (kJ/mol), -3.52 to -4.95 (kJ/mol), and -3.30 to -3.88 (kJ/mol) for the adsorption of HM-ions of Pb(II), Cd(II), and Cu(II), respectively, onto modified NK adsorbent. In this domain, The primary adsorption of the examined HM-ions was verified to be a physically motivated process. Additionally, the physical adsorption of Pb(II), Cd(II), and Cu(II) ions onto modified NK was successfully achieved with (ΔS^o) values of 84.83, 71.64, and 28.81 (J/mol), respectively. This indicates that the nucleation sites at the adsorbent surface are appropriately random and that there are sufficient driving forces at the aqueous medium interface. When deportation of investigated HM-ions occurs on a modified NK surface, the hydrated water molecules undergo re-substitution before adhering to the surface or penetrating its structure. This reduces heterogeneity, hence increasing the relevant entropy. The adsorption process is endothermic as was highlighted by the positive numbers of (ΔH^o).

3.8 NK reusability and comparison with pertinent adsorbents

The life cycle of NK adsorbent is an important criterion to comprehend its practicality in HM-ions uptake from an aqueous medium, and how feasible its reusability is for repeated cycles from an economic point of view. Figure 10 depicts the percentage removal of heavy HM-ions from modified NK adsorbent versus cycles of reusability, for an initial HM-ions concentration of 40 mg/$L_{solution}$, pH reading of 5.5, and medium temperature of 303.15 K. There is a devaluation in the performance of the modified NK towards the deportation of HM-ions out of the aquatic environment in reverence of implementing re-cycled adsorbent. This finding is attributed to the protonation of the adsorbent surface since some of the positively charged HM-ions are kept attracted to the surface of the regenerated adsorbent due to the electrostatic forces, hence causing a blockage of few nucleation sites. Particularly, the modified NK adsorbent can be regenerated up to four cycles with tolerable performance,

due to the robust textural characteristics that promote the migration of HM-ions from aqueous solutions and ensure high structural stability of the modified NK adsorbent during the desorption stage.

Table 3. Thermodynamic parameters of HM-ions adsorption onto modified NK adsorbent.

HM-ion	T	K_a	ΔG^o	ΔH^o	ΔS^o
	[K]	[$L_{solution}$/g]	[kJ/mol]	[kJ/mol]	[J/(mol.K)]
Pb(II)	293	4.67	3.79-	21.07	84.83
	303	6.42	4.63-		
	313	8.11	5.48-		
Cd(II)	293	4.22	3.52-	17.47	71.64
	303	5.44	4.24-		
	313	6.67	4.95-		
Cu(II)	293	3.88	3.30-	5.14	28.81
	303	4.15	3.59-		
	313	4.44	3.88-		

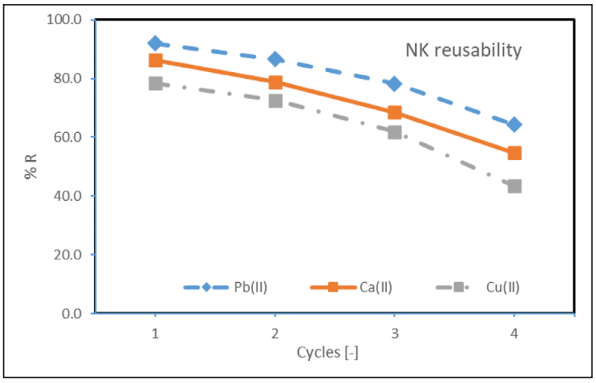

Figure 10. Removal efficiency of HM-ions onto modified NK adsorbent vs. cycles of reusability with C_o = 40 mg/$L_{solution}$, 303.15 K, and initial pH figure of 5.5.

For comparison with pertinent adsorbents, Table (4) summarizes the maximal absorption capacity of the modified NK adsorbent to that reported in the pertinent literature. By employing sulfate-modified KC rather than natural Kaolinite, Adebowale et al. (2005) appear to have improved the removal of HM-ions from aqueous media. The chemical modification increased the absorption capacity of the examined HM-ions. On the other hand, Wang et al. (2006) found modest outcomes from chemical treatment when utilizing natural Kaolinite. Regarding the outcomes of Unuabonah et al. (2008) using polyvinyl alcohol modified Kaolin, Amer et al. (2010) using phosphate modified KC, and Adewuyi et al., 2019 using amine modified KC, respectively, significant accomplishments were noted, which are attributed to the combination of physical and chemical treatment approaches. Whereas poor results were attained when using solely natural Kaolinite (Jiang et al., 2010; Shahmohammadi-Kalalagh et al., 2011; David et al., 2020). On the other hand, promising results were obtained in the investigations of Amer et al, 2010; Ogbu et al., 2019; and Al Rabadi and Awwad, 2021, where Silica oxides contributed to advanced uptake capacity for HM-ions onto modified adsorbent from aqueous media. In general, the observed differences in adsorption uptake can be attributed due to the physico-chemical characteristics of each adsorbent such as surface area and pore volume, modification technique, and the main functional groups in the matrix structure of the adsorbent. By comparing current findings with relevant investigations, a remarkable HM-ions uptake of modified NK adsorbent has been achieved. Consequently, the removal of HM-ions from aqueous solution using modified NK could be effective, eco-friendly, and budgeted-feasible adsorbent for the uptake of HM-ions such as Pb(II), Cd(II), and Cu(II) from aquatic streams even by elevated concentrations, and hence prompting the remediation of environment and protection of public health.

Table 4. Comparison of maximum uptake of HM-ions onto modified NK with relevant studies.

Adsorbent	q_{max} [$mg/g_{adsorbent}$]			Reference
	Pb(II)	Cd(II)	Cu(II)	
Modified NK	250.0	232.6	222.2	Current investigations
Kaolinite	87.26	35.92	71.95	Adebowale et al., 2005
Sulfate modified KC	89.09	42.57	77.09	Adebowale et al., 2005
Natural Kaolinite	-	-	16.79	Wang et al., 2006
Polyvinyl alcohol modified Kaolin	56.18	41.67	-	Unuabonah et al., 2008
Phosphate modified KC	93.89	41.66	80.94	Amer et al., 2010
Kaolinite clay	2.35	0.88	1.22	Jiang et al., 2010
Kaolinite	7.75	-	4.42	Shahmohammadi-Kalalagh et al., 2011
Saw-dust Kaolinite	125	125	-	Ogbu et al., 2019
Amine modified KC	36.41	24.41	-	Adewuyi et al., 2019
Raw Kaolinite	5.42	-	-	David et al., 2020
Alkaline modification of Kaolinite	25.64	-	-	David et al., 2020
nKSOC	172.41	158.73	-	Al Rabadi and Awwad, 2021

4. Conclusion

Based on the addressed findings, a novel solution was introduced for the deportation of HM-ions of Pb (II), Cd (II), and Cu (II) from an aqueous environment. To synthesize an eco- and budgeted-friendly NK adsorbent, the natural KC was structurally modified by integration of physical and chemical methodologies. Under a variety of different constraints, including medium pH and temperature, adsorbent dose, initial HM-ions concentration, and contact time, the modified NK demonstrated efficient behavior for the uptake of HM-ions from aqueous solutions. According to the positive values of (ΔS^o) and (ΔH^o), the thermodynamic scrutiny has shown that the adsorption of HM-ions results is a spontaneous process that is associated with an enhanced randomness at the solid-medium interface. Whilst negative (ΔG^o) figures confirm the endothermic elimination of HM-ions from modified NK. The Langmuir and Freundlich isotherms performed adequately by reproducing experimental adsorption data. This innovative approach could potentially be used for wastewater pollutants remediation in comparison to the deportation by pertinent adsorbents, described in the literature, and with the effective recovery performance.

Acknowledgments

Sincere thanks to Al-Balqa Applied University and the Royal Scientific Society for the conduction of this research in subordinate facilities.

Conflicts of Interest

The authors declare that this study is their own original work. It was not copied (in whole or in-part) from any other work. Also, to declare that no similar work has been submitted or published in somewhere else, either in English or in any other language, without the written consent of the Publisher.

Authors Contributions

A. Awaad contributed to basic idea for the current study, acquisition of experimental data, M. Mahasneh interpreted the experimental results, and S. Al Rabadi drafted the manuscript. All authors have seen and approved the final manuscript and agreed to its submission for publication by JJEES.

Funding

No funding to be disclosed.

Competing Interests

The authors have no competing interests to declare that are relevant to the content of this study.

References

Abdallah, S. (2019). Remediation of Copper and Zinc from wastewater by modified clay in Asir region southwest of Saudi Arabia. Open Geosciences 11: 505-512.

Alasadi, A.M., Khaili, F.I., Awwad, A.M. (2019). Adsorption of Cu(II), Ni(II) and Zn(II) ions by nano kaolinite: Thermodynamics and kinetics studies. Chemistry International 5:258-268.

Al-Essa, K., and Khalili, F. (2018). Heavy Metals Adsorption from Aqueous Solutions onto Unmodified and Modified Jordanian Kaolinite Clay: Batch and Column Techniques, American Journal of Applied Chemistry 6: 25-34.

Al-Mubaidin, M., Al-Hamaiedeh, H., El-Hasan, T. (2022). Impact of the Effluent Characteristics of Industrial and Domestic Wastewater Treatment Plants on the Irrigated Soil and Plants. Jordan Journal of Earth and Environmental Sciences, 13 (3): 223-231.

Al Rabadi, S., and Awwad, A., (2021). Immobilization of heavy Pb(II) and Cd(II) ions from aqueous discharges. Jordanian Journal of Engineering and Chemical Industries, 4: 96-105.

Al-Rousan, S., Al-Shloul, R., Al-Horani, F., Abu-Hilal, A. (2012). Heavy metals signature of human activities recorded in coral skeletons along the Jordanian coast of the Gulf of Aqaba, Red Sea. Environmental Earth Sciences volume 67: 2003–2013.

Al Tarawneh, W.M. (2014). Urban Sprawl on Agricultural Land (Literature Survey of Causes, Effects, Relationship with Land Use Planning and Environment) A Case Study from Jordan (Shihan Municipality Areas). Journal of Environment and Earth Science, 4: 97 – 124.

Al-Zboon, K., Al-Harahsheh, M., Bani Hani, F. (2011). Fly ash based geopolymer for Pb removal from aqueous solution. J. of Hazardous Mat., 188: 414–421.

Adebowale, K.O., Unuabonah, E.l, Olu-Owolabi, B.I. (2005). Adsorption of some heavy metal ions on sulfate- and phosphate-modified kaolin. Applied Clay Science 29:145-148.

Adewuyi, A., Pereira, F.V., Adewuyi, O.A. (2019). Amine modified kaolinite clay from Nigeria: A resource for removing Cd2+ and Pb2+ ions from aqueous solution., J. Appl. Res. Technol. 17: 78-91.

Amer, M.W., Khalili, F.I., Awwad, A.M. (2010). Adsorption of lead, zinc and cadmium ions on polyphosphate-modified kaolinite clay. Journal of Environmental Chemistry and Ecotoxicology 2:001-008.

Aragão, D.M., Arguelho, M.L.P.M., Prado, C.M.O., Alves, J.P.H. (2014). Use of natural kaolinite clay as an adsorbent to remove Pb(II), Cd(II), and Cu(II) from aqueous solution. Materials Science Forum 805:581-584.

Awwad, A.M., Shammout, M., Amer, M.W. (2021). Fe(OH)3/kaolinite nanoplatelets: Equilibrium and thermodynamic studies for the adsorption of Pb(II) ions from aqueous solution. Chemistry International 7:90-102.

Bkour, Q., Faqir, N., Shawabkeha, R., Ul-Hamid, A., Bart, H.A. (2016). Synthesis of a Ca/Na-aluminosilicate from kaolin and limestone and its use for adsorption of CO2. Journal of Environmental Chemical Engineering 4:973–983.

Chukwuemeka-Okorie, H.O., Ekemezie, P.N., Akpomie, K.G., Olikagu, C.S. (2018). Calcined corncob-kaolinite combo as new sorbent for sequestration of toxic metal ions from polluted aqua media and desorption. Front. Chem. 6: 1-13

David, M.K., Okoro, U.C., Akpomie, K.G., Okey, C., Oluwasola, H.O. (2020). Thermal and hydrothermal alkaline modification of kaolin for the adsorptive removal of lead(II) ions from aqueous solution. SN Appl. Sci. 2:1134.

El-Maghrabi, H.H., and Mikhail, S. (2014). Removal of heavy metals via adsorption using natural clay material. Journal of Environment and Earth Science 4: 38-45.

Freundlich, H., and Hellen W. (1939). The adsorption of cis- and trans-azobenzene, J. of the American Chem. Society, 61: 2228-2230.

Gougazeh, M. (2018). Removal of iron and titanium contaminants from Jordanian kaolins by using chemical leaching. Journal of Taibah University for Science, 12: 247–254.

Hameed, B.H., Ahmad, A.A., Aziz, N. (2007). Isotherms, kinetics and thermodynamics of acid dye adsorption on activated palm ash. Chemical Engineering Journal 133 (1–3): 195-203.

Huang, R., Lin, Q., Zhong, Q., Zhang, X., Wen, X., Luo, H.

(2020). Removal of Cd(II) and Pb(II) from aqueous solution by modified attapulgite clay. Arabian Journal of Chemistry 13: 4994-5008.

Jiang, M.Q., Jin, X.Y., Lu, X.Q., Chen, Z.I. (2010). Adsorption of Pb(II), Cd(II), Ni(II) and Cu(II) onto natural kaolinite clay. Desalination 252: 33-39.

Khaleque, A., Alam, M.M., Hoque, M., Mondal, S., Bin Haider, J., Xu, B., Johir, M. A.H., Karmakar, K .A. Zhou, J. L., Ahmed, M. B., Moni M.A. (2020). Zeolite synthesis from low-cost materials and environmental applications: A review", Env. Advances 2:100019.

Kurapati, S., and Srivastava, P.K. (2018). Application of Debye-Scherrer Formula in the determination of Silver nano particles shape. International Journal of Management, Technology And Engineering 8: 81-84

Langmuir, I. (1918). The adsorption of gases on plane surfaces of glass, mica and platinum. Journal of the American Chemical Society 40: 1361-1403.

Lawal, J.A., Odebunmi, E.O., Adekola, F.A. (2020). Adsorption of Fe, Pb, Zn and Cr ions from aqueous solutions using natural ammonium oxalate and sodium hydroxide modified kaolinite clay. Journal of Science 22:1-22.

Mahandrimanana, A. (2020). Analysis of Specific Surfaces of Composite Material: Clays of Madagascar and TiO2. International Journal of Materials and Chemistry 10: 1-4.

Mojoudi, N., Mirghaffari, N., Soleimani, M., Belver, C., Bedia, J. (2019). Phenol adsorption on high microporous activated carbons prepared from oily sludge: equilibrium, kinetic and thermodynamic studies. Scientific Reports 919352. https://doi.org/10.1038/s41598-019-55794-4.

Mustapha, S. Ndamitso, M.M., Abdulkareem, A.S., Tijani, J.O., Mohammed, A.K., Shuaib, D.T. (2019). Potential of using kaolin as a natural adsorbent for the removal of pollutants from tannery wastewater. Heliyon 5: e02923.

Ogbu, I.C., Akpomie, K.G., Osunkunle, A.A., Eze, S.I. (2019). Sawdust-kaolinite composite as efficient sorbent for heavy metal ions. Bangladesh J. Sci. Ind. Res. 54: 99-110.

Panda, A.K., Mishra, B.G., Mishra, D.K., Singh, R.K. (2010). Effect of sulphuric acid treatment on the physico-chemical characteristics of kaolin clay, Colloids and Surfaces A: Physicochemical and Engineering Aspects, 363 (1-3): 98-104.

Somyanonthanakun, W., Ahmed, R., Krongtong, V., Thongmee, S. (2023). Studies on the adsorption of Pb(II) from aqueous solutions using sugarcane bagasse-based modified activated carbon with nitric acid: Kinetic, isotherm and desorption, Chemical Physics Impact, 6:100181,

Sari, A., Tuzen, M., Citak, D., Soylak, M. (2007). Equilibrium, kinetic and thermodynamic studies of adsorption of Pb(II) from aqueous solution onto Turkish kaolinite clay. Journal of Hazardous Materials 149: 283-291.

Shahmohammadi-Kalalagh, Sh., Babazadeh, H., Nazemi, A.H., Manshouri, M. (2011). Isotherm and Kinetic Studies on Adsorption of Pb, Zn and Cu by Kaolinite. Caspian J. Env. Sci. 9: 243-255.

Sigma-Aldrich Chemie (2022). "Solubility Table of Compounds in Water at Temperature." https://www.sigmaaldrich.com/JO/en/support/calculators-and-apps/solubility-table-compounds-water-temperature (Oct. 13, 2022).

Tarawneh, K., Eleyan, L., Alalwan, R., Sallam, S., Hammad, S. (2021). Assessment of heavy metals contamination levels in surfaces soil in Baqa'a area, Jordan. Jordan Journal of Earth and Environmental Sciences, 12 (4): 285-294.

Tran, H.N. (2022). Improper Estimation of Thermodynamic Parameters in Adsorption Studies with Distribution Coefficient KD (qe/Ce) or Freundlich Constant (KF): Considerations from the Derivation of Dimensionless Thermodynamic Equilibrium Constant and Suggestions. Adsorption Science and Technology, 5553212:1-23. https://doi.org/10.1155/2022/5553212.

Unuabonah, E.I., Olu-Owolabi, B.I., Adebowale, K.O., Yang, L.Z. (2008). Removal of lead and cadmium ions from aqueous solution by polyvinyl alcohol-modified kaolinite clay: A Novel nano-clay adsorbent. Adsorption Science and Technology 26: 383-405.

Wang, X.S., Wang, J., Sun, C. (2006). Removal of copper(II) ions from aqueous solutions using natural kaolinite. Adsorption Science and Technology 24: 517-530.

المملكة الأردنية الهاشمية

صندوق دعم البحث العلمي

الجامعة الهاشمية

المجلة الأردنية
لعلوم الأرض والبيئة

JJEES

مجلة علمية عالمية محكمة

المجلد (١٤) العدد (٤)

http:// jjees.hu.edu.jo/

ISSN 1995-6681

المجلة الأردنية لعلوم الأرض والبيئة

مجلة علمية عالمية محكمة

المجلة الأردنية لعلوم الأرض والبيئة: مجلة علمية عالمية محكمة ومفهرسة ومصنفة، تصدر عن عمادة البحث العلمي في الجامعة الهاشمية وبدعم من صندوق البحث العلمي - وزارة التعليم العالي والبحث العلمي، الأردن.

ترسل البحوث إلكترونيا إلى البريد الإلكتروني التالي:

رئيس تحرير المجلة الأردنية لعلوم الأرض والبيئة

jjees@hu.edu.jo

لمزيد من المعلومات والأعداد السابقة يرجى زيارة موقع المجلة على شبكة الانترنت على الرابط التالي:

www.jjees.hu.edu.jo

المملكة الأردنية الهاشمية صندوق دعم البحث العلمي الجامعة الهاشمية

Indexed by Scopus ELSEVIER

JJEES

المجلة الأردنية لعلوم الأرض والبيئة

المجلد (14) العدد (4)

مجلة علمية عالمية محكمة تصدر بدعم من صندوق دعم البحث العلمي

ISSN 1995-6681 jjees.hu.edu.jo كانون ثاني 2023